CCLAB Composite Construction Laboratory

ÉCOLE POLYTECHNIQUE FÉDÉRALE DE LAUSANNE

Appendix B - Technical Report n° CCLab2000.1b/2

Experiments on Double-lap Joints with Epoxy, Polyurethane and ADP Adhesives

Julia de Castro San Román

Version: March 28th, 2005

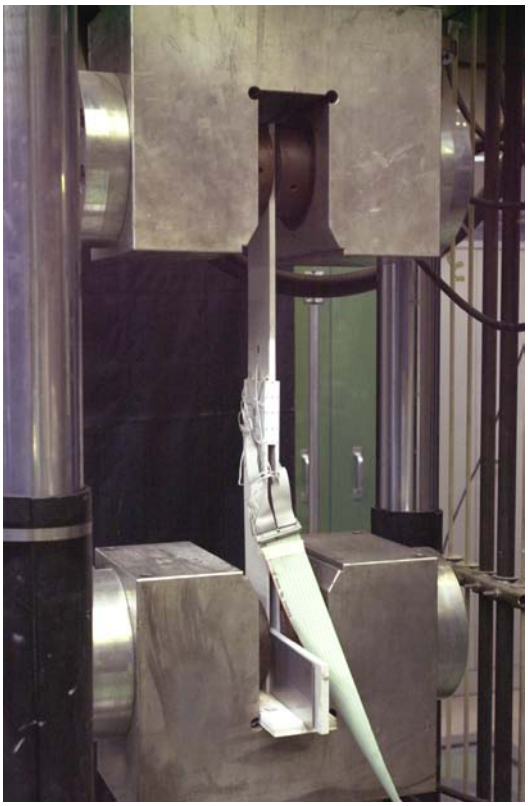

Table of Contents

1 Introduction

1.1 Formulation of the Problem

Fiber-reinforced polymer (FRP) elements are commonly joined with mechanical connections such as steel profiles. However, the use of bolts and rivets is not material-adapted due to the anisotropic character and brittle behavior of FRP materials, and usually leads to over-sizing of components (Keller 2003). Adhesively bonded connection is far more appropriate and allows better load transfer. Nevertheless the stiff and relatively brittle epoxy adhesives currently used cause shear and through-thickness peaks at joint edges (Figure 1). The use of ductile and/or flexible adhesives reduces shear and through-thickness stress concentrations and creates even distribution, increasing the joint's robustness (Figure 1). In addition, ductile and flexible adhesives allow large deformations and develop elastoplastic or elastic hinges in the structures, which for compensate the lack of ductility of FRP materials (de Castro 2005 b). Bonded joints with ductile and flexible adhesives are adapted to FRP elements.

The experimental program consists of testing bonded joints using different adhesives (brittle and ductile, stiff and soft) to study the effect on load transfer, related to stress distribution, and joint stiffness, related to joint elongation.

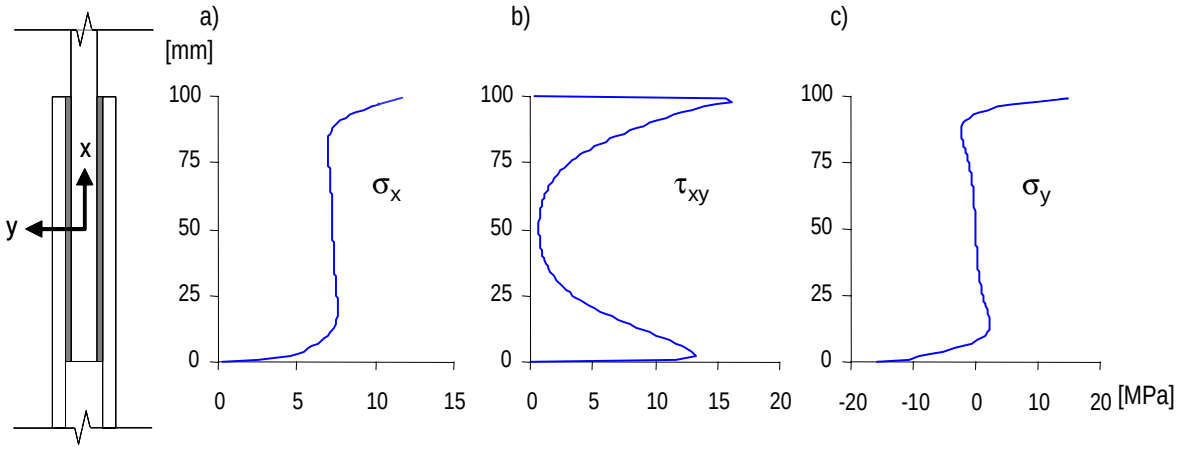

Figure 1 (a) Axial; (b) shear and (c) through-thickness stress distribution along overlap length of adhesively bonded double-lap joint (5 and 10 mm thick GFRF laminates from Fiberline Composites S/A, connected with a 2 mm thick layer of SD330 epoxy adhesive from SIKA AG)

1.2 Objectives

To investigate the mechanical behavior of bonded double-lap joints in GFRP elements using different adhesives, experiments were carried out in collaboration with the adhesive supplier and partner, SIKA AG, Zurich, Switzerland.

The experimental series focus on four objectives:

- determination of joint elongation and joint stiffness;
- determination of load transfer along the joint and its effect on joint strength;
- determination of the adhesive suitable for the development of ductile joints;
- acquisition of experimental data for validation of the developed FEA model.

1.3 Experimental Program

The experimental program consists of thirteen experimental series which examine the effect on joint behavior of the following parameters:

- adhesive mechanical properties;
- manufacturing process (including surface treatment and curing time);
- overlap length.

Three adhesives were considered in the research program: an epoxy resin, designated EP; a polyurethane adhesive, designated PU and an acrylic adhesive, designated ADP. The EP adhesive exhibits linear elastic behavior while the PU and ADP adhesives exhibit ductile behavior. The EP adhesive is stronger and stiffer than the PU and ADP adhesives. Reasons concerning their choice and mechanical properties are given in 2.3.2.

Eight manufacturing processes were tested combining different applied surface treatments and curing times (Table 1). The supplier recommended surface treatment including the application of chemical products such as primer and activator for PU and ADP adhesives. The primer improves adhesion and/or stabilizes and protects the adherends prior to application of the adhesive. The activator activates polymerization. Several combinations of these products were tested to determine the most suitable for each adhesive (2.3.1). Usually, the stiffness and strength of bonded joints improve with time but remain stable after one or two weeks of curing. EP and PU joints present their maximal stiffness and strength after one week (SIKA AG, personal communication). The curing time effect on ADP joints was tested. Two overlap lengths, 100 mm and 200 mm, were tested with the EP stiff adhesive and for the ADP soft adhesive.

Table 1 summarizes the test series and their characteristics. Figure 2 shows joint configuration.

Tensile experiments were carried out between 2002-2004 in the IS laboratory of the EPFL in Lausanne at 23 ± 2°C.

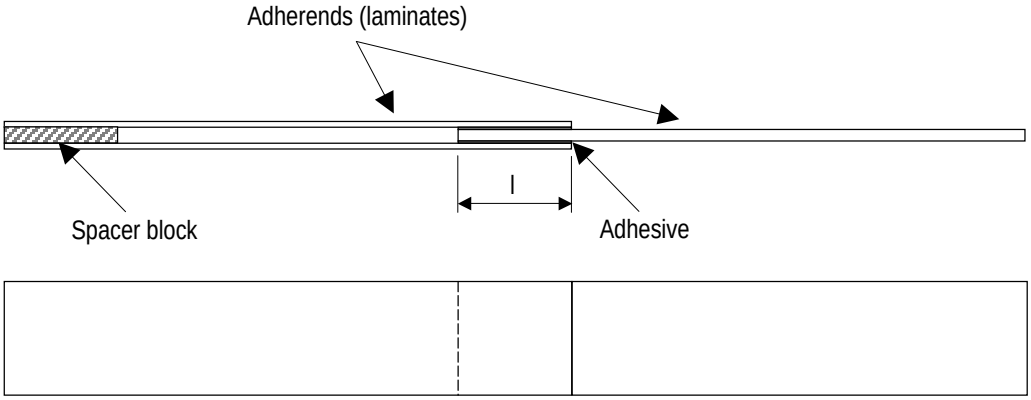

Figure 2 Adhesively bonded double-lap joint

Table 1 Specimen series (see 2.3.1 for surface treatment)

Series	Number of specimens	Adhesive	Manufacturing processes	Surface Treatment[1]	Curing time (weeks)	Overlap length l(mm)
EP.A	12	EP	1	-	1	100
EP.D	3	EP	1	-	1	200
PU.A	3	PU	2	activator+primer 1	1	100
PU.B	6	PU	1	-	1	100
PU.C	1	PU	3	primer 1	1	100
ADP.A	3	ADP	2	activator+primer 1	1	100
ADP.B1	1	ADP	4	-	5	100
ADP.B2	1	ADP	5	primer 1	5	100
ADP.B3	2	ADP	6	activator+primer 2	5	100
ADP.B4	3	ADP	7	activator+primer 1	5	100
ADP.C	9	ADP	7	activator+primer 1[2]	5	100
ADP.D	3	ADP	7	activator+primer 1	5	200
ADP-EP.A	6	ADP/EP	8	-	5	100

[1] all manufacturing processes include sanding and degreasing treatments

[2] ADP.B4 and ADP. C series were identical but manufactured at a different time, and thus analyzed separately

2 Experimental Specimens

2.1 Dimensions

Specimen dimensions are shown in Figure 3. The double-lap specimens were manufactured with three laminates of 500 mm length and 100 mm width. The double-lap configuration is easy to manufacture and eliminates bending moments due to load eccentricity, unlike the single-lap joint. The laminate length guarantees some distance between grip and joint areas; thus, the joint area is not influenced by load introduction. The inner laminate was 10 mm thick and the outer laminates 5 mm. The inner laminate was twice as thick as the outer laminate in order to guarantee a constant section area and constant axial stress. The bonded areas varied with the test series (Table 2); 11 were 100x100mm and 2 were 200x100mm (test series EP.D, ADP.D). The choice of adhesive thickness was a trade-off. A thin layer, as for steel or traditional composite joints, 0.05-0.5 mm (Gleich 2002), is not feasible due to laminates' manufacturing tolerances. The measurement systems (gages and wires) inside the joint constrained the minimal thickness of the adhesive layer (Figure 14). The adhesive thickness used was 2 mm. For series ADP-EP.A, an additional 0.5 mm thick layer of EP adhesive was applied to the laminate bonded areas before connecting them with the 2 mm thick ADP adhesive layer (see 2.3.1). Global adhesive thickness was 3 mm in this series.

Specimen with two rather than four bonded areas was chosen to reduce eccentricity and bonded areas. In fact, the specimen fails when one of the bonded areas fails.

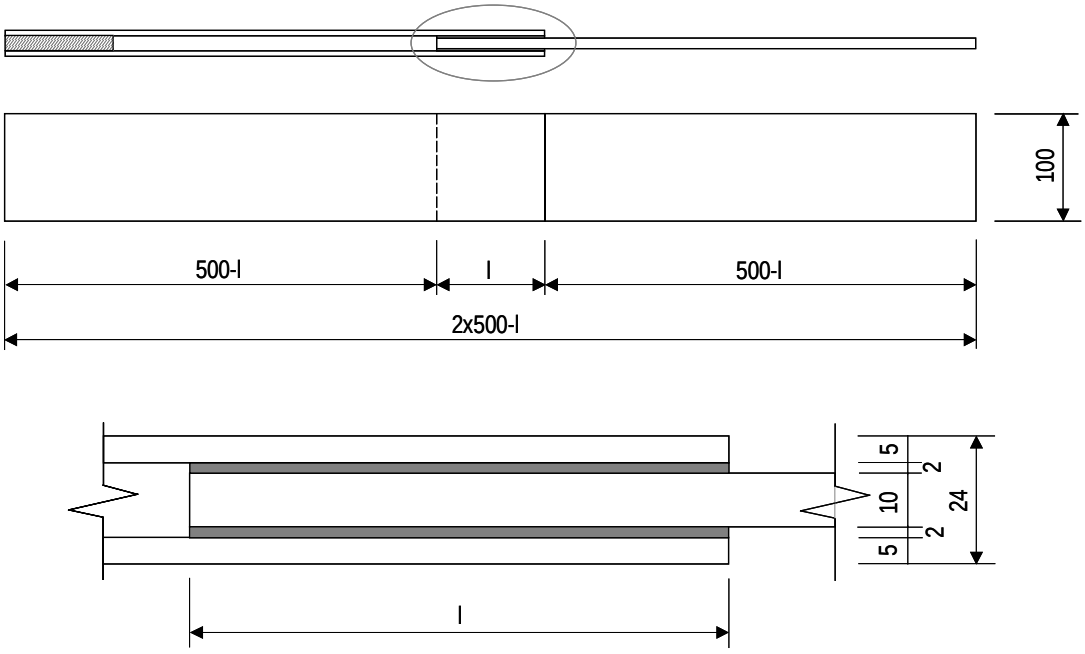

Figure 3 Dimensions of all double-lap joint specimens, except ADP-EP.A series

2.2 Materials

2.2.1 GFRP Laminates

The laminates used in this investigation were pultruded glass-fiber reinforced polymers (GFRP) manufactured by Fiberline Composites S/A (DK), using E-glass G666P and an isophtalic polyester P4506. The manufacturer supplied the laminates of the required dimensions which were cut from the web of standard structural profiles:

- I200x100x10 profiles were used for the 10 mm laminates;
- U140x40x5 profiles were used for the 5 mm laminates.

Structural profiles are composing of a succession of layers of (Figure 4):

- roving mix;
- mat/weave;
- surface veil.

The number of layers and their fiber content depend on profile thickness. The roving mix layer consists of a combination of unidirectional fibers in the longitudinal direction (the x direction) which is the profile's main loading direction, and provides longitudinal strength. It has a 4:1 ratio of straight to blown glass rovings. The mat/weave reinforcement provides shear resistance and contributes to improving bolt bearing capacity and transversal bearing strength (Anon 2003). It consists of a combination of chopped strand mat (CSM) and woven glass mat (0°/90°), stitched together using a special process whereby hundreds of needles are punched through the two mats. The needles have small hooks that push filaments from one mat to the other, thereby combining them (Anders Korsgaard, Fiberline Composites S/A, personal communication). The thin polyester surface veil (40 g/mm^2) was added on the outside to protect the fiber reinforcement from ultra-violet degradation and corrosive attacks.

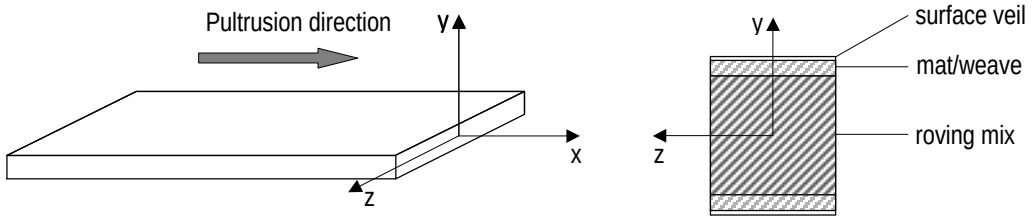

Figure 4 (a) Local axis; (b) schematic drawing of laminate section (not to scale)

Profiles are manufactured by pultrusion (Figure 6), an automated process used for the production of straight or curved profiles with a constant section and high fiber content. The fibers are pulled through a heated die at a specific temperature and speed where they are impregnated with the resin. The resin is

then polymerized and the composite cured in the final profile geometry. Lastly, profiles are cut into the desired lengths by a "floating" suspended saw. This pultrusion process guarantees constant quality.

Material properties are different for each laminate thickness due to their different fiber architecture and content. Fiber weight normally accounts for 40-80 % (Anon 1995). Thus, material tests must be carried out for each thickness. Burning-off tests conducted by T. Tirelli (2003) defined the fiber architecture and fractions listed in Table 2. The 5 and 10 mm thick laminates contain a similar fiber amount but the 5 mm laminate has a higher UD-fiber fraction than the 10 mm. The fiber architecture of the 10 mm laminates is shown in Figure 5(a). The fiber fractions were determined by weighing specimen before and after resin burn-off in a furnace at 450°. Volume fractions were calculated using an E-glass density of 2.56 g/cm^3. Calculations assumed that there were no internal voids. This was checked by some cross-section investigation using a microscope, which confirmed very good fiber embedment without any voids (Figure 5(b)).

Table 2 GFRP laminates technical characteristics (Tirelli 2003)

Reinforcement	5 mm			10 mm		
	Architecture	% by vol.	% by weight	Architecture	% by vol.	% by weight
Rovings (UD)	4:1 straight and blown	37	53	4:1 straight and blown	32	47
Combined mats [g/m2]:	2x1			2x2		
- CSM	300	5	7	450	6	9
- woven 0°/90°	150/150	5	7	300/300	8	11
Total		47	67		46	67

Figure 5 10 mm GFRP laminate (a) fiber architecture after matrix burn-off (without surface veil), (b) microscopic section through thickness: rovings in centre, mats on outside (Tirelli 2003)

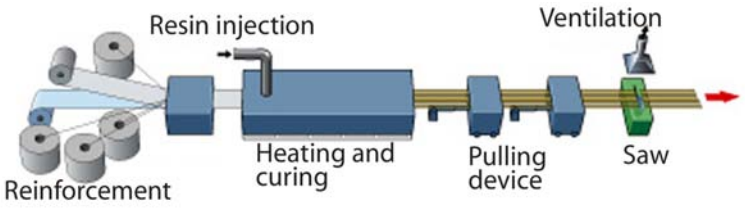

*Figure 6 Pultrusion process (*http://www.fiberline.com*)*

In addition to material differences, the operator starting profile manufacture is allowed to change the amount of roving if production problems arise, providing stiffness does not drop below a certain limit measured in a standard three-point bending test. Unfortunately Fiberline's stocking system does not differentiate between different productions of the same profile. Different productions are stocked together and mixed. Nonetheless, material tests carried out by the CCLab indicated that the laminates used in double-lap joint specimens had similar mechanical properties, which proved constant material quality (Table 3).

Laminates are orthotropic materials due to their manufacturing process, so their matrix is characterized by nine elastic coefficients. Different tests were carried out by Tirelli (2003) and Vallée (2003) at the IS laboratory of the EPFL in Lausanne to determine some of the essential mechanical properties of laminates for joint behavior analysis. The laminate test program consists of a series of test specimens per laminate type:

- longitudinal tensile tests (x direction), quasi-static, destructive testing;
- through-thickness tensile tests (y direction), quasi-static, destructive testing.

The longitudinal tensile tests were carried out on specimens 5 and 8 (laminates reinforced with tabs at ends) for the 5 and 10 mm respectively (Tirelli, 2003). The through-thickness tensile tests were carried out on 10 square specimens using a special testing machine, the CCLab Tensile-Shear Device, developed by Vallée (2004). The following table summarizes the average values and in most cases standard deviations of the principal mechanical characteristics.

Table 3 GFRP laminates mechanical characteristics (supplier's properties)

Laminate	E_x [MPa]	$\sigma_{x,u}$ [MPa]	$\varepsilon_{x,u}$ [%]	ν_{xz} [-]	E_y [MPa]	$\sigma_{y,u}$ [MPa]
5 mm	34'622±719 (23'000)	429±15 (240)	1.27±0.06	0.27±0.02 (0.23)	3500 (7000)	9.08±0.91 (50)
10 mm	32'505±1'303 (23'000)	332±14 (240)	1.03±0.07	0.27±0.02 (0.23)	3500 (7000)	7.94±0.79 (50)

The laminates exhibited almost linear-elastic behavior up to failure (Figure 7). The 5 mm laminates were stiffer and stronger than the 10 mm laminates, mainly due to the higher UD-fiber fraction

(see Table 2). Average values differ considerably from the those in the supplier's design manual (Anon 2003) indicated in brackets. They are conservative for longitudinal mechanical properties whereas they overevaluate through-tickness properties. Vallée (2004) observed and analyzed these differences.

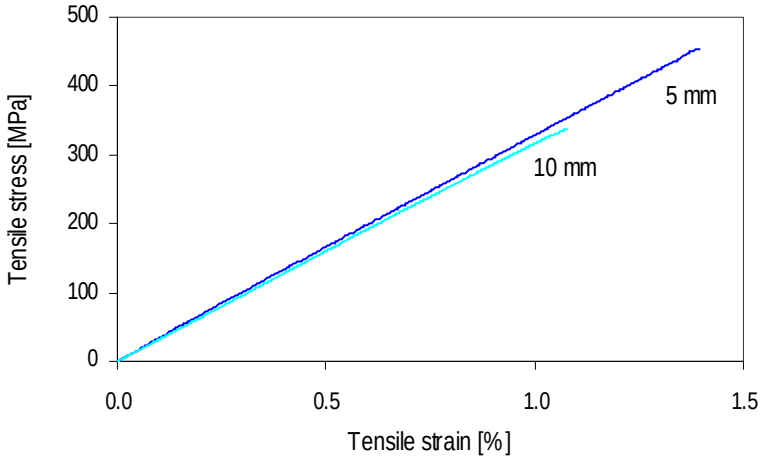

Figure 7 GFRP laminates: average tensile stress-strain curves (Tirelli, 2003)

2.2.2 Adhesives

The three structural adhesives considered in the research program are resins rather than adhesive films since adhesive thickness can vary and thus, compensate the lack of flatness of the adherends. Appropriate viscosity is required to guarantee easier application. The adhesives considered are (Figure 8):

- cold-cured two-component epoxy resin SD 330, designated EP in this project;
- cold-cured two-component polyurethane adhesive S-Force 7851, designated PU;
- fast-curing two-component adhesive SikaFast 5221, based on ADP technology, designated ADP.

Figure 8 (a) EP (SD 330); (b) PU (S-Force 7851) and (c) ADP (SikaFast 5221) in a cartridge container useful for small series (215 ml and 250 ml), and the appropriate static mixer tube

SD 330 is a resin developed for impregnation of carbon-fiber fabrics used for strengthening purposes. It offers high strength and stiffness but presents brittle failure. Since epoxies are commonly used for structural bonding, it seems worthwhile to compare their behavior with new adhesives chosen for the same application.

Because the aim of this project is to create ductile joints that develop larger deformations and increase joint strength, adhesives with nonlinear behavior are preferred. The S-Force 7851 was developed for structural bonding of car-body parts made from carbon-fiber reinforced epoxy resins. It is more flexible and ductile than the epoxy. The SikaFast 5221 adhesive, based on ADP (Acrylic Double Performance) technology, was developed specially for structural bonding. ADP technology offers a new generation of fast-curing soft adhesives designed to substitute welding and mechanical-fastening techniques. It is very flexible and ductile. The following table shows some technical data; more information is available at www.sika.ch.

Table 4 Adhesive technical characteristics

Adhesive	EP	PU	ADP
Chemical base	two-component epoxy resin	two-component polyurethane adhesive	two-component acrylic based
Supplier	Sika	Sika	Sika
Glass transition temperature T_g[1]	+45°C (23°, 7 days cured)	+40 °C	+50°C (23°, 1 day cured)
Consistency	thixotropic	thixotropic	thixotropic
Cure	ambient temperature	ambient temperature	ambient temperature
Working time [2]	40 min at max. +23°C	15 min at +25°C	9 min at +23°C
Application temperature (environment and supports)	+10°C to +25°C	+15°C to +100°C	+10°C to +40°C
Surface treatment	sand and degrease	sand and degrease apply activator apply primer	sand and degrease apply activator apply primer

[1] supplier data
[2] period after mixture of components during which joint must be assembled, similar to open time

To determine the adhesives' mechanical properties, different tests were carried out in collaboration with the adhesive supplier, SIKA AG, and the Strength and Technology Department of the EMPA, Dübendorf. The adhesive test program consists of a series of 3-5 specimens per adhesive type:

- tensile tests according to EN ISO 527 (1997), quasi-static, destructive testing;
- compressive tests according to ASTM D 695-96 (1996), quasi-static, destructive testing;
- shear napkin-ring tests designed at the EMPA (Schmid and Kieslbach 2001), based on the former EN ISO 11003-1, quasi-static, destructive testing.

The compression and tensile tests were carried out on bulk specimens on August 30, 2001 in the laboratory of SIKA AG, Zurich. The shear tests were carried out during April 2002 in the EMPA.

Results are summarized in report CCLab2000.1b/1 (de Castro 2005 a). The following table presents some mechanical characteristics.

Table 5 Adhesive mechanical characteristics

Adhesive	E_t [MPa]	$\sigma_{t,u}$ [MPa]	$\varepsilon_{t,u}$ [%]	E_c [MPa]	$\sigma_{\chi,max}$ [MPa]	$\varepsilon_{c,max}$ [%]	G [MPa]	ν [-]
EP	4552±138	38.1±2.6	1.0±0.1	3050±33	80.7±2.1	3.5±0.1	-	0.37
PU	571±56	18.4±1.0	37.1±1.5	371±37	-	-	355	0.42
ADP	208±18	11.1±0.7	164.1±11.2	9±2	-	-	33	0.40

The EP adhesive exhibits almost linear elastic behavior and brittle failure while the PU and ADP adhesives exhibit ductile behavior. The EP adhesive is stronger and stiffer than the PU and ADP adhesives.

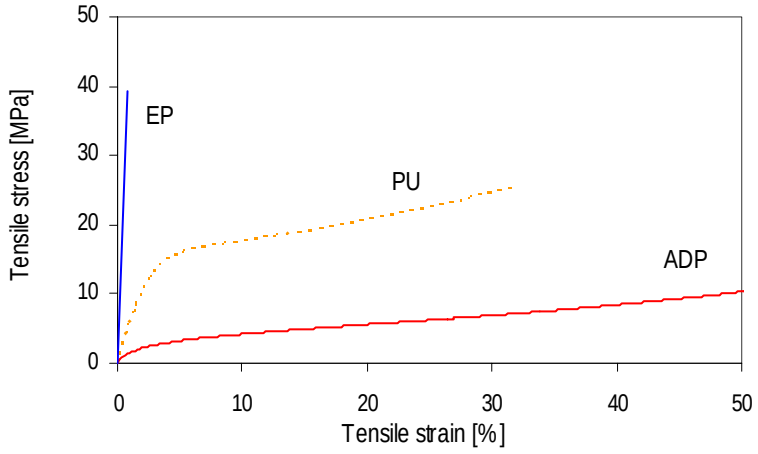

Figure 9 Adhesive tensile average stress-strain curves

2.3 Manufacture and Quality Control

2.3.1 Manufacture

The specimens were manufactured in three main steps:

- surface treatment;
- bonding;
- cure.

Joint resistance and durability depend on adhesive type and surface treatment. The surface treatment eliminates the layers of grease and release agents as well as low cohesion layers (dust, oxides) and improves anchorage between adhesive and adherends by increasing the roughness of the latter. This improves the adherence of the adhesive and adherends. Several treatments are usually carried out: degreasing, mechanical preparation and chemical, physical or physicochemical treatments. The

application of additional layers such as a primer layer modifies adherend geometry or adds new chemical groups which guarantee better adhesion. The primer can stabilize and protect the adherends prior to adhesive application. Each primer is associated with a specific adhesive. If no primer has been developed for a specific adhesive, preliminary tests must be carried out with existing primers in order to select the most suitable. The application of an activator activates polymerization.

Surface treatment could be avoided by applying a special rough fabric, called a peel-ply, to the future bonding area before resin polymerization. This fabric, peeled off just before bonding, protects the bonding surface during manufacture and handling of the elements and provides a clean, rough surface. Several researchers in the past reported relatively low joint strengths using peel-ply surface preparation compared to preparation by mechanical abrasion (Crane et al. 1976; Pocius and Wenz 1985). Hart-Smith et al. (1990) attributed the low strength to the entrapment of air in the textured surface caused by the peel-ply removal and maintained it can reduce the effective bonding area by up to 40%. In order to preclude this, they also suggested "sanding the clean surface to roughen the bottoms of all the depressions left by the wave in the peel-ply". However, the peel-ply technique has recently been improved and is now frequently used (Hollaway and Head 2001).

In this study, surface treatment of the GFRP laminates started with degreasing, sanding and cleaning the future bonded area (Figure 10). Isopropanol or acetone solvents compatible with the polyester, the composite material resin, were used to degrease surfaces. A Bosch GDA280E sander with 80-grit abrasive paper was used to remove the polyester and surface veil until the mat appeared at approximately 0.1 mm depth, taking care not to damage the first fiber layer. The bonded areas were degreased again with the solvent to remove deposited abrasive particles. The EP specimens were then ready for adhesive application. The PU and ADP specimens required the application of two products: an activator and a primer, according to the supplier's (SIKA AG) specifications.

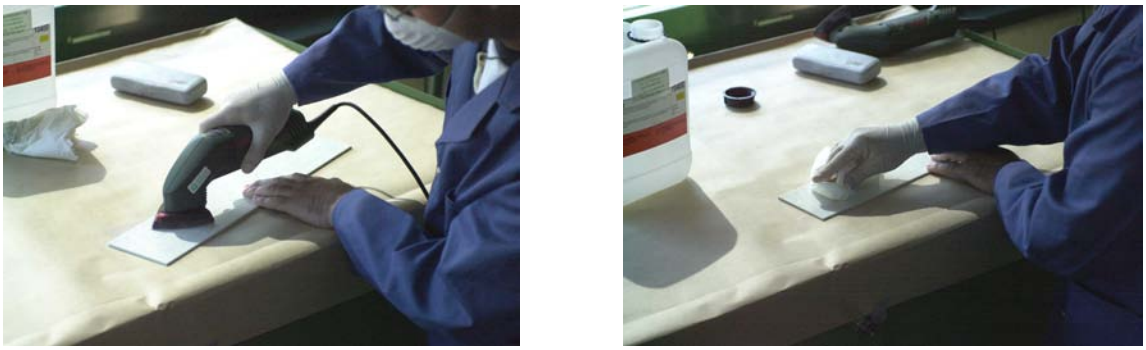

Figure 10 Surface treatment: (a) sanding, (b) degreasing

SIKA Technology AG, Zurich, carried out preliminary tests on February 2003 to check the effect of the activator and four primers: 206 G+P (primer 2), 209, 210 and 215 (primer 1), and primer drying time, 1 or 24 hours (Tsuno 2003). Single-lap joints with steel and GFRP adherends were manufactured and tested. Results indicated that application of primers 206 G+P and 215 dramatically

increased adhesion and joint strength, while the activator slightly improved adhesion. Specified drying time is between 1 and 24 hours but test results indicated no differences. Because of the different specimen configuration and dimensions compared to the double-lap joints studied and the use of a steel adherend, different tests series were carried out to define appropriate surface treatment and curing time. Only primers 206 G+P and 215 were used for the large-scale joint specimens. Table 1 shows the test series and their corresponding manufacturing process (1-8).

The bonding was prepared according to the supplier's specifications. The two components were mixed using the suitable static mixer tube and the uncured adhesive was then spread onto one outer laminate. Four glass balls of 2 mm diameter were placed on the bonding area to guarantee adequate adhesive layer thickness. Then the inner laminate was laid and pressed. The laminates were aligned with a rule. Weights were placed to produce pressure during curing time. After one day of cure, the second outer laminate was bonded following the same process. The specimens were cured under ambient laboratory conditions, 23 ± 2°C, for one or five weeks, depending on the test series.

For ADP-EP.A specimens, two EP adhesive layers of 0.5 mm thick were first applied to the laminates. After one day of cure, the specimens were manufactured in the way previously described. The ADP adhesive was spread directly onto the EP layer without applying any primer and activator. The EP layer was applied between the ADP and laminates to avoid adhesion failure in ADP specimens (see 4.3.2).

2.3.2 Quality Control

Several quality controls were performed during joint manufacture and before testing to obtain constant performances and improved reliability. These controls were in accordance with the Quality Assurance in Adhesive Technology (1998) resulting from the EUREKA Project EU716. This document specifies control tools and techniques for fulfilling established joint requirements. As suggested, a specific checklist document was developed describing all joint manufacture steps (Siebrecht and Vallée 2001).

During the manufacturing process it was crucial to verify:

- adhesive : product's conformity, storage conditions, open time, mixture reactivity, viscosity;
- activator and primer : product's conformity, storage conditions, open time, dry time and thickness;
- surface : moisture and ambient temperature, operation times, solvent.

After bonding, final inspections using non-destructive testing techniques must be carried out to identify joint defects. Typical defects found on bonded joints are shown in Figure 11. Adams and Cawley (1989) classified them as adhesive defects or adhesive/adherend interface defects. Table 6 summarizes the types of defects, their causes and the appropriate control techniques for their detection.

Porosity and voids could be detected by basic visual and acoustic inspections and/or advanced and expensive testing techniques commonly called non-destructive evaluating (NDE) techniques. Visual

inspection consists of examination of adhesive surround. Acoustic inspection consists of hitting the bonded area with a rule. These basic inspections are fast and economical techniques but are also limited and subjective. The advanced testing techniques most commonly used are infrared radiation, radiography or ultrasonic methods. Although bad cohesion and bad adhesion defects could be detected by fine ultrasonic analysis and acoustic emission, these techniques are currently considered unreliable and research is continuing in this field. More details concerning these non-destructive testing and commercial instruments are available in Adams et al. (1997), Adams (1990), Adams and Cawley (1989) and Lambert et al. (1994).

In this experimental study, final inspection consists of basic visual and acoustic controls. A visual inspection of failed specimens was made after testing to check the presence of defects. No large defects were detected on specimens.

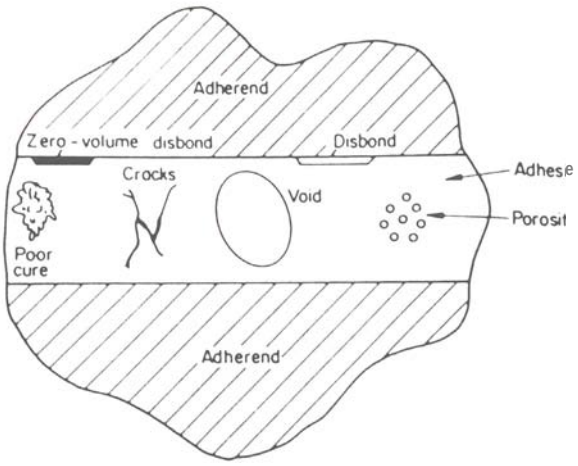

Figure 11 Typical defects in bonded joints (Adams and Cawley, 1989)

Table 6 Causes of bonded joint defects and appropriate control techniques

Defects	Causes	Inspection techniques
Porosity	Volatile and entrained gases (principally air and water vapor)	Visual and acoustic inspection Infrared radiation
	Bad or insufficient application of adhesive	Radiography
Voids	Air entrapment during laying of adhesive Relative displacement of adherends Adhesive flow	Ultrasonic
Bad cohesion	Incorrect or contaminated mixing Incorrect storage Bad polymerization	Ultrasonic spectroscopy Acoustic emission
Cracks	Bad polymerization Thermal shrinkage	
Bad adhesion	Contamination before bonding (oil deposit or loose oxide layer) Formation of a skin in adhesive layer when adherend is applied after working time	Acoustic emission

3 Experimental Procedure

3.1 Test Set-up and Loading Equipment

Specimens were subjected to an axial tensile loading via a SCHENK Hydropuls-Zylinder Typ PL testing machine with a capacity of 1000 kN in static loading (tension as well as compression) and possible displacements up to ± 250 mm (Figure 12). The diameter of the horizontal hydraulically-controlled circular jaws was 150 mm. Grip lengths were 140 mm and 100 mm for the 10 mm and 5 mm laminates respectively, thus specimen lengths between grips were 660 mm for the 100 mm overlap length and 560 mm for the 200 mm. A 14 mm thick spacer block was placed between the 5 mm laminates in the grip area to assure in-plane loading. The tests were conducted in a laboratory environment at room temperature without impact of temperature changes or moisture. The load was applied at a constant displacement rate of 0.6 mm/min until specimen failure.

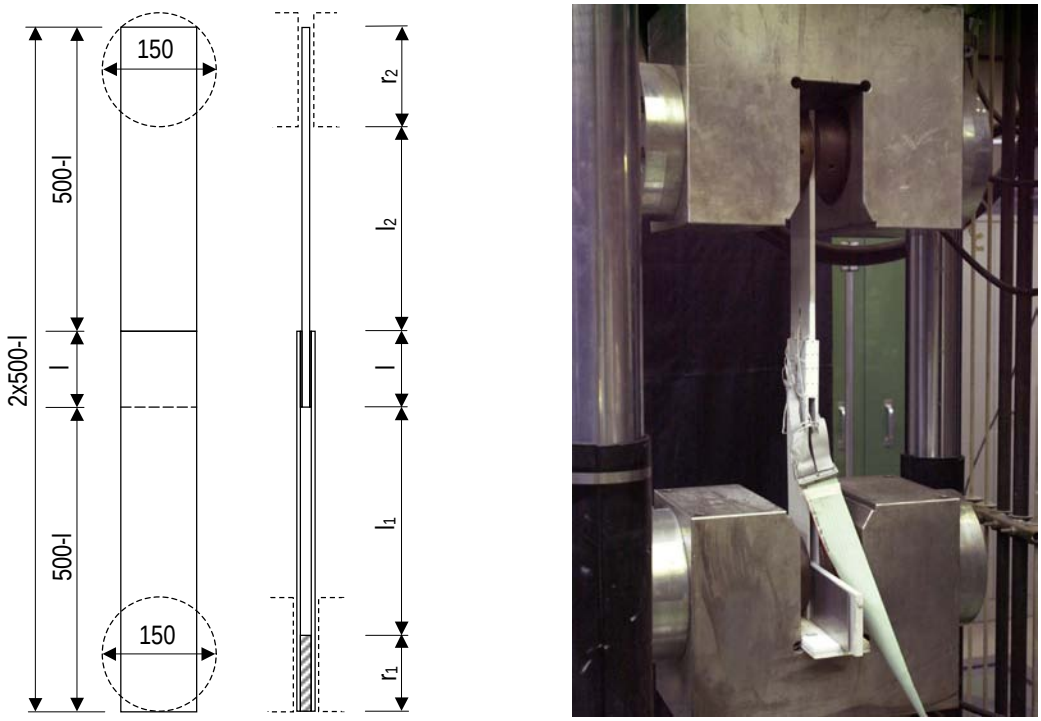

Figure 12 Tensile testing device

3.2 Instrumentation

3.2.1 Classic Instrumentation

All tests were instrumented with automated measurements every 2-3 s. The data acquisition unit was a HBM UPM 60 with 60 channels (Hottinger Baldwin Messtechnik, Darmstadt, D). A data acquisition program was developed in LABVIEW programming language for this experimental work. This

program enabled test evolution to be followed and data acquisition to be checked on different graphs. The recorded data were:

- load and displacement of the machine with a load and displacement cell;
- axial strain on some laminate sections measured with strain gages;
- axial strain on bonded overlap measured with strain gages.

Two kinds of axial strain gages were glued to specimens, the 6/120LY13 and 1.5/120LY13 produced by HBM. The connecting areas were degreased and gage positions precisely defined and marked before the gages were stuck using an appropriate adhesive.

Axial strain on laminates sections

The 6/120LY13 has a 6mmx2.8mm measuring grid, 13mmx6mm measuring-grid carrier and an electric resistance of 120 x. These ten gages are referred to as external gages. Their labeling and positions are indicated in Figure 13. They were placed on four sections. Two gages, s0 and s5, were placed on the 10 mm laminate and the other eight were placed on the 5 mm laminates. Gages s0-4 were on the upper side and gages s5-9 on the lower side. Measurements indicated any load eccentricity in direction y. Eight gages were placed on the specimen's longitudinal axis in order to measure the strain on different sections close to the joint area. Two gages were placed 10 mm from the edge in order to determine any loading eccentricity in direction z.

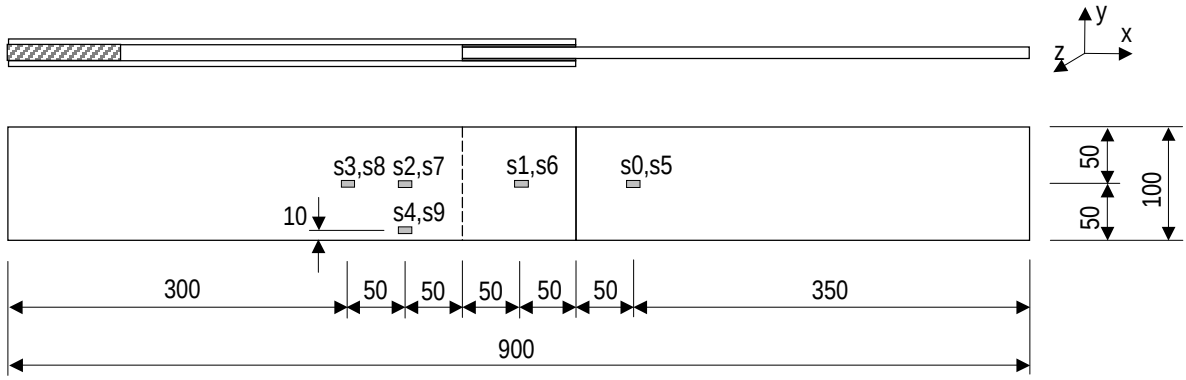

Figure 13 External strain gage positions

Axial strain on bonded overlap

The 1.5/120LY13 has a 1.5mmx1.2mm measuring grid, 6.5mmx4.7mm measuring-grid carrier and an electric resistance of 120 Ω. These gages are referred to as internal gages because they were placed on the bonded area. They were placed on the 10 mm laminate, which was loaded in tension, unlike the 5 mm laminates, which were loaded in flexion due to joint configuration. Their labeling and positions are indicated in Figure 14. There were two position configurations.

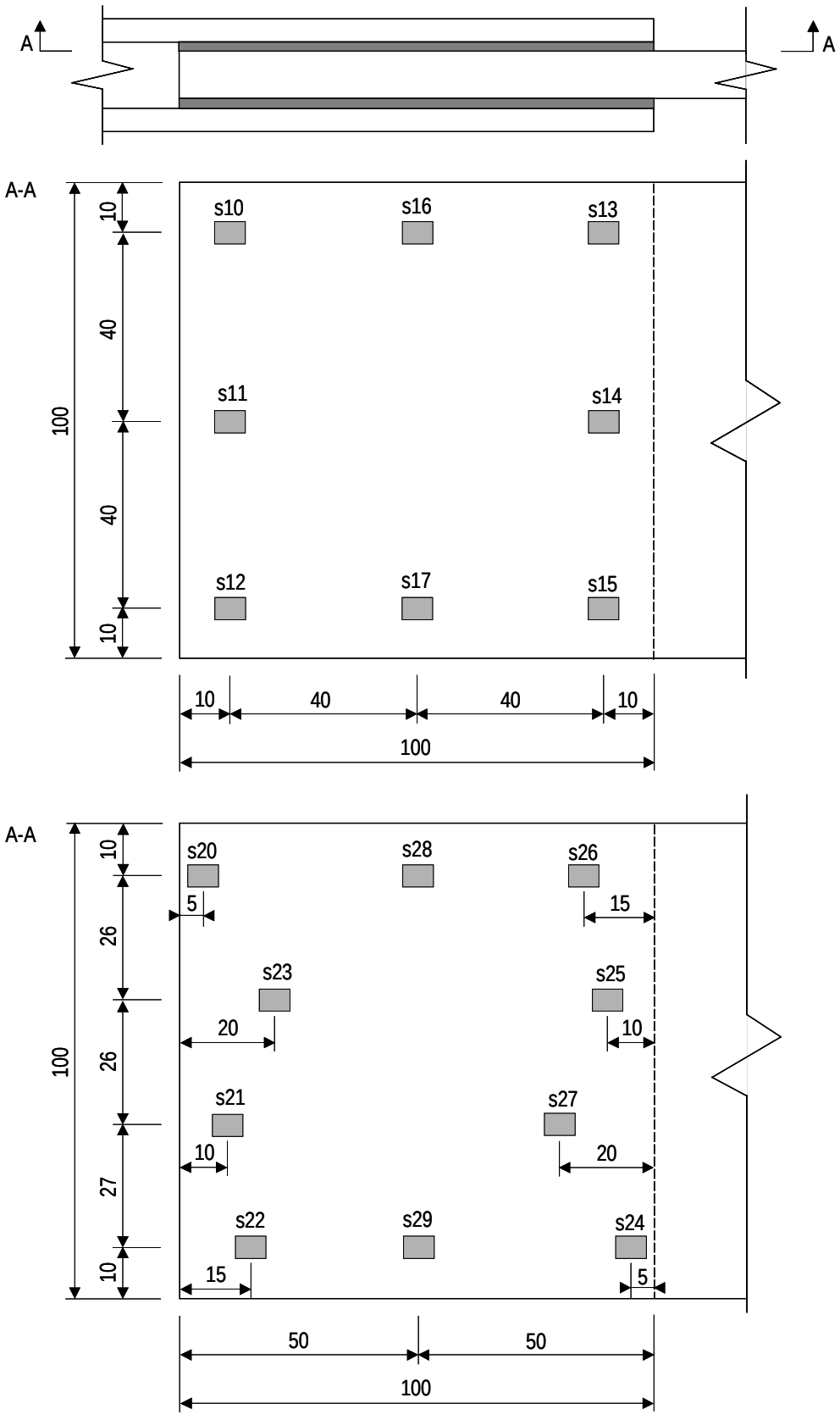

Figure 14 Internal strain gage positions: (a) configuration 1 and (b) configuration 2

Configuration 1 consists of eight gages placed along three sections: the outer (s10-12), middle (s16-17) and inner (s13-15) sections. Their measurements indicated if the strains in the edge and middle of the joint width and the strain on the inner and outer sections were identical. This indicated the 2-dimensional or 3-dimensional effect of the joint. Configuration 2 consists of ten gages (s20-29), placed along nine different sections, giving more accurate information about strain distribution along the overlap length. As strains greatly increase at the ends compared to the middle area of the joint, most of the gages were placed between 5 and 20 mm from the ends. On these two configurations, the gages placed on the middle section of the bonded area indicated any loading eccentricity in direction z.

Test results for joints with and without internal gages were compared, which led to the conclusion that the gages did not affect joint behavior (see 4.1.1, 4.2.1 and 4.3.1).

3.2.2 Displacements Measured with Video-extensometer

The position of fifteen points in the joint area were automatically measured with a video-extensometer every 1 s (Figure 15(a)). The video-extensometer is an image-processing system, intended to determine displacements. The image is digitized by a CCD (Charge Coupled Device)-camera and processed in real time by a PC-supported video processor. The camera-image is digitized in 640x480 discrete pixels whose grey-scales are resolved again in 256 shades. Consequently, the smallest displacement that can theoretically be detected corresponds to 1:100000 of the camera's field of view. For the generated field of view, accuracy was ± 2 μm.

To assure good data acquisition, the selected points must be sufficiently wide, 2-3mm in diameter, and contrasted with the surface. The joint was first painted white, then the selected points were drawn in black. A light spot was used to increase the contrast. Visualization of the spectrum histogram allowed the contrast to be checked (Figure 15(b)).

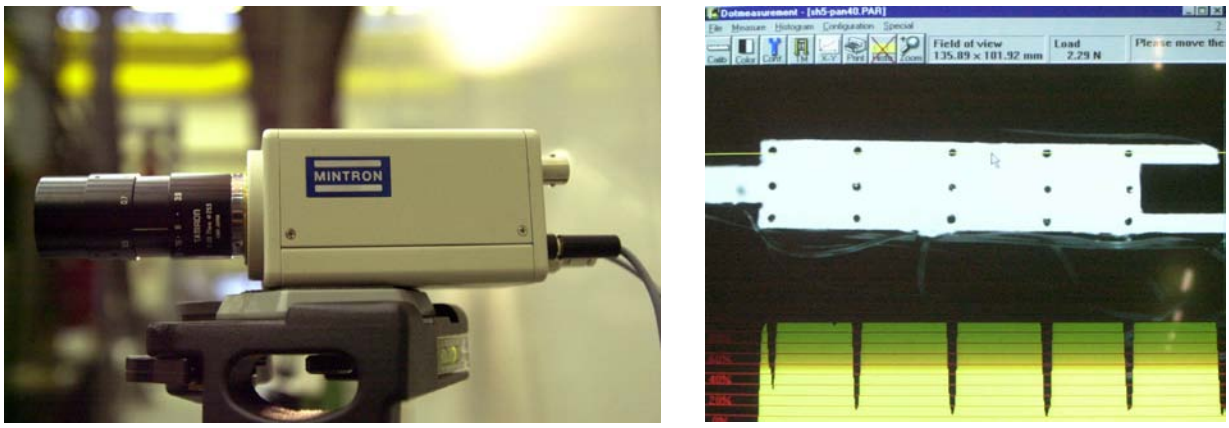

Figure 15 (a) Video-extensometer; (b) PC, running Windows software, generating monitor indicating contrast spectrum histogram

Fifteen points were drawn in the joint area but not all of them were followed by the video-extensometer because of a serious contrast problem (Figure 15(b)). There were five points on each axial

line of the laminates with a distance of 22 or 25 mm between them (Figure 16). Point positions were determined by the video-extensometer, then the displacements in directions x and y were calculated. Thus, joint stiffness was estimated with the relative displacement of the laminates in direction x and through-thickness strain with the relative displacement of the laminates in direction y.

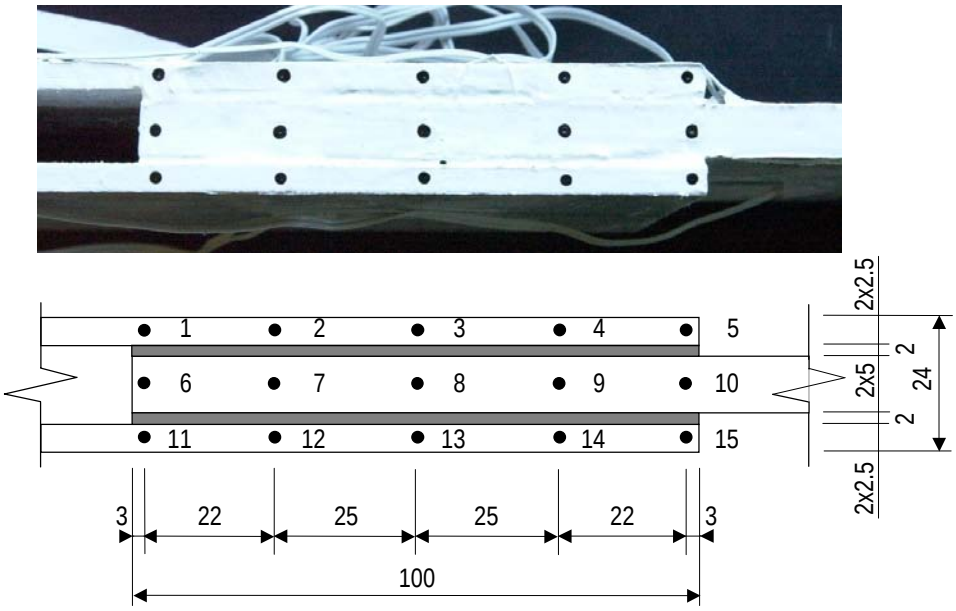

Figure 16 Position of video-extensometer measurement points

Not all specimens were fully instrumented. Table 7 indicates the instrumentation used for each specimen. There are for instance three kinds of EP.A specimens:

- poorly instrumented (1,2,3);
- moderately instrumented (4,5,6);
- fully instrumented (7,8,9) (Figure 17).

Figure 17 Fully-instrumented specimen

Table 7 Specimen series

Series	Specimen	External gage numbers	Internal gage numbers	Video extensometer
EP.A	1,2,3	2 (s0,s2)	-	-
	4,5,6	3 (s0,s2,s7)	10 (configuration 2)	-
	7 ,8	10 (s0-s9)	8 (configuration 1)	×
	9	10 (s0-s9)	8 (configuration 1)	-
	10,11	-	-	-
	12	-	-	×
EP.D	1,2,3	3 (s0,s2,s7)	-	-
PU.A	1,2	3 (s0,s2,s7)	-	-
	3	-	-	-
PU.B	1,2	3 (s0,s2,s7)	-	-
	3	-	-	-
	4,5,6	3 (s0,s2,s7)	-	-
PU.C	1	3 (s0,s2,s7)	-	-
ADP.A	1,2	2 (s0,s2)	-	-
	4	2 (s0,s2)	10 (configuration 2)	-
ADP.B	1.1, 2.1, 3.2, 4.2	-	-	-
	3.1, 4.1, 4.3	2 (s0,s2)	-	-
ADP.C	1,2,3	3 (s0,s2,s7)	-	-
	4,5,6	10 (s0-s9)	10 (configuration 2)	-
	7,8,9	3 (s0,s2,s7)	8 (configuration 1)	×
ADP.D	1,2,3	3 (s0,s2,s7)	-	-
ADP-EP.A	1,2,3	3 (s0,s2,s7)	-	-

Table 8 shows the measurement system's accuracy.

Table 8 Measurements and accuracy

Measurement	Instruments	Number of measurements	Measurement range	Accuracy
Load	load cell of the machine	1	± 1000 kN	± 0.1%
Elongation	displacement cell of the machine	1	± 250 mm	± 0.1%
	video-extensometer	0-15	-	± 2 m
Strain	6/120LY13 HBM gages	0-3-10	± 5%	± 2 m
	1.5/120LY13 HBM gages	0-6-10	± 5%	± 2 m

3.2.3 Potentially Measurement Systems

Joint behavior can also be analyzed with optical fiber sensors or speckle interferometry but these techniques are not suitable for this experimental study as explained below.

Optical fiber sensors measure strain locally with high resolution and accuracy. Traditional optical sensors measure the strain in one location, so there are as many sensors as defined locations. The Fiber-optic Bragg (FBG) sensor developed by Hill et al. in 1978 has the advantage of measuring strains in different locations with only one single optical fiber (Haung et al. 1998, Masskant et al. 1997); this technique is called "multiplexing" measurement. Since FBG optical fiber's diameter is relatively small (≈250μm) compared to adhesive thickness, they could be embedded in the adhesive layer and certainly do not influence the joint's mechanical properties. This assumption must however be verified, according to Abbott and Scott (2002). They suggested including the embedded sensor in the FEM model developed for joint analysis to optimize its placement. Thus the critical positions where the embedded sensor significantly reduces load capacity are avoided. Despite these advantages, FBG sensors are too expensive for this kind of experimental study. They are nonetheless suitable in real structures as monitoring sensors to provide strain data and damage detection under service conditions (Lau et al. 2001).

The speckle interferometry (ESPI: Electronic Speckle pattern Interferometry) measures the surface displacements (Jones and Wykes 1983). It is commonly used to determine deformations and the loss of strength and to detect the debonded areas and the crack propagation in joints (Asundi 1987, Bassetti 2001). The surface roughness lighted up with a coherent light as a laser produce interference phenomenon when the surface roughness is the same or higher than the wave length. The phenomenon varies the light intensity leading to speckles. The displacements are determined comparing the surface at the reference state with the one at the loading state. Interferometry measurements could be carried out in collaboration with NAM Laboratory (Laboratoire de nanophotonique et métrologie) in the EFPL. No experiments have been performed using this technology due to experienced technicians need.

4 Results

4.1 Epoxy Adhesive

4.1.1 Load-Displacement Relationship

Detailed data concerning test series EP.A (l=100 mm) and EP.D (l=200 mm) are given in Appendix 7.1 and 7.2 respectively. The global load-elongation curves of series EP.A (blue) and EP.D (green) are represented in Figure 18. Tables 9 and 10 summarize the ultimate load, F_u, and the ultimate displacement, u_u, of specimens EP.A and EP.D respectively. They also include the corresponding ultimate average shear stress, τ_u, joint efficiency, J_{eff}, average values and standard deviations. The average shear stress is calculated by dividing the load by the two bonded areas. Joint efficiency is defined as the ratio of joint ultimate load to laminate ultimate load (Sotiropoulos et al. 1994). The latter is 332 kN and corresponds to the 10 mm laminate strength, which is lower than the 5 mm laminate, 2x215 kN (see Table 3). The average values and standard deviations did not take into account specimen EP.A7, due to its premature failure caused by bad handling, and specimens EP.A10,12, due to their higher stiffness compared to the others.

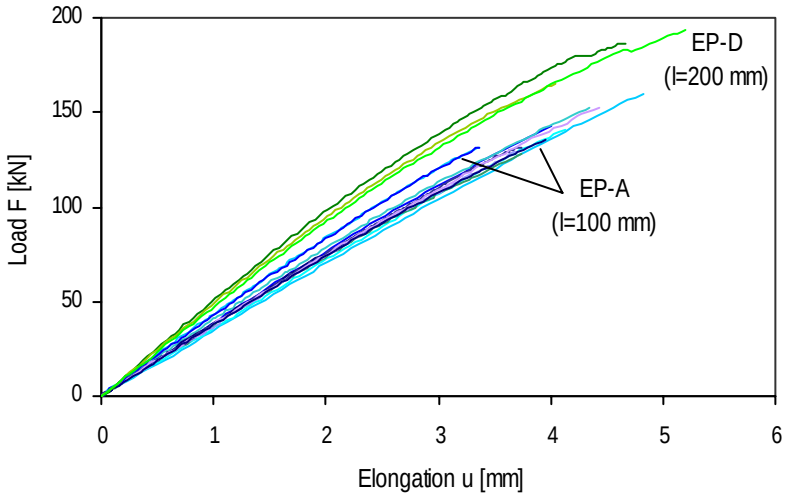

Figure 18 Load-elongation curves for series EP.A (blue) and EP.D (green)

Load-elongation curves for specimens EP.A were identical except for specimens EP.A10,12, which exhibited higher stiffness. Behavior was linear up to approximately 40 and 60 kN (approximately 35% of failure load). At this load level, a slight decrease in global stiffness was observed. The stiffness decrease coincided with the beginning of noise emissions. The average failure load was 141 kN and average global elongation was 4.1 mm. The ultimate average shear stress was 7.1 MPa. Average joint efficiency was 0.43.

Load-elongation curves for specimens EP.D were similar to those for specimens EP.A. Behavior was linear up to approximately 60 and 80 kN (approximately 40% of failure load). At this load level, as for specimens EP.A, a slight decrease in global stiffness was observed coinciding with noise emissions. The

average failure load was 182 kN, 28% higher than for specimens EP.A, and average global elongation was 4.6 mm. The ultimate average shear stress was 4.5 MPa, which is 37% lower than that corresponding to specimens EP.A (7.1 MPa). Average joint efficiency was 0.55.

Joint efficiency varied nonlinearly with overlap length. Doubling overlap length induced a joint efficiency increase of 29%. This is related to the well-known non-uniform shear stress distribution in bonded joints (Adams et al. 1997).

Table 9 Test results for series EP.A

Specimen	F_u [kN]	u_u [mm]	J_{eff} [-]	τ_u [MPa]
EP.A1	143	4.0	0.43	7.1
EP.A2	160	4.8	0.48	8.0
EP.A3	141	4.1	0.42	7.0
EP.A4	152	4.4	0.46	7.6
EP.A5	128	3.7	0.38	6.4
EP.A6	130	3.7	0.39	6.5
EP.A7	*93*	*2.5*	*0.28*	*4.7*
EP.A8	132	3.7	0.40	6.6
EP.A9	153	4.4	0.46	7.7
EP.A10	*132*	*3.4*	*0.40*	*6.6*
EP.A11	135	4.0	0.41	6.8
EP.A12	*132*	*3.4*	*0.40*	*6.6*
m	141	4.1	0.43	7.1
s	11	0.4	0.03	0.6

Table 10 Test results for series EP.D

Specimen	F_u [kN]	u_u [mm]	J_{eff} [-]	τ_u [MPa]
EP.D1	187	4.7	0.56	4.7
EP.D2	165	4.1	0.50	4.1
EP.D3	194	5.2	0.58	4.8
m	182	4.7	0.55	4.5
s	15	0.6	0.04	0.4

Test results for specimens EP.A4-9 with internal gages and specimens EP.A1-3 and EP.A10-12 without internal gages were compared in order to check the influence of gages. Load-elongation curves and failure loads are similar in both cases; thus gages did not affect joint behavior and load transfer. Strains measured with the internal gages are considered as the strain existing in a non-instrumented joint.

4.1.2 Failure Modes

Failure of specimens EP.A and EP.D occurred in the 5 and 10 mm laminates between the two outer fiber layers or inside one layer of mat. More precisely it took place between the mat and roving layers

of the 5 mm laminates and between the two mats or inside the first mat of the 10 mm laminates (Figure 19). Figures 51 and 52 (Appendix 7.1) and Figure 62 (Appendix 7.2) show the failure mode of EP.A and EP.D series respectively. According to the failure mode classification described in ASTM D 5573-94, it was a "fiber-tear failure" but it is traditionally called interlaminar adherend failure. It is a common failure mode of composite material joints due to the weak transversal properties of composites, mainly influenced by matrix properties (Hart-Smith 1987). It could be caused by in-plane through-thickness shear and/or through-thickness tension (through-thickness). Failures occurred in a brittle manner without the previous appearance of cracks in joint area. Because of the brittle failure and large dissipation of energy leading to extensive secondary damage, it is difficult to define where failure really started. In order to investigate the crack initiation and failure process, Vallée (2004) carried out similar EP specimen tests involving a high-speed camera. He concluded that failure seems to be initiated in the inner laminate, the 10 mm laminate, and demonstrated that the cracks in the 5 mm laminate occurred due to dynamic effects. This assumption tallies with FEA model predictions (de Castro 2005 b) and Hart-Smith's fracture description (Hart-Smith 1987) (Figure 20). The main failure surfaces are inside the 10 mm laminates at approximately 0.5 mm depth. Depth varies slightly due to variability of fiber layer position (Figure 5(b)).

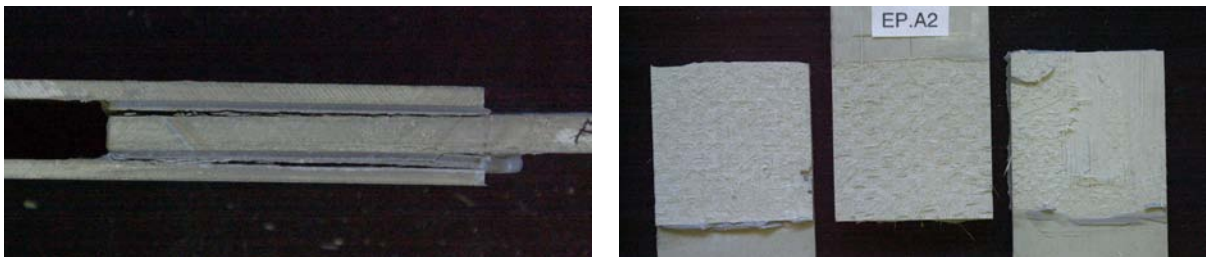

Figure 19 Failure mode of specimen EP.A4

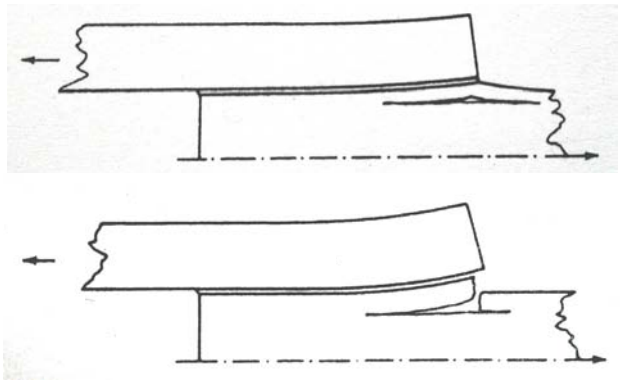

Figure 20 Interlaminar failure modes (Hart-Smith 1987)

4.1.3 Load-Strain Relationship on Laminates

Figure 21(a) represents the load-strain curves of the external strain gages placed on specimen EP.A9. Comparison of s0-s4 gage measurements with s5-s9 gage measurements indicates that there is no

loading eccentricity in direction y (Figure 21(b)). The initial slope varies due to initial torsion when closing testing machine jaws. Comparison of s2/s7 gage measurements with s4/s9 gage measurements indicates that there is no loading eccentricity in direction z. Specimens EP.A7-8 showed similar results (Appendix 7.1). Table 11 summarizes the measured strains on several locations of specimens EP.A7-9 at 50 kN.

Table 30 in Appendix 7.1 indicates the Young's modulus of the 5 mm and 10 mm thick laminates estimated with strain measurements from gages s2/s7 and s0/s5 respectively. Average values are 32950 MPa and 26160 MPa for the 5 mm and 10 mm thick laminates respectively. These mechanical properties will be introduced in the developed FEA model (de Castro 2005 b, Chapter 5). It is important to note that both laminates were loaded in tension but the 5 mm thick laminates were also subjected to bending. The FEA model demonstrates that strains at gage locations were slightly influenced by bending, the calculated strain being 3% lower than that assuming only tension. Thus the Young's modulus of the 5 mm thick laminates is slightly overestimated.

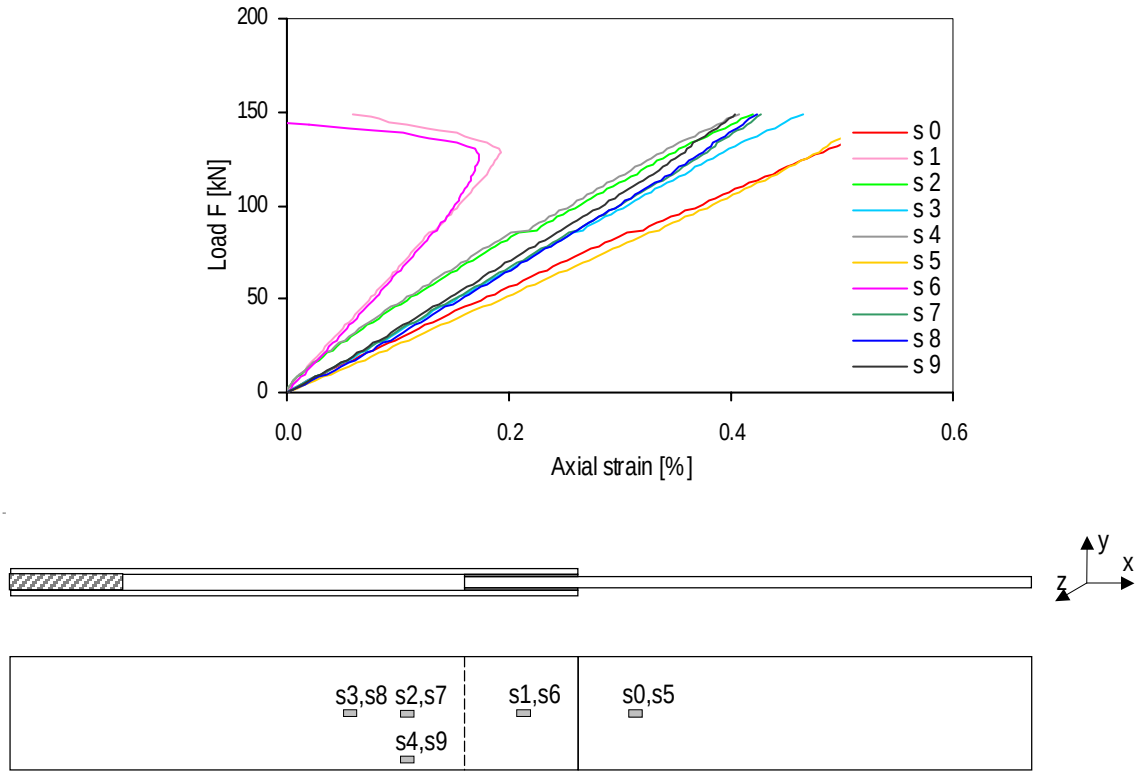

Figure 21 (a) Load-strain curves of external gages in specimen EP.A9; (b) Gage positions

Table 11 Measured strains [%] for specimens EP.A7-9 at 50 kN

	s0	s5	s1	s6	s2	s7	s4	s9	s3	s8
EP.A7	0.143	0.169	0.077	0.070	0.178	0.170	0.144	0.139	0.161	0.149
EP.A8	0.170	0.209	0.070	0.064	0.144	0.142	0.139	0.126	0.142	0.135
EP.A9	0.177	0.194	0.075	0.079	0.139	0.135	0.151	0.145	0.151	0.145

4.1.4 Strain Distribution on the Overlap

The data are presented in Appendix 7.1.

Configuration 1

Load-strain curves for specimens are presented in Appendix 7.1. Figure 22 represents axial strain distribution across the joint width of specimens EP.A7-9 in two different sections, the outer (s10-s12) and inner (s13-s15) (Figure 14) at 50 kN. Strains in the edge were usually higher than those in the middle of the joint width; in one case deviations reached 25 to 50% of the value in the middle. Non-uniform load transfer across the width is in agreement with Richardson et al. (1993).

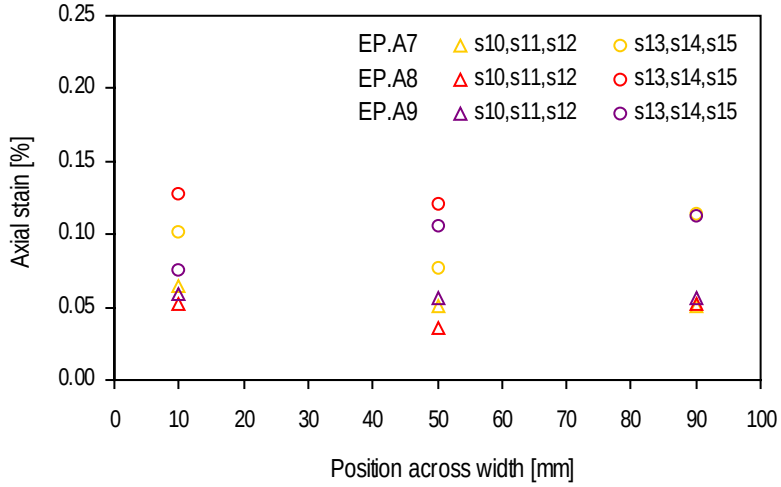

Figure 22 Axial strain distribution across width for specimens EP.A7-9 at 50 kN

Configuration 2

In configuration 2, ten gages are placed on nine different sections in order to measure strain distribution along overlap length. Load-strain curves for specimens EP.A4-6 are presented in Appendix 71.

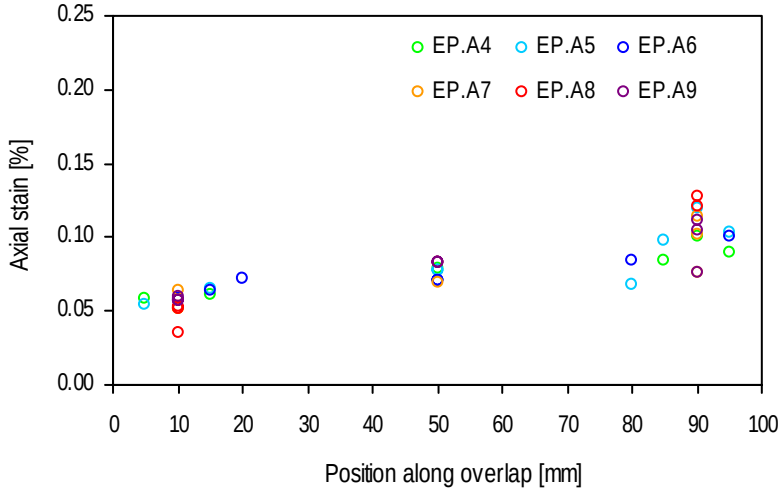

Figure 23 Axial strain distribution along overlap length of specimens EP.A4-9 at 50 kN

Figure 23 shows axial strain distribution along overlap length of specimens EP.A4-6 (config. 2) and specimens EP.A7-9 (config. 1) at 50 kN. Axial strain distribution in specimens EP.A4-9 exhibited a sharp slope at the ends of the overlap, between 0 and 10 mm from the edges, which signifies large load transfer in these lengths. Thus, the rest of the overlap length did not really contribute to the transfer.

4.1.5 Joint Elongation

Fifteen point positions were measured by the video-extensometer, then the elongations in directions x and y could be determined (Figure 24). Elongations in direction y were on almost the same scale as video-extensometer accuracy for the selected field of view (± 2 μm). So, no indication concerning through-thickness strain was obtained. However, it is important to note for future work that reduction of the camera's field of view will increase accuracy. In this way, elongations in direction y could probably be measured.

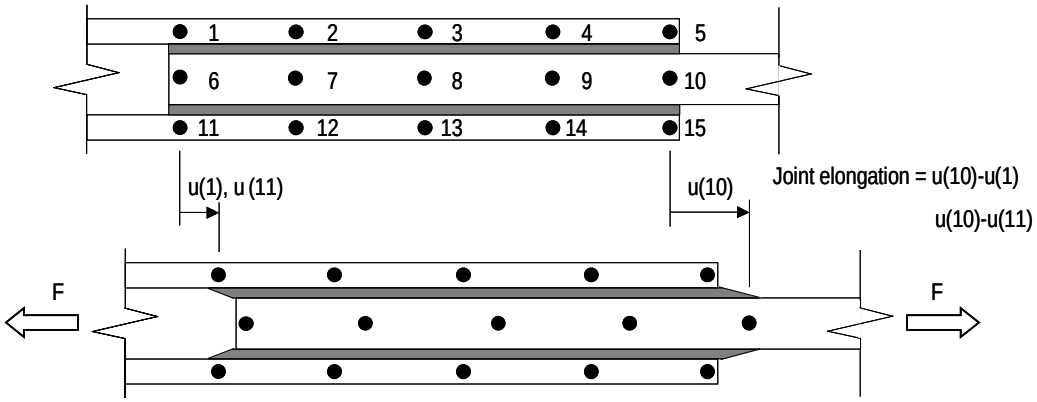

Figure 24 Joint elongation

Figure 25 shows the raw data for specimen EP.A8. The raw data are interpolated with a straight line. The processed data for specimens EP.A7,8,12 are presented in Appendix 7.1. Table 12 resumes the measured elongations of specimens EP.A7,8,12 at 50 kN.

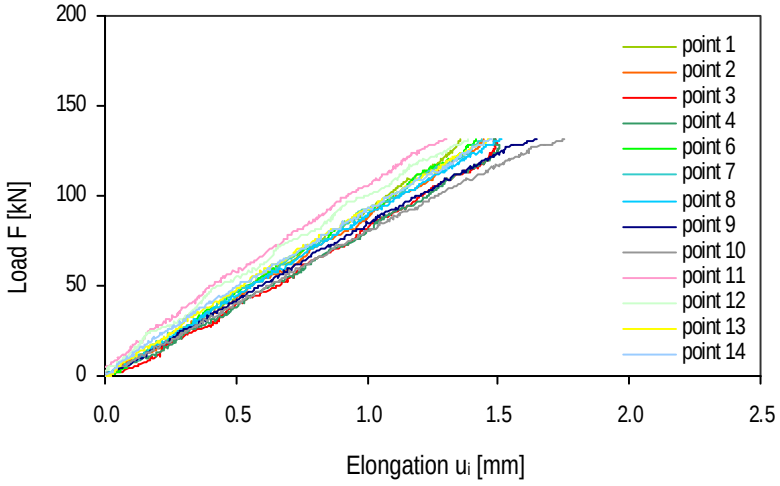

Figure 25 Load-elongation curves in the joint, u_i, for specimen EP.A8

Joint elongation and stiffness are estimated from the relative elongation of the laminates in direction x. They are calculated with positioning of points 1, 10 and 11 as indicated in Figure 24. Figure 26 shows joint elongation, u_j, and global elongation, u, of specimens EP.A7,8,12. Figure 27 includes the joint stiffness, ratio of joint elongation to global elongation and ratio of laminate elongation to global elongation of specimen EP.A8. Table 13 summarizes joint stiffness and the ratio of joint elongation to global elongation of specimens EP.A7,8,12.

Table 12 Measured elongations [mm] for specimens EP.A7,8,12 at 50 kN

	1	11	2	12	3	13	4	14	5	15
EP.A7	-	0.586	0.607	0.604	-	0.623	0.644	-	0.655	-
EP.A8	0.528	0.527	0.556	0.556	0.580	0.552	0.595	0.572	-	-
EP.A12	0.530	0.519	0.558	0.544	-	0.566	0.591	0.567	0.594	0.586

	6	7	8	9	10
EP.A7	-	0.617	0.632	0.659	0.692
EP.A8	0.545	0.549	0.563	0.593	0.633
EP.A12	0.548	0.555	0.576	0.607	0.631

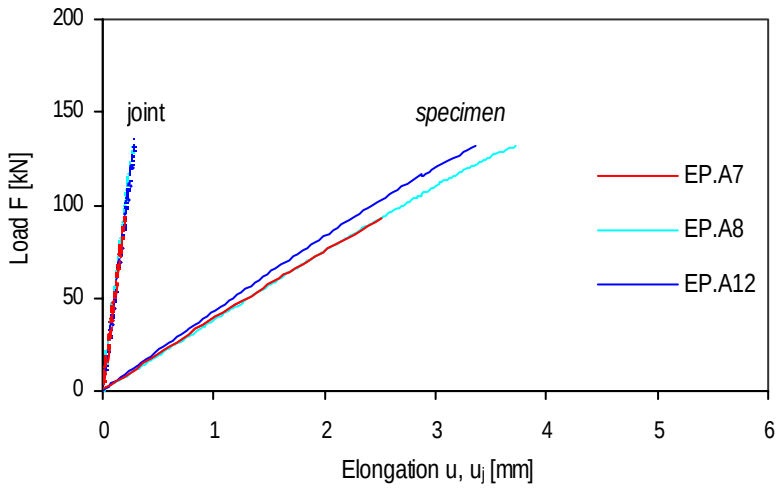

Figure 26 Load-elongation curves of joint, u_j, and global specimen, u, of specimens EP.A7,8,12

Table 13 Joint stiffness and ratio of joint elongation to global elongation of specimens EP.A 7,8,12

Specimen	Joint stiffness (kN/mm)	u_j/u (%)
EP.A7	470	8
EP.A8	475	8
EP.A12	478	9

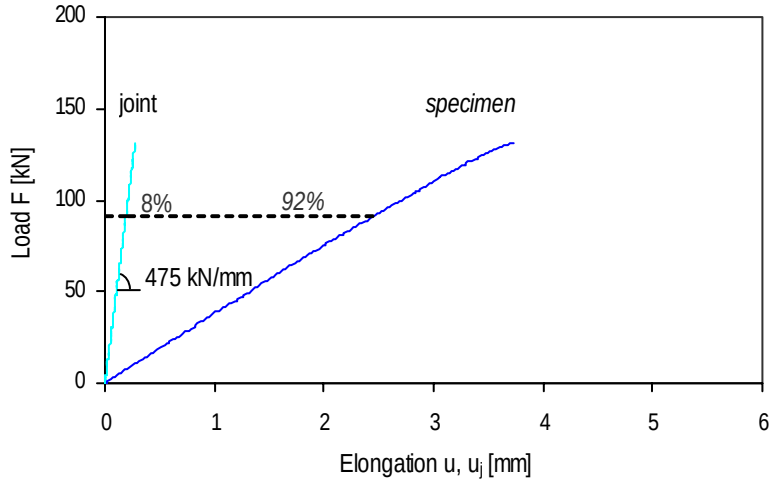

Figure 27 Load-elongation curve of joint, u_j, and global specimen, u, of specimen EP.A8

4.2 Polyurethane Adhesive

4.2.1 Load-Elongation Relationship

Detailed data concerning test series PU.A-C are presented in Appendixes A.3-5 respectively. The global load-elongation curves of specimens PU.A (orange), PU.B (green) and PU.C (red) are represented in Figure 28. Tables 14-16 summarize the ultimate load, F_u, and the ultimate elongation, u_u, of specimens PU.A-C respectively. They also include the corresponding ultimate average shear stress, τ_u, joint efficiency, J_{eff}, average values and standard deviations. Specimens PU.A3 and PU.B6 were not taken into account in average values and standard deviations due to premature failure and inappropriate surface treatment respectively (see 4.2.2).

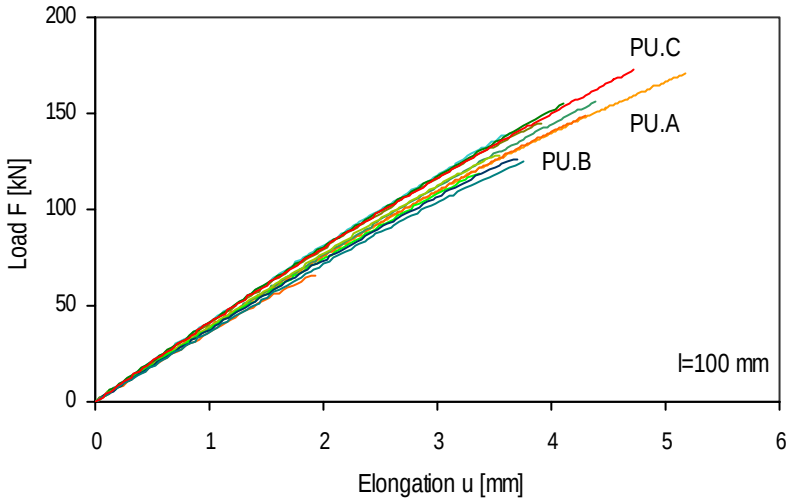

Figure 28 Load-elongation curves for series PU.A (orange), PU.B (green), PU.C (red)

The load-elongation curves for PU specimens were identical but ultimate loads were widely scattered due to the adhesion failure mode (see 4.2.2). Behavior was linear up to approximately 60 and 80 kN (approximately 40-50% of failure load). At this load level, a slight decrease in global stiffness was observed, coinciding with the beginning of noise emissions. Average failure loads were 160 kN and 140 kN and average global elongations 4.8 mm and 3.9 mm for series PU.A and PU.B respectively. The corresponding ultimate average shear stresses were 8.0 and 7.0 MPa.

Specimen PU.C1 reached a higher ultimate load than the other joint series. The applied surface treatment (primer 1) seems the most appropriate for the PU adhesive and GFRP adherends but no conclusion could be drawn with only one specimen. Failure load was 173 kN, corresponding global elongation was 4.6 mm and ultimate shear stress was 8.7 MPa.

Average joint efficiency of series PU.A, PU.B and PU.C was 0.48, 0.41 and 0.52 respectively.

Table 14 Test results for series PU.A

Specimen	F_u [kN]	u_u [mm]	J_{eff} [-]	τ_u [MPa]
PU.A1	171	5.2	0.52	8.6
PU.A2	149	4.3	0.45	7.5
PU.A3	*66*	*1.9*	*0.20*	*3.3*
m	160	4.8	0.48	8.0
s	16	0.6	0.05	0.8

Table 15 Test results for series PU.B

Specimen	F_u [kN]	u_u [mm]	J_{eff} [-]	τ_u [MPa]
PU.B1	157	4.4	0.47	7.9
PU.B2	129	3.6	0.39	6.5
PU.B3	145	3.9	0.44	7.3
PU.B4	141	3.7	0.42	7.1
PU.B5	155	4.1	0.47	7.8
PU.B6	*119*	*3.4*	*0.36*	*6.0*
PU.B7	126	3.7	0.38	6.3
PU.B8	125	3.8	0.38	6.3
m	140	3.9	0.42	7.0
s	13	0.3	0.04	0.7

Table 16 Test results for series PU.C

Specimen	F_u [kN]	u_u [mm]	J_{eff} [-]	τ_u [MPa]
PU.C1	173	4.6	0.52	8.7

4.2.2 Failure Modes

Figures 58, 63 and 65 (Appendix 7.3-5) show the failure mode of series PU.A-C respectively. Specimens PU.A1-3 and PU.C1 exhibited a combination of adhesive failure and interlaminar adherend failure (Figure 29(a)). According to the failure mode classification described in ASTM D 5573-94, it was a "mixed failure" combining an "adhesion promoter to substrate failure" and a "light-fiber-tear failure". The light-fiber-tear failure occurred in the laminate, near the surface. The adhesion promoter to substrate failure occurred in the interface between primer and activator layers in specimens PU.A and between primer and laminate in specimen PU.C1(surface treatment without activator). The adhesive failure revealed inappropriate surface treatment and is not usually accepted in adhesive technology (Hutchinson 1999).

Specimens PU.B1-5 and PU.B8 exhibited "light-fiber-tear failure" (Figure 29(b)). Specimens PU.B3,5 showed a large void at one edge point of insufficient application of adhesive (Figure 29(c)). Specimens PU.B.6,7 exhibited a "mixed failure" combining "adhesive failure", between adhesive and laminate, and "light-fiber-tear failure". The adhesive failure extended to two thirds of one bonded area of specimen PU.B6 (Figure 29(d)). Visual control of laminates surfaces revealed they were not sanded, which might explain the large adhesion failure areas. The average failure load and elongation values in Table 15 do not take into account specimen PU.B6. Adhesion failure was mainly observed around the gage locations in specimen PU.B7. The adhesive used for gage installation probably extended beyond the edges.

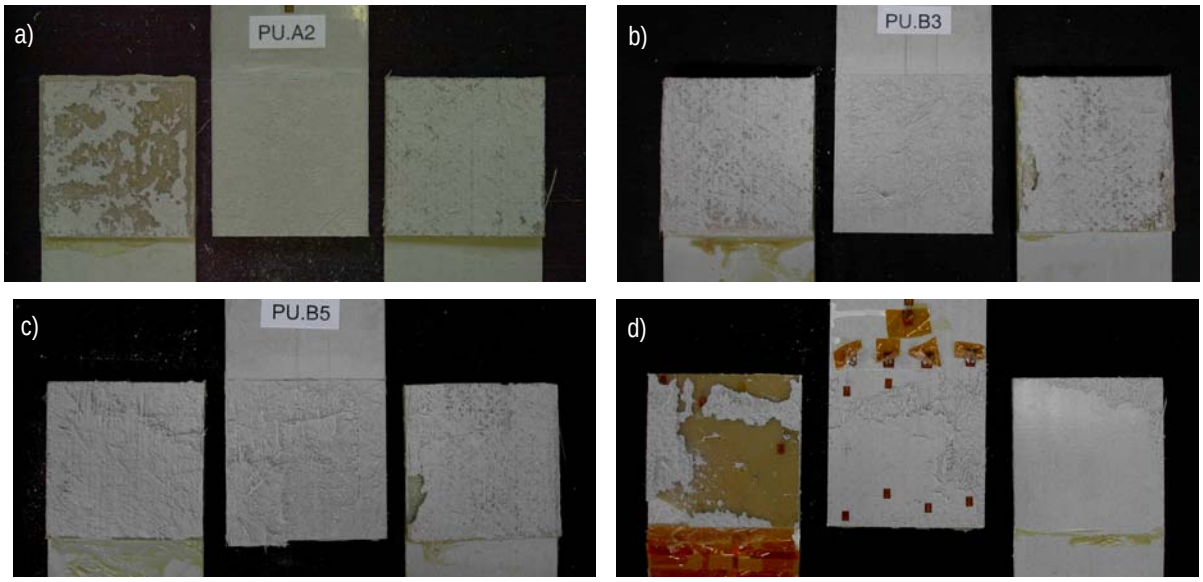

Figure 29 Failure modes of specimens (a) PU.A2, (b) PU.B3, (c) PU.B5, (d) PU.B6

4.2.3 Load-Strain Relationship on Laminates

Data are presented in Appendix 7.4. Comparison of gage s2/s7 measurements indicates that there is no large loading eccentricity in direction y. The initial slope varies due to initial torsion when closing testing-machine jaws.

Table 31 in Appendix 7.4 indicates the Young's modulus of the 5 mm and 10 mm laminates estimated with strain measurements from gages s2/s7 and s0/s5 respectively. Average values are 32130 MPa and 28260 MPa for the 5 mm and 10 mm laminates respectively. These mechanical properties will be introduced in the developed FEA model (de Castro 2005 b, Chapter 5). As for specimens EP.A, it is important to note that both laminates were loaded in tension but the 5 mm thick laminates were also subjected to bending. The FEA model demonstrates that strains at gage locations were slightly influenced by bending, the calculated strain being 3% lower than that assuming only tension. Thus the Young's modulus of the 5 mm thick laminates is slightly overestimated. Table 17 summarizes the measured strains of specimens PU.B6-8 at 50 kN.

Table 17 Measured strains [%] for specimens PU.B6-8 at 50 kN

	s0	s2	s7
PU.B6	0.182	0.162	0.150
PU.B7	0.171	0.160	0.145
PU.B8	0.191	0.172	0.172

4.2.4 Strain Distribution on the Overlap

Configuration 2

Data are presented in Appendix 7.4. Ten gages are placed on nine different sections in order to describe strain distribution along overlap length. Load-strain curves of specimens PU.B6-8 are presented in Appendix 7.4. Figure 30 shows the axial strain distribution of these specimens along the overlap length. Axial strain distribution in specimens PU.B6-8 exhibited an important slope at the ends of the overlap, between 0 and 10 mm from the edges, which signifies an important load transfer in these lengths. The slope in the rest of the overlap remained quite constant.

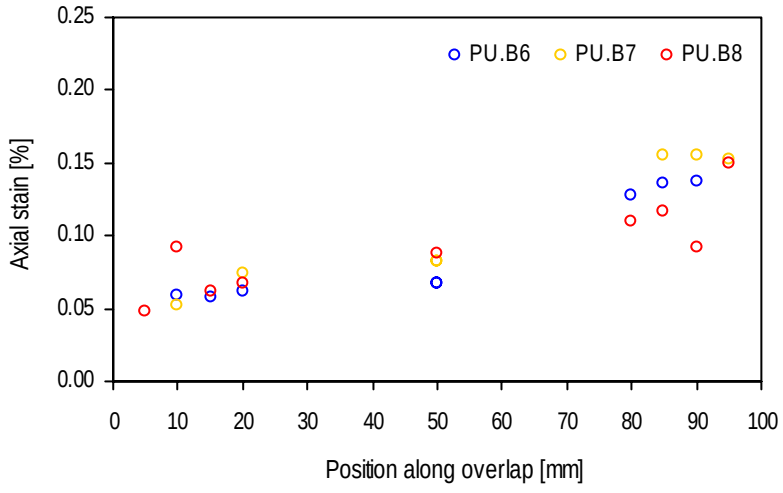

Figure 30 Axial strain distribution along overlap length of specimens PU.B6-8 at 50 kN

4.2.5 Joint Elongation

Figure 31 shows the raw data for specimen PU.B7. Raw data are interpolated with a straight line as for series EP.A. The processed data for specimens PU.B6-8 are presented in Appendix 7.4. Table 18 resumes the measured elongations of specimens PU.B6-8. As for series EP.A, joint displacement and joint stiffness are estimated from the relative displacement of the laminates in direction x (Figure 24). Figure 32 shows joint elongation, u_j, and global elongation, u, of specimens PU.B6-8. Figure 33 includes the joint stiffness, ratio of joint elongation to global elongation and ratio of laminate elongation to global elongation for specimen PU.B7. Table 19 summarizes joint stiffness and the ratio of joint elongation to global elongation of specimens PU.B6-8.

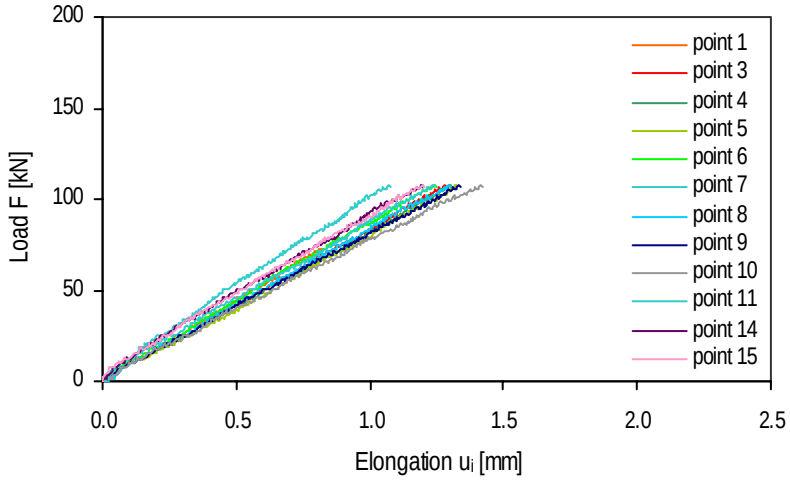

Figure 31 Load-elongation curves in the joint, u_i, for specimen PU.B7

Table 18 Measured elongations [mm] for specimens PU.B6-8 at 50 kN

	1	11	2	12	3	13	4	14	5	15
PU.B6	0.584	0.541	0.619	0.574	0.648	0.607	-	0.611	0.680	0.639
PU.B7	0.560	0.505	-	-	0.596	-	0.606	0.569	0.624	0.570
PU.B8	-	0.504	0.594	0.596	0.611	0.617	0.642	0.631	0.643	0.644

	6	7	8	9	10
PU.B6	0.623	0.628	0.643	0.669	0.689
PU.B7	0.566	0.556	0.597	0.625	0.658
PU.B8	0.619	0.618	0.634	0.665	0.699

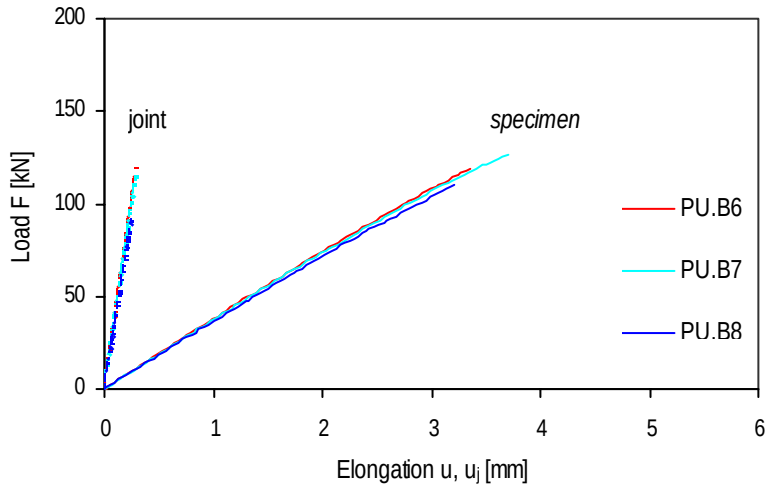

Figure 32 Load-elongation curves for joint, u_j, and global specimen, u, of specimens PU.B6-8

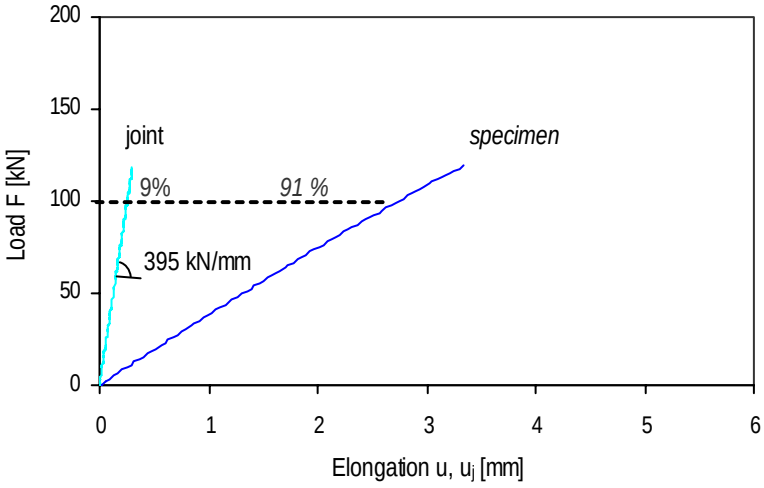

Figure 33 Load-displacement curve of joint, u_j, and global specimen, u, of specimen PU.B7

Table 19 Joint stiffness and ratio of joint elongation to global elongation of specimens PU.B6-8

Specimen	Stiffness (kN/mm)	u_j/u (%)
PU.B6	400	9
PU.B7	395	9
PU.B8	360	10

4.3 ADP Adhesive

4.3.1 Load-Displacement Relationship

Detailed data concerning test series ADP.A-D are given in Appendixes A.6-9. The global load-elongation curves for specimens ADP.A-D are represented in Figures 34(a)-(d). All are represented in Figure 35. Tables 20-23 summarize the ultimate load, F_u, and ultimate elongation, u_u, of specimens ADP.A-D respectively. They also include, except Table 21, the corresponding ultimate average shear stress, τ_u, joint efficiency, J_{eff}, average values and standard deviations. Table 21 does not contain these average values because series ADP.B includes specimens with different surface treatments.

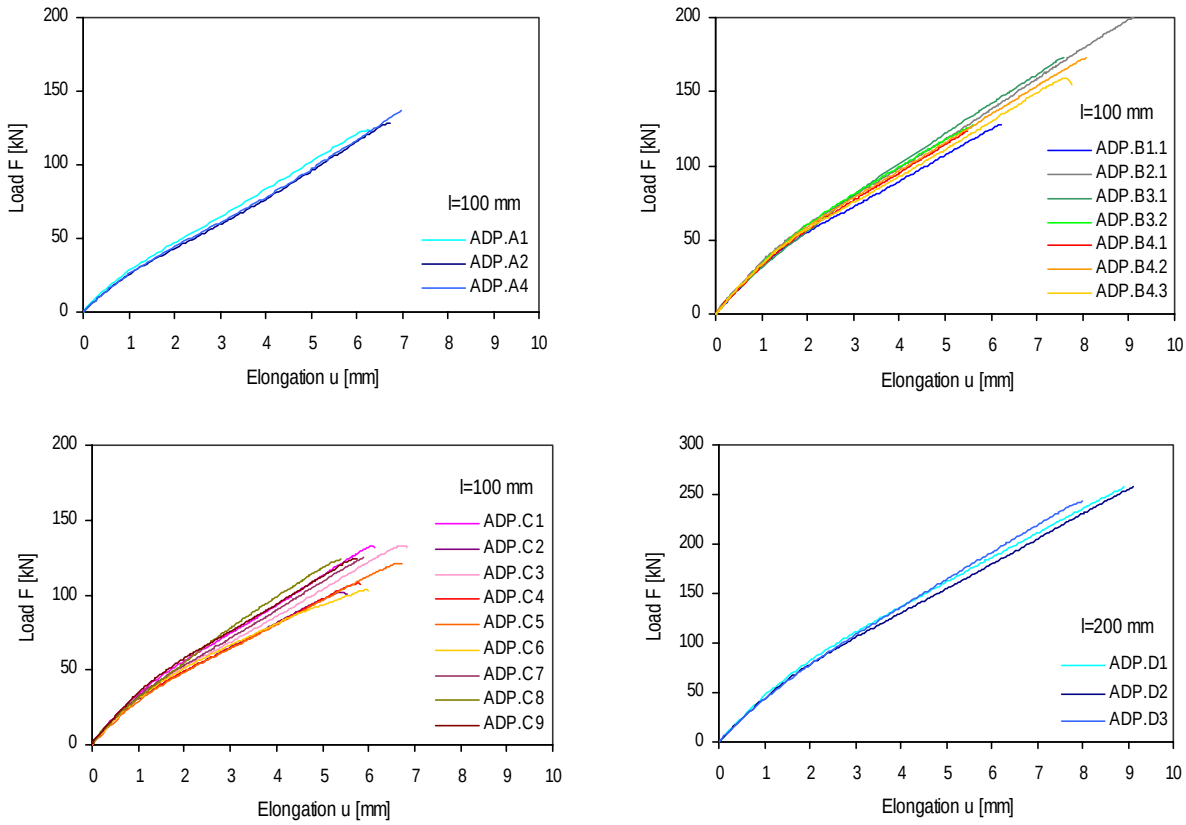

Figure 34 Load-elongation curves for series (a) ADP.A, (b) ADP.B, (c) ADP.C, (d) ADP.D

The load-elongation curves for specimens ADP.A-C were similar but their ultimate loads were widely scattered due to adhesion failure mode (see 4.3.2). The specimens showed bilinear behavior. Global stiffness changed at 20 and 30 kN (approximately 20% of failure load) for series ADP.A and 25 kN and 45 kN (approximately 30% of failure load) for series ADP.C. At this load level a decrease in global stiffness was observed as it was for the ADP adhesive (Figure 9). Series ADP.A was initially softer than series ADP.C. This may be due to the different curing time (series ADP.A, 1 week, series ADP.C, 5

weeks). Nevertheless the ADP adhesive is fast-curing and should not be affected by this parameter. Average failure loads were 130 kN and 119 kN and average global elongations 6.7 mm and 6.0 mm for series ADP.A and ADP.C respectively. Average joint efficiency of series ADP.A and ADP.C was 0.39 and 0.36 respectively, while average global elongations increased by 63% and 46% respectively.

Series ADP.B includes specimens with different surface treatments. Specimen ADP.B2.1 reached a higher strength than the others and exhibited higher global stiffness. The applied surface treatment (primer 1) seems the most appropriate for the ADP adhesive and GFRP adherends but no conclusion could be drawn with only one specimen. Failure load was 202 kN and global elongation 9.2 mm. Joint efficiency was 0.61.The corresponding ultimate shear stress was 10.1 MPa. Global stiffness changed at 40 kN (approximately 20% of failure load).

Load-elongation curves for specimens ADP.D were identical and similar to those of series ADP.A-C. Behavior was bilinear and global stiffness changed at 60 and 80 kN (approximately 30% of failure load). At this load level, as for series ADP.A-C, a decrease in global stiffness was observed as it was for the ADP adhesive (Figure 9). The average failure load was 253 kN and average global elongation 8.7 mm. Unlike the other ADP series, failure loads were narrow scattered. Ultimate average shear stress was 6.3 MPa, 5% higher than that corresponding to series ADP.C (6.0 MPa). Average joint efficiency was 0.76.

Using the ADP adhesive, joint efficiency varied almost linearly with overlap length. Doubling overlap length induces a joint efficiency increase of 110%. This value is higher than 100% because of the adhesion failure mode. A fiber-tear failure, as for specimens with the EP adhesive, will result in 100% at the most, assuming constant shear distribution along overlap and small through-thickness stresses at joint edges.

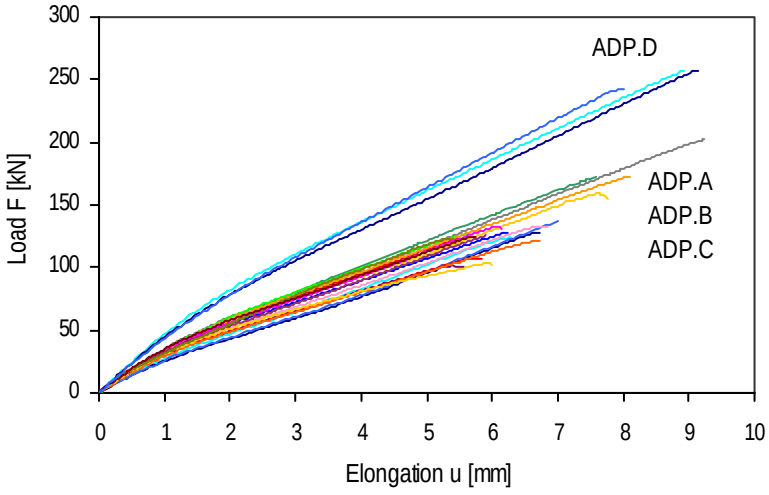

Figure 35 Load-elongation curves for series ADP

Table 20 Test results for series ADP.A

Specimen	F_u [kN]	u_u [mm]	J_{eff} [-]	τ_u [MPa]
ADP.A1	124	6.3	0.37	6.2
ADP.A2	128	6.7	0.39	6.4
ADP.A4	137	7.0	0.41	6.9
m	130	6.7	0.39	6.5
s	7	0.4	0.02	0.3

Table 21 Test results for series ADP.B

Specimen	F_u [kN]	u_u [mm]	J_{eff} [-]	τ_u [MPa]
ADP.B1.1	64	2.4	0.19	3.2
ADP.B2.1	202	9.2	0.61	10.1
ADP.B3.1	173	7.6	0.52	8.7
ADP.B3.2	127	5.6	0.38	6.4
ADP.B4.1	130	5.9	0.39	6.5
ADP.B4.2	173	8.1	0.52	8.7
ADP.B4.3	159	7.8	0.48	8.0

Table 22 Test results for series ADP.C

Specimen	F_u [kN]	u_u [mm]	J_{eff} [-]	τ_u [MPa]
ADP.C1	132	6.1	0.40	6.6
ADP.C2	100	5.6	0.30	5.0
ADP.C3	133	6.9	0.40	6.7
ADP.C4	108	5.8	0.33	5.4
ADP.C5	121	6.7	0.36	6.1
ADP.C6	103	6.0	0.31	5.2
ADP.C7	127	6.1	0.38	6.4
ADP.C8	124	5.4	0.37	6.2
ADP.C9	124	5.8	0.37	6.2
m	119	6.0	0.36	6.0
s	12	0.5	0.04	0.6

Table 23 Test results for series ADP.D

Specimen	F_u [kN]	u_u [mm]	J_{eff} [-]	τ_u [MPa]
ADP.D1	257	8.9	0.77	6.4
ADP.D2	258	9.1	0.78	6.5
ADP.D3	243	8.0	0.73	6.1
m	253	8.7	0.76	6.3
s	8	0.6	0.03	0.2

4.3.2 Failure Modes

Figures 68, 71, 78 and 79 (Appendix 7.6-9) show the failure mode of series ADP.A-D respectively. The premature adhesive failure of specimen ADP.B1.1 (manufacturing process 4) at 66 kN revealed that surface treatment required the application of a primer (Figure 36(a)). The others specimens exhibited a "mixed failure" combining an "adhesive to adhesion promoter failure", between adhesive and primer, and a "fiber-tear failure" and/or "light-fiber-tear failure". The bad adhesion area depended on surface treatment efficiency and is related to failure load. Specimen ADP.B3.1 failed at 173 kN and showed a small surface with adhesion failure (Figure 36(c)), whereas specimen ADP. C2 failed at 100 kN and exhibited adhesion problems in almost the entire bonded area (Figure 36(d)). Specimen ADP.B2.1 failed at 202 kN, the maximal failure load of series ADP.A-C, and showed a "mixed failure" combining the previously mentioned failures modes and "cohesive failure" (Figure 36(b)). This could be caused by shear. The applied surface treatment (primer 1) seems to most appropriate for the ADP adhesive and GFRP adherends but no conclusion could be drawn with only one specimen. The adhesion failure revealed inappropriate surface treatment and is not usually accepted in adhesive technology (Hutchison 1999).

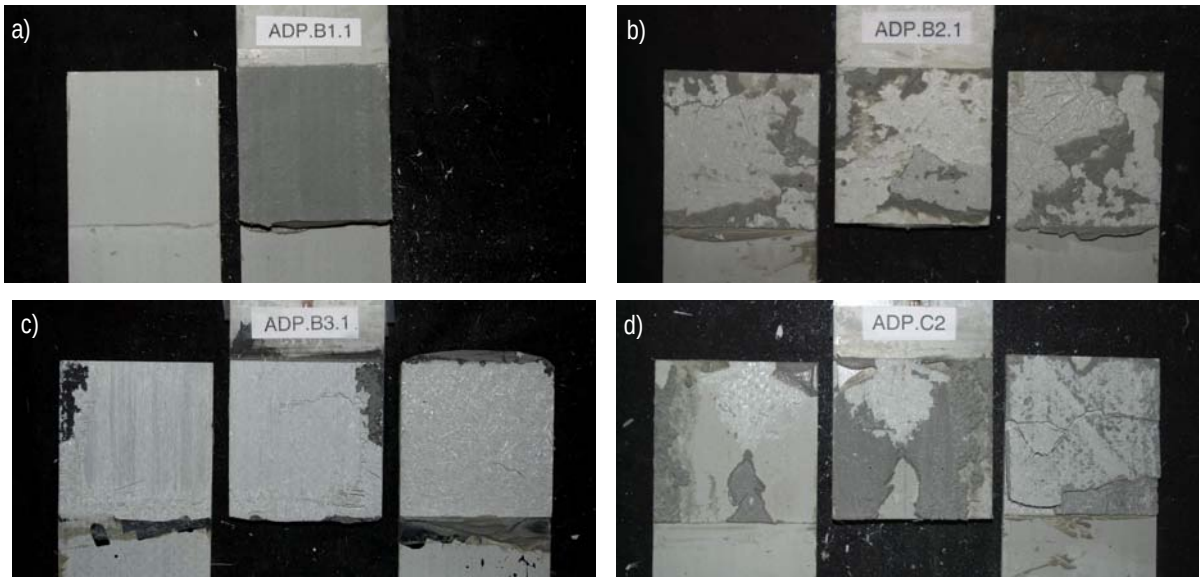

Figure 36 Failure modes of specimens (a) ADP.B1.1, (b) ADP.B2.1, (c) ADP.B2.1, (d) ADP.C2

4.3.3 Load-Strain Relationship on Laminates

Figure 37(a) represents the load-strain curves of the external strain gages placed on specimen ADP.C9. Comparison of gage s0-s4 measurements with gage s5-s9 measurements indicates that there is no loading eccentricity in direction y ((Figure 37(b)). The initial slope varies due to initial torsion when closing testing-machine jaws. Comparison of gage s2/s7 measurements with gage s4/s9 measurements indicates that there is no loading eccentricity in direction z. Specimens ADP.C7-9 showed similar

results (Appendix 7.8). Tables 24 and 25 summarize the measured strains on several locations of specimens ADP.C7-9 at 50 kN.

Table 32 in Appendix 7.8 indicates the Young's modulus of the 5 mm and 10 mm laminates estimated with strain measurements from gages s2/s7 and s0/s5 respectively. Average values are 31880 MPa and 30380 MPa for the 5 mm and 10 mm laminates respectively. These mechanical properties will be introduced in the developed FEA model (de Castro 2005 b, Chapter 5). It is important to note that both laminates were loaded in tension but the 5 mm thick laminates were also subjected to bending. The FEA model demonstrates that strains at gage locations were slightly influenced by bending, the calculated strain being 4% lower than that assuming only tension. Thus the Young's modulus of the 5 mm thick laminates is slightly overestimated. Some Young's moduli of the 10 mm laminates are higher than those estimated in series EP.A and PU.C. Burning-off tests were conducted on pieces from specimens ADP.C4 and ADP.C9, giving quite different Young's moduli, 25449 and 33977 MPa respectively. Tests showed that the laminate from specimen ADP.C4 had lower fiber rovings amount than specimen ADP.C9 which corresponds with the variations in Young's modulus. Thus, the laminates are not identical, which could explain scattered measurements.

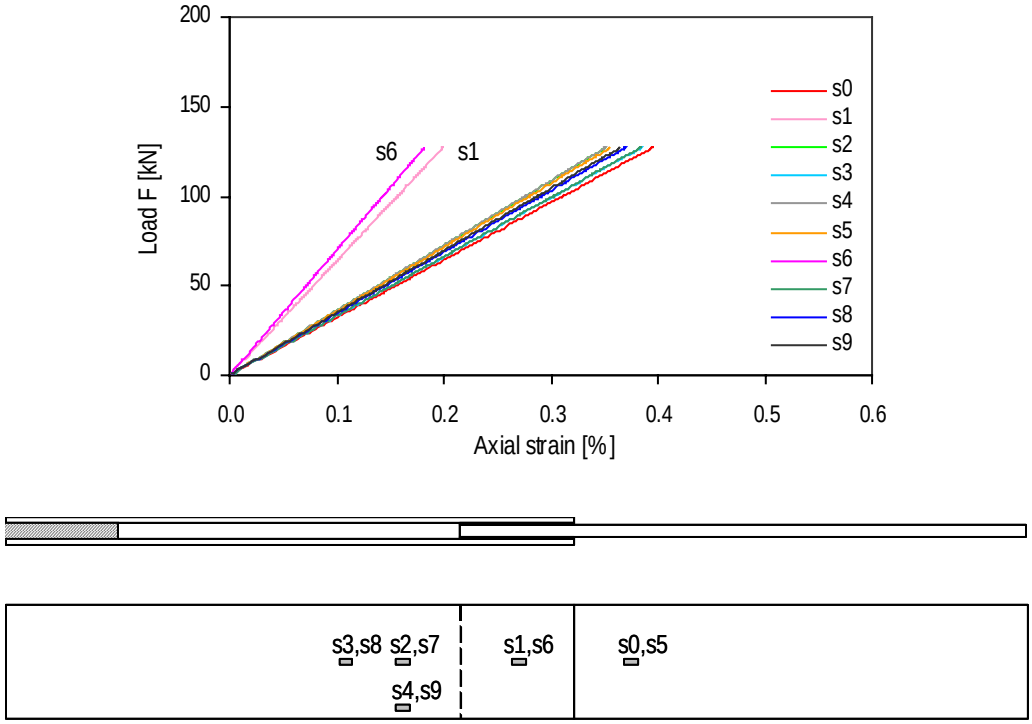

Figure 37 (a) Load-strain curves of external gages in specimen ADP.C9; (c) Gage positions

Table 24 Measured strains [%] for specimens ADP.C7-9 at 50 kN

	0	5	1	6	2	7	4	9	3	8
ADP.C7	0.156	0.140	0.078	0.072	0.139	0.138	0.151	0.144	0.152	0.146
ADP.C8	0.171	0.149	0.071	-	0.136	0.141	0.149	0.123	0.154	0.145
ADP.C9	0.143	0.151	0.070	0.081	0.150	0.138	0.146	0.133	0.139	0.150

4.3.4 Strain Distribution on the Overlap

Data are presented in Appendix 7.8.

Configuration 1

Figure 38 represents axial strain distribution across joint width of specimens ADP.C7-9 in two different sections, the outer (s10-s12) and inner (s13-s15) (Figure 14). There were insufficient measurements in the outer edge to define a tendency. Gages in the border of the inner section revealed strain deviations of 10 to 20% compared with those in the middle of the joint width. The non-uniform load transfer across the width is in agreement with Richardson et al. (1993) but for a low stiffness adhesive such as ADP, strain distribution is nearly linear.

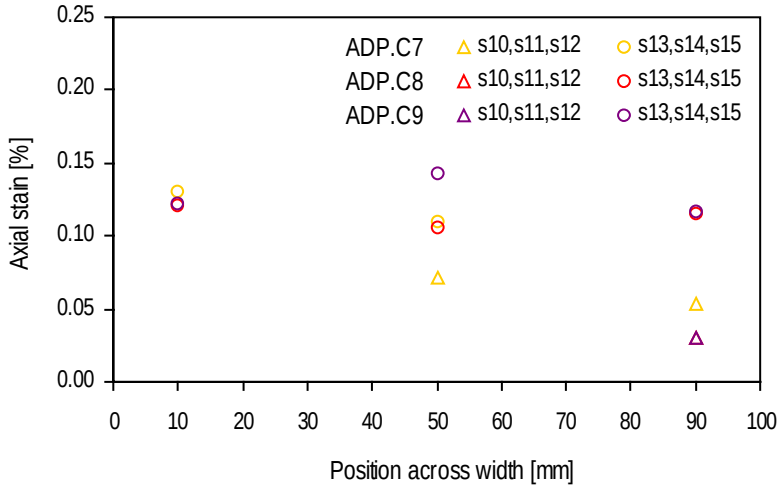

Figure 38 Axial strain distribution across width for specimens ADP.C7-9 at 50 kN

Configuration 2

Ten gages are placed on nine different sections in order to describe strain distribution along overlap length. Load-strain curves for specimens ADP.C4-6 are presented in Appendix 7.8.

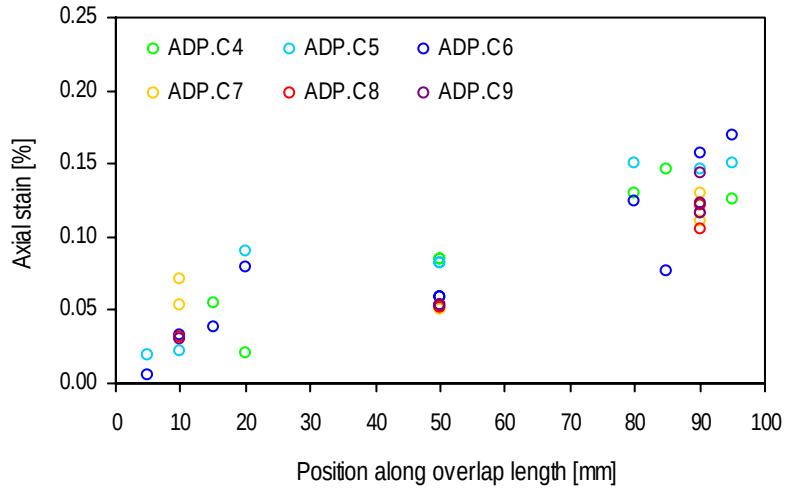

Figure 39 Axial strain distribution along overlap length for specimens ADP.C4-9 at 50 kN

Figure 39 shows the axial strain distribution along overlap length of specimens ADP.C4-6 (config. 2) and specimens ADP.C7-9 (config. 1) at 50 kN. Axial strain distribution on specimens ADP.C4-9 exhibited a fairly constant slope along overlap length, which signifies uniform load transfer.

4.3.5 Joint Elongation

Figure 40 shows raw data for specimen ADP.C9. The points placed in the 5 mm laminates (1-5 and 11-15) exhibited linear elongations whereas points placed in the 10 mm laminates (6-10) exhibited bilinear elongations. The raw data are interpolated with a polynomial curve of the 6th degree. The processed data for specimens ADP.C7-9 are presented in Appendix 7.8. Tables 26 and 27 resume the measured elongations of specimens PU.B6-8 at 20 kN and 100 kN respectively. Two load levels are considered instead of one as for the other series due to the bilinear behavior.

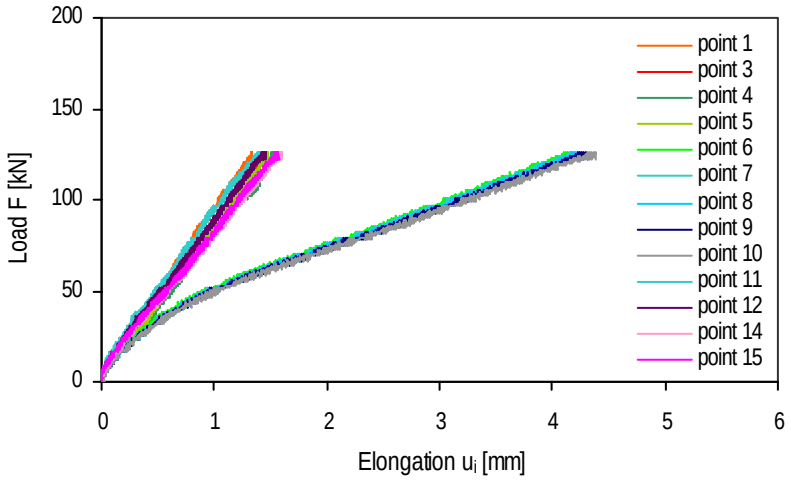

Figure 40 Load-elongation curves in joint, u_i, for specimen ADP.C9

Table 25 Measured elongations [mm] for specimens ADP.C7-9 at 50 kN

	1	11	2	12	3	13	4	14	5	15
ADP.C7	0.148	0.127	0.148	0.125	0.164	0.123	0.156	0.161	0.168	0.133
ADP.C8	0.150	0.169	0.147	0.164	0.155	0.193	0.184	-	0.173	0.159
ADP.C9	0.198	0.129	-	0.157	0.203	-	0.207	0.177	0.215	0.170

	6	7	8	9	10
ADP.C7	0.220	0.223	0.229	0.245	0.231
ADP.C8	0.278	0.273	0.267	0.302	0.302
ADP.C9	0.239	0.238	0.243	0.241	0.231

Table 26 Measured elongations [mm] for specimens ADP.C7-9 at 50 kN

	1	11	2	12	3	13	4	14	5	15
ADP.C7	0.502	0.487	0.519	0.498	0.552	0.519	0.565	0.556	0.579	0.545
ADP.C8	0.451	0.476	0.467	0.508	0.489	0.489	0.521	-	0.518	0.515
ADP.C9	0.517	0.483	-	0.583	0.559	-	0.611	0.525	0.580	0.559

	6	7	8	9	10
ADP.C7	1.128	1.138	1.145	1.174	1.193
ADP.C8	1.206	1.217	1.218	1.245	1.279
ADP.C9	0.939	0.972	0.984	0.999	1.032

As for series EP.A and PU.B, joint displacement and stiffness are estimated from the relative displacement of laminates in direction x (Figure 24). Figure 41 shows the joint elongation, u_j, and global elongation, u, of specimens ADP.C7-9. Figure 42 includes the joint stiffness, ratio of joint elongation to global elongation and ratio of laminate elongation to global elongation of specimen ADP.C9. Table 28 summarizes joint stiffness at 20 kN (characterizing the first linear part), 50 kN and 100 kN (characterizing the second linear part) and the ratio of joint elongation to global elongation at 20 kN, 50kN and 100 kN of specimens ADP.C7-9. The initial joint stiffness (at 20 kN) decreased four times (at 100kN) in the second linear part. Thus the ratio of joint elongation to global elongation was 25% at 20 kN and increased to 50% at 100 kN.

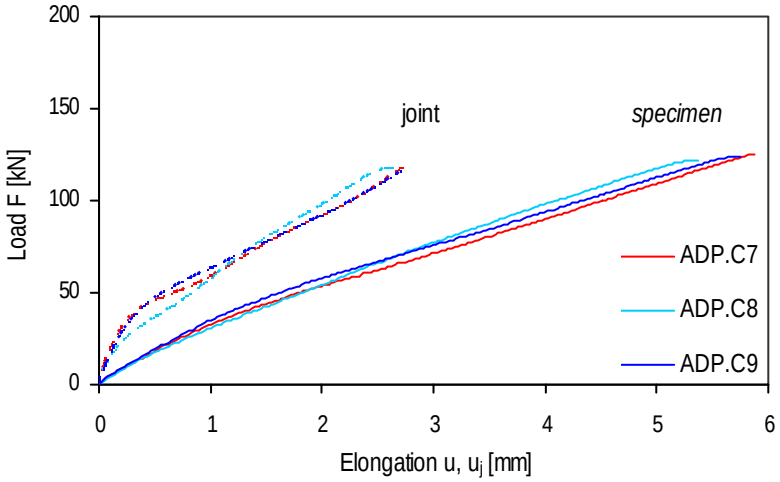

Figure 41 Load-elongation curves for joint, u_j, and global specimen, u, of specimens ADP.C7-9

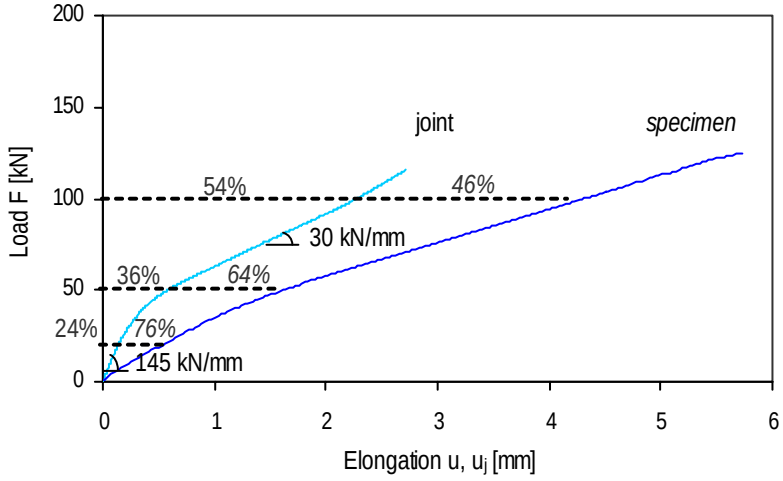

Figure 42 Load-displacement of joint, u_j, and global specimen, u, of specimen ADP.C9

Table 27 Joint stiffness and ratio of joint elongation to global elongation of specimens ADP.C7-9

Specimen	Stiffness (kN/mm)			u_j/u (%)		
	20 kN	50 kN	100 kN	20 kN	50 kN	100 kN
ADP.C7	160	70	30	20	38	50
ADP.C8	100	60	40	29	45	50
ADP.C9	145	95	30	24	36	54

4.4 ADP-Epoxy Adhesives

4.4.1 Load-Displacement Relationship

Detailed data concerning test series ADP-EP.A are given in Appendix 7.10. Global load-elongation curves are represented in Figure 43. Table 29 summarizes the ultimate load, F_u, ultimate elongation, u_u, corresponding ultimate average shear stress, τ_u, joint efficiency, J_{eff}, average values and standard deviations.

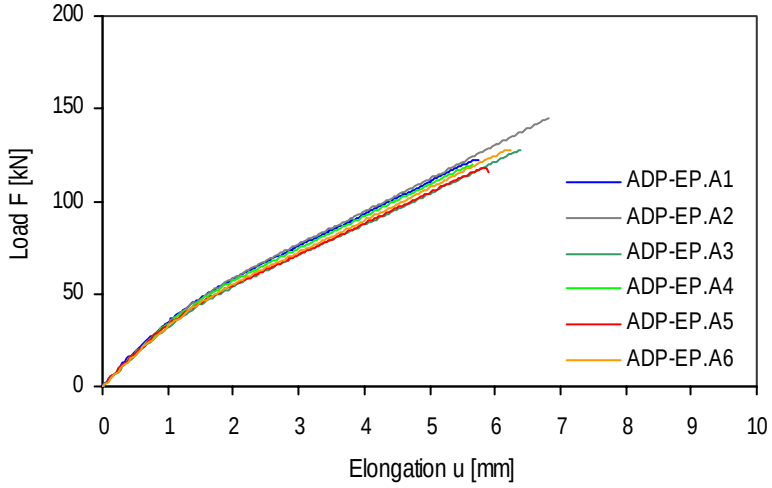

Figure 43 Load-elongation curves for series ADP-EP.A

Load-elongation curves for specimens ADP-EP.A were similar to series ADP.C. The specimens showed bilinear behavior. Global stiffness changed at 40 and 50 kN (approximately 35% of failure load). At this load level a decrease in global stiffness was observed as it was for the ADP adhesive (Figure 9). Average failure load was 127 kN and average global elongation 6.1 mm. Average joint efficiency was 0.38.

Table 28 Test results for series ADP-EP.A

Specimen	F_u [kN]	u_u [mm]	J_{eff} [-]	τ_u [MPa]
ADP-EP.A1	123	5.8	0.37	6.2
ADP-EP.A2	145	6.8	0.44	7.3
ADP-EP.A3	128	6.4	0.39	6.4
ADP-EP.A4	120	5.7	0.36	6.0
ADP-EP.A5	118	5.9	0.36	5.9
ADP-EP.A6	127	6.2	0.38	6.4
m	127	6.1	0.38	6.3
s	10	0.4	0.03	0.5

4.4.2 Failure Modes

Figure 84 (Appendix 7.10) shows the failure mode of series ADP-EP.A. The specimens exhibited a "mixed failure" combining "adhesive failure", between adhesives, and "fiber-tear failure" and/or "light-fiber-tear failure" (Figure 44).

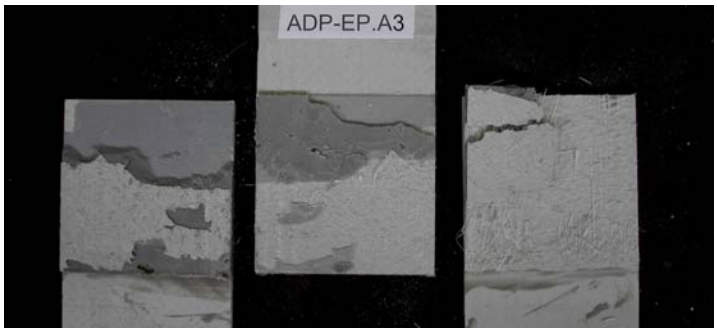

Figure 44 Failure mode of specimen ADP-EP.A3

5 Summary

Quasi-static tensile experiments on adhesively double-lap joint with different adhesive were performed in order to quantify the adhesive behavior effect. The conclusions from the adhesive double-lap joint are:

- The epoxy (EP) and polyurethane (PU) joints exhibited linear behavior up to the brittle failure and thus constant stiffness. The PU adhesive remained elastic and did not reach plastic deformations as elastic strain was too high. Comparing both joints indicates that reducing the adhesive Young's modulus approximately 7.5 times has a low effect on joint stiffness whilst increasing joint strength.
- The acrylic (ADP) joints exhibited bilinear behavior as for the ADP adhesive, with a joint stiffness reduction of approximately 75% when reaching plastic deformations in 100 mm overlap length joints.
- The EP and polyurethane PU joint failure occurred in the laminates by fiber-tear or light-fiber-tear failure (commonly called interlaminar failure), while ADP joints exhibited a mixed failure including adhesion failure and fiber-tear or light-fiber-tear failure. The adhesion failure led to a lower strength than expected, which was related to bad adhesion area dimensions. ADP joints with the large overlap length (200 mm) were 40 % stronger than EP joints. Nevertheless, few joints with the short overlap length (100 mm) showed a higher strength than the EP and PU series. Thus, applying the appropriate surface treatment will improve results. The supplier must carry out research to solve the adhesion problem.
- The flexible ADP joints with highly nonlinear adhesive characteristics allowed large elongation deformations and provided a favorable load transfer. Nevertheless, because of their premature failure due to adhesion problems, their potential was not reached.
- Adhesively-bonded joint efficiency using a highly nonlinear adhesive (76% for ADP joints with 200-mm overlap length) was greater than mechanical joint efficiency (50% according to Matthews (1987)) and thus adhesive-bonding is more appropriate to the anisotropic character and brittle behavior of FRP materials.
- The strain distribution across the joint width indicated higher strains at the edge than in the middle. The deviations reached 20% when assuming a transversal uniform distribution. Thus, a uniform approximation is assumed for numerical and analytical analyses leading to 2-D rather than 3-D models.

6 Acknowledgements

The author wishes to acknowledge the support of the Swiss Innovation Promotion Agency CTI (Contract No. 4676.1), Fiberline Composites A/S, Denmark (supplier of the pultruded profiles) and Sika AG, Zurich, Switzerland (supplier of the adhesives). Special thanks to Mr Venetz of SIKA AG for his assistance with the bonded joint manufacture.

7 Appendix

7.1 Curves and Failure Pictures of Specimens EP.A

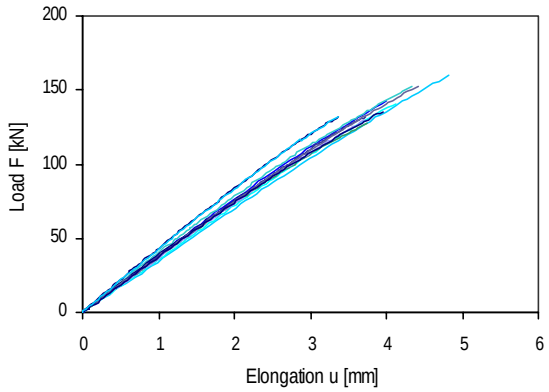

Figure 45 Load-elongation curve of specimens EP.A

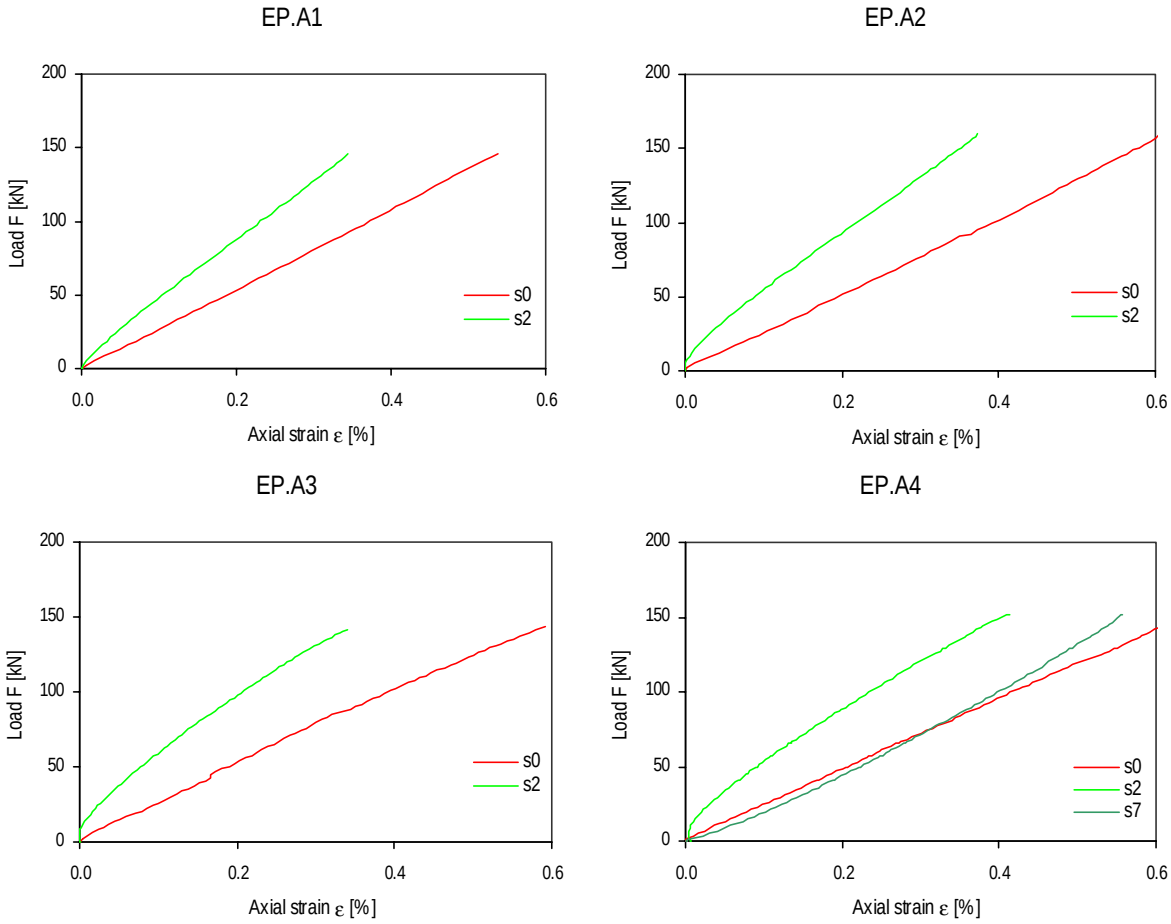

Figure 46 Load-strain curve of specimens EP.A1-4

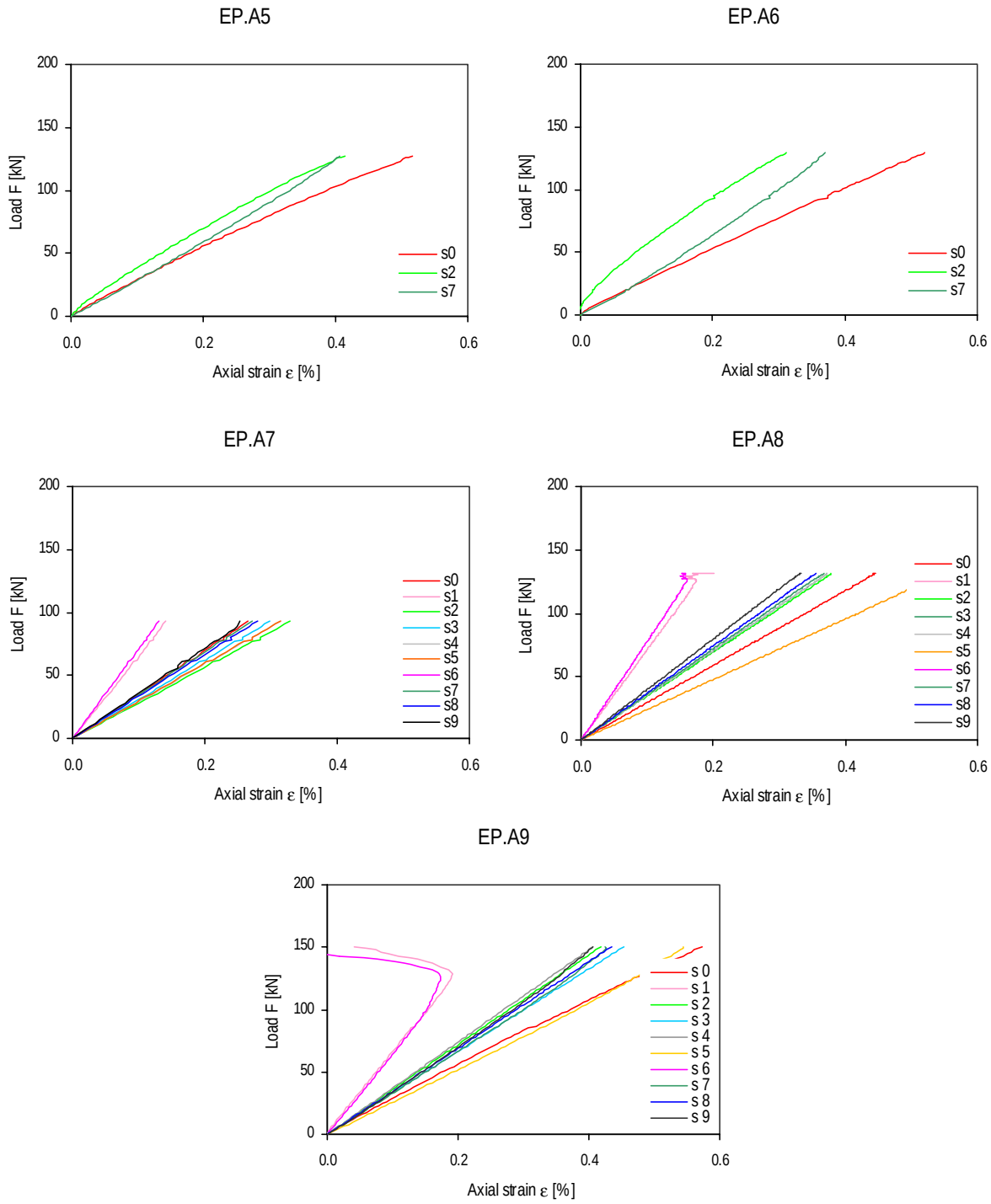

Figure 47 Load-strain curve of specimens EP.A5-9

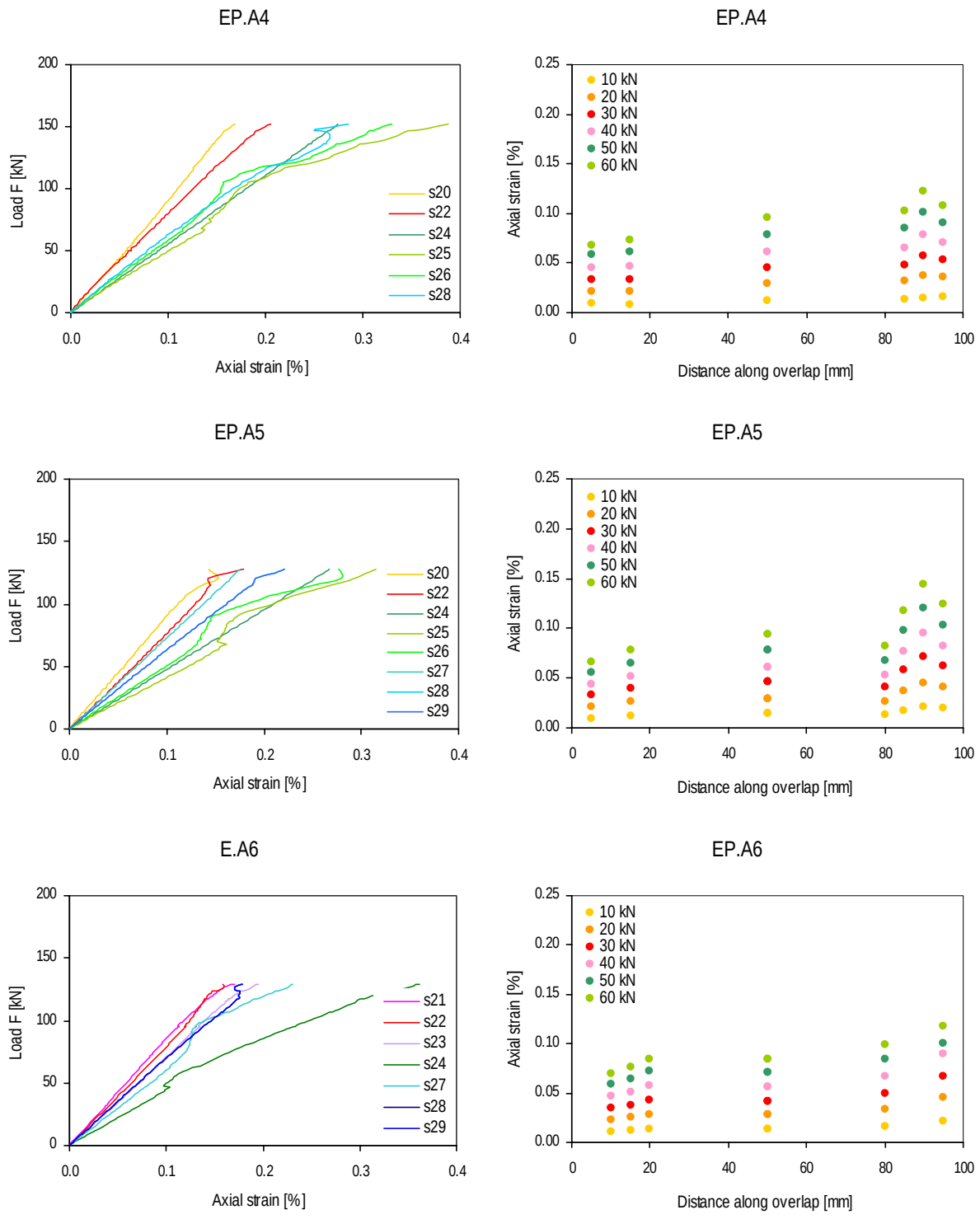

Figure 48 (a) Load-strain curves in joint; (b) Axial strain distribution along overlap length for different load levels of specimens EP.A4-6

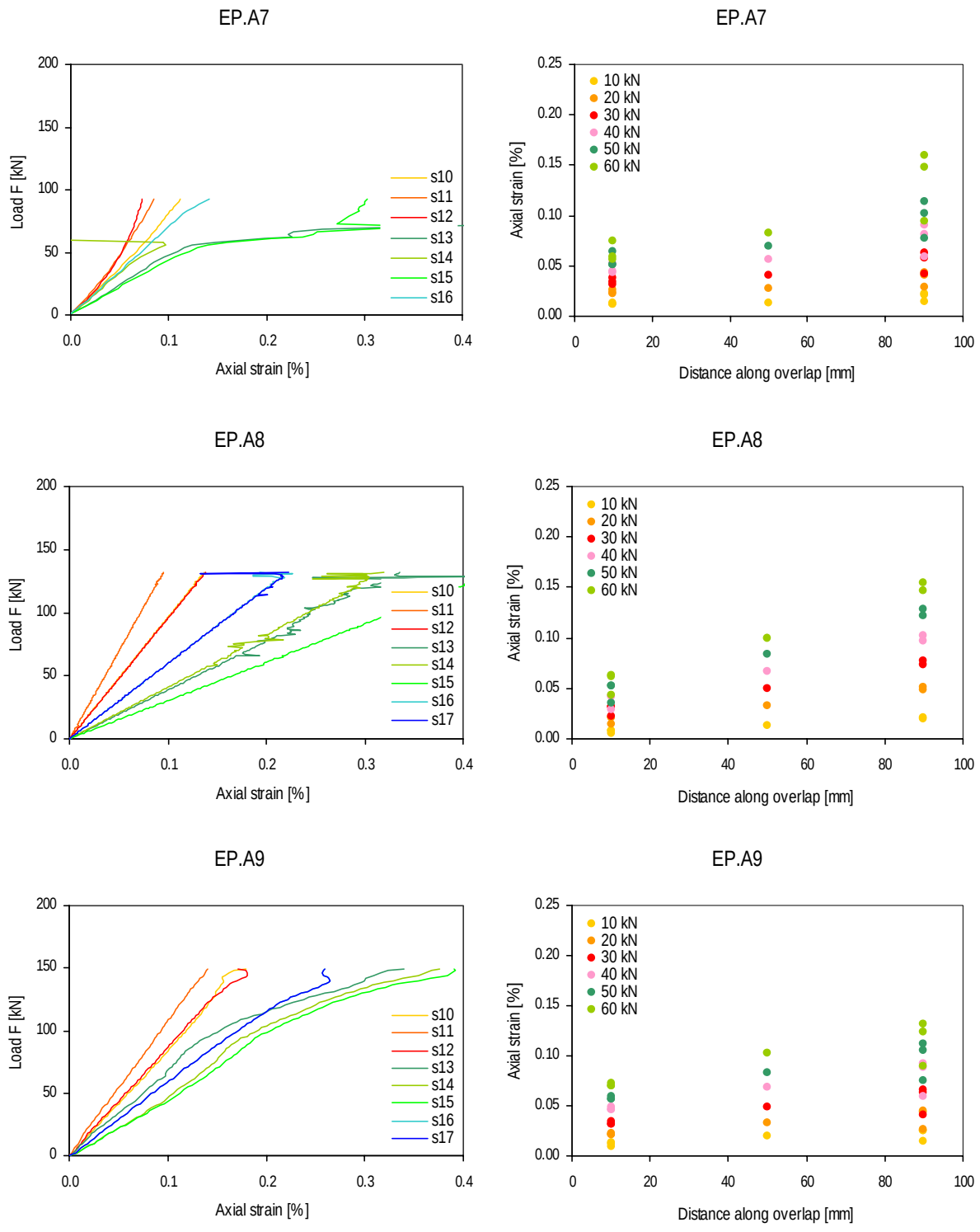

Figure 49 (a) Load-strain curves in joint; (b) Axial strain distribution along overlap length for different load levels of specimens EP.A7-9

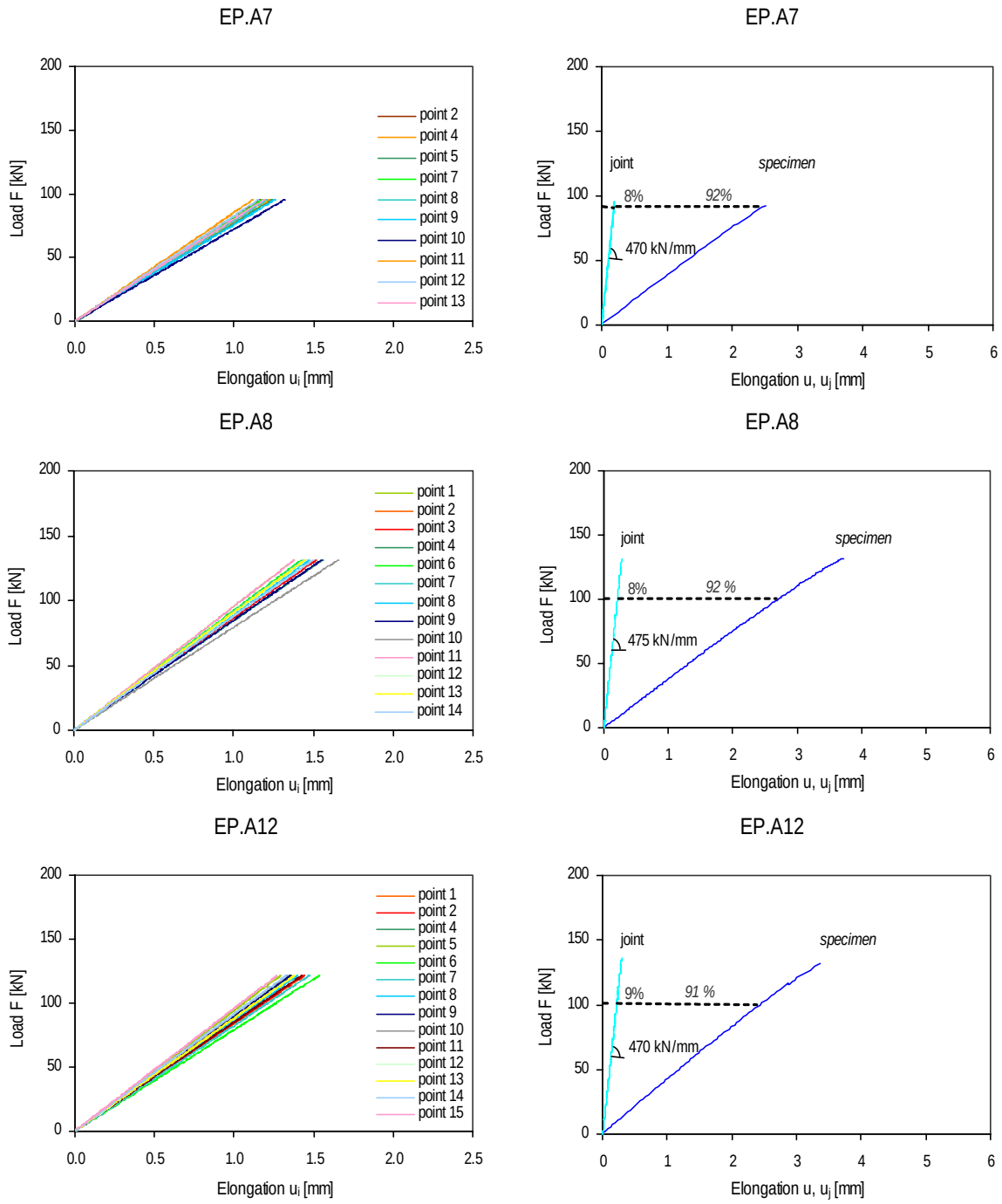

Figure 50 (a) Load-displacement curves measured with video-extensometer; (b) Load-displacement curves of joint and global specimen for specimens EP.A7,8,12

Table 29 Young's modulus of laminates for series EP.A [MPa]

Specimen	Laminates	
	5 mm	10 mm
EP.A1	26964	38788[1]
EP.A2	27929	37867[1]
EP.A3	26811	33549
EP.A4	23807	29758
EP.A5	25438	30667
EP.A6	24831	35254
EP.A7	32229[1]	31216
EP.A8	26665	35366
EP.A9	26828	34827
m	26159	32948
s	1348	2361

[1] not considered in average and standard deviation values

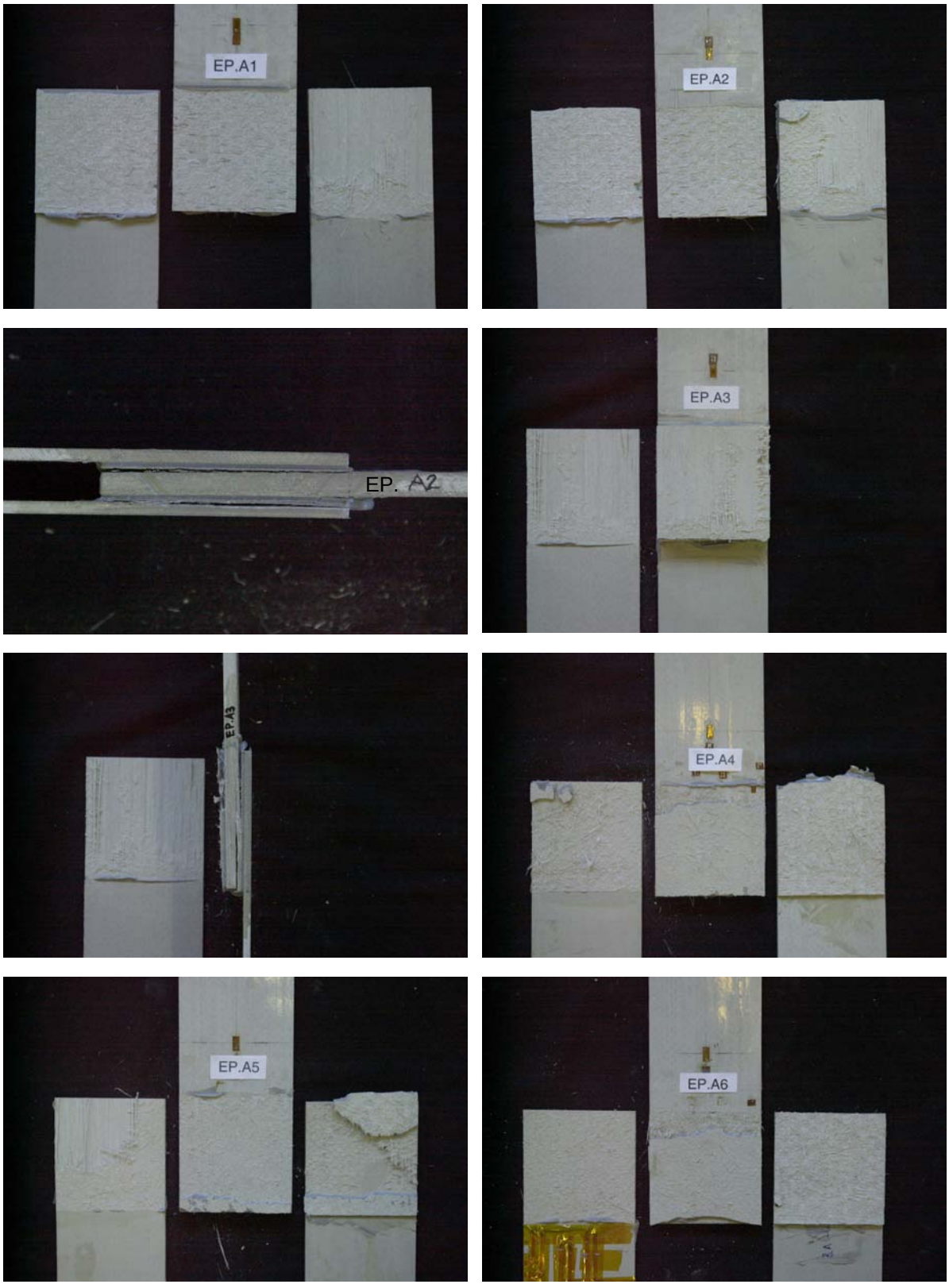

Figure 51 Failure of specimens EP.A1-6

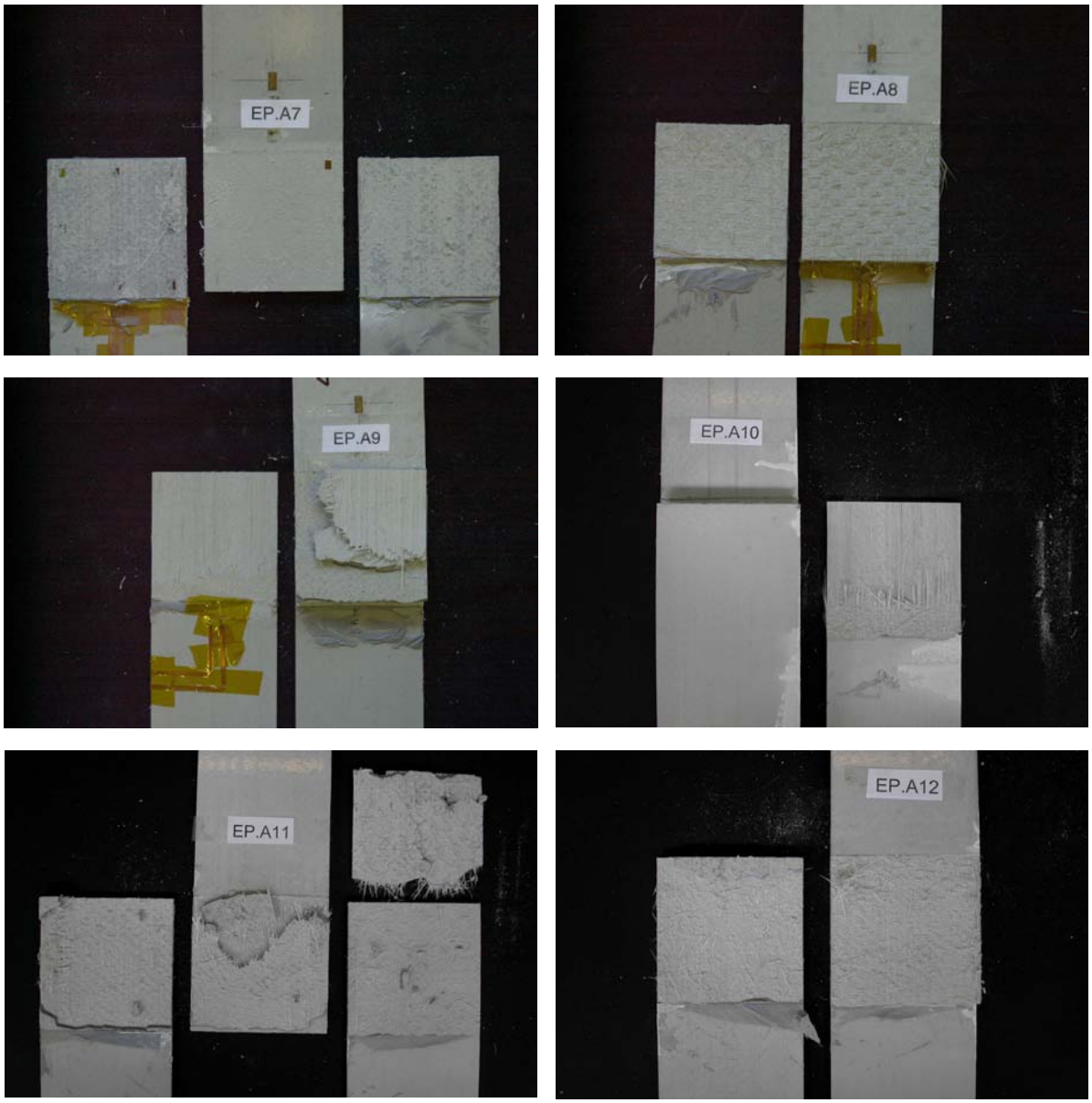

Figure 52 Failure of specimens EP.A7-12

7.2 Curves and Failure Pictures of Specimens EP.D

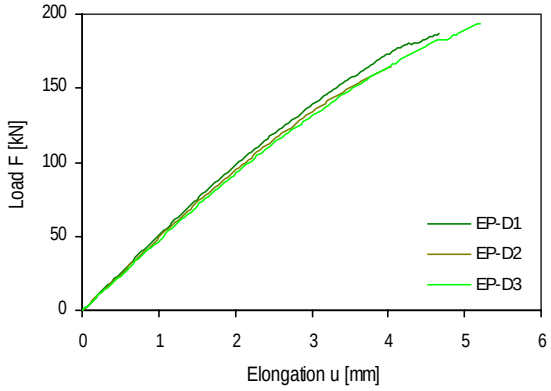

Figure 53 Load-elongation curve of specimens EP.D

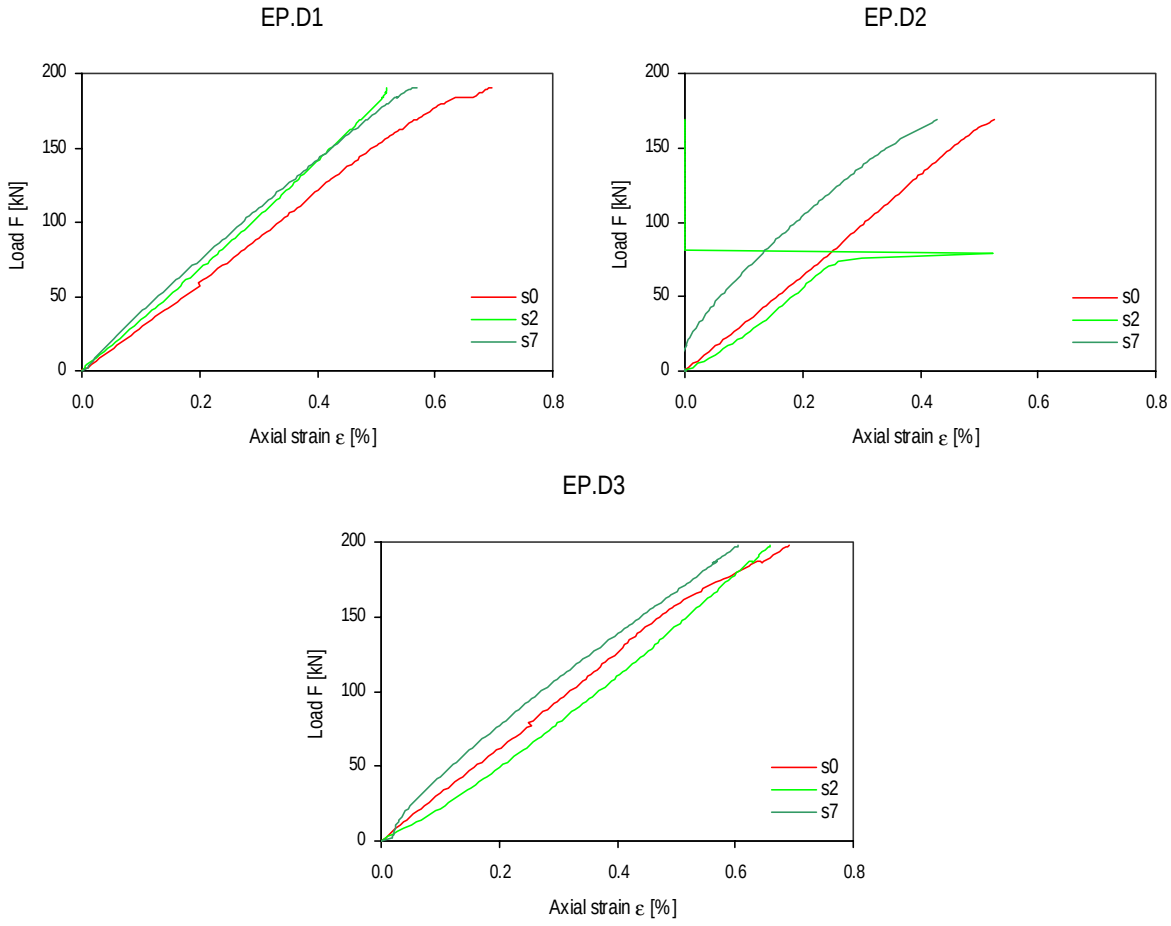

Figure 54 Load-strain curve of specimens EP.D

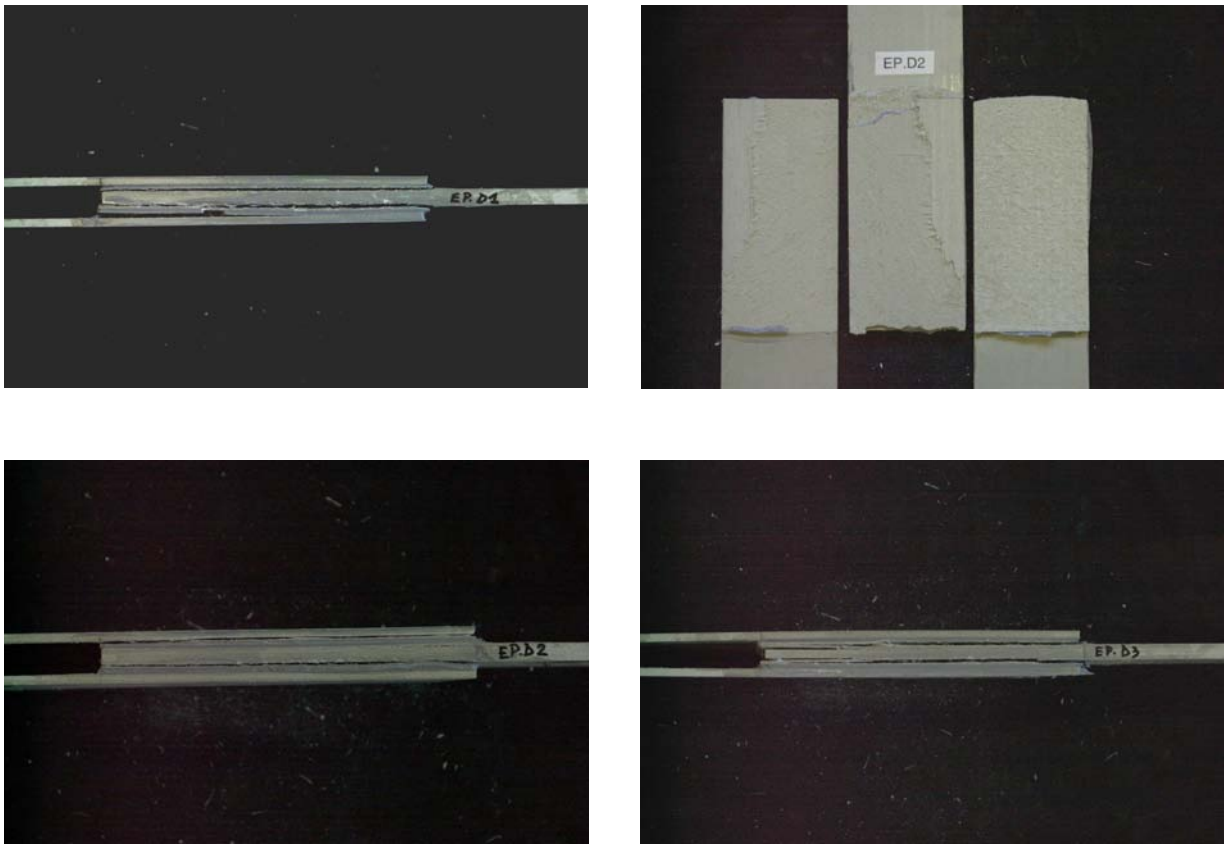

Figure 55 Failure of specimens EP.D

7.3 Curves and Failure Pictures of Specimens PU.A

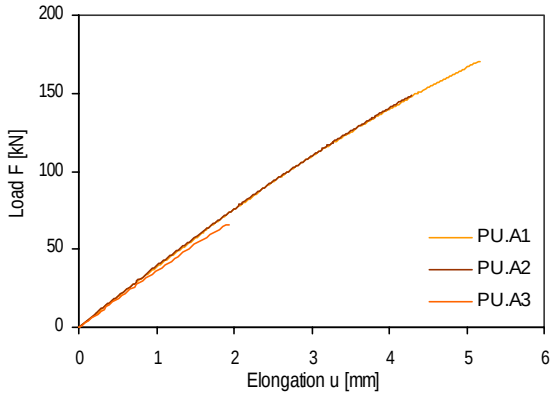

Figure 56 Load-elongation curve of specimens PU.A

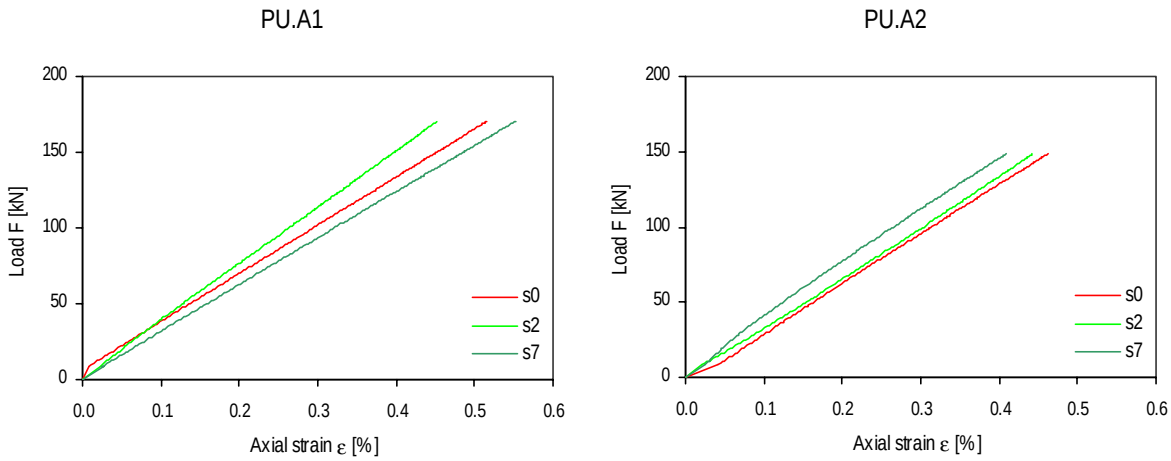

Figure 57 Load-strain curve of specimens PU.A1,2

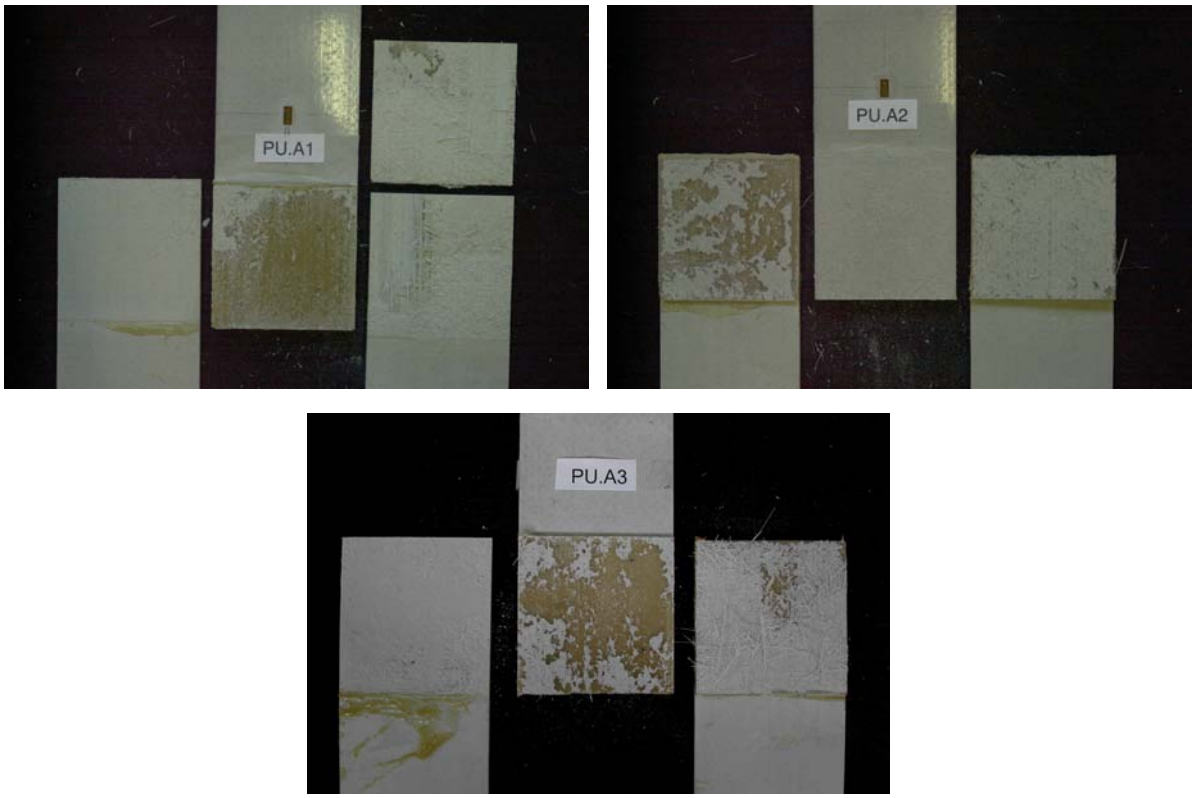

Figure 58 Failure of specimens PU.A

7.4 Curves and Failure Pictures of Specimens PU.B

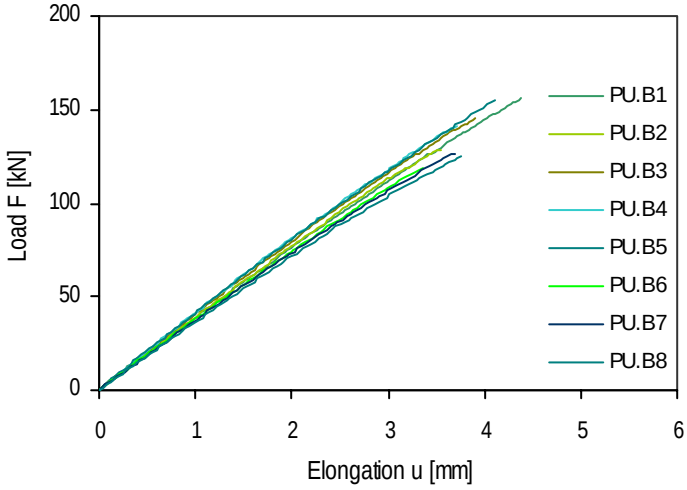

Figure 59 Load-elongation curve of specimens PU.B

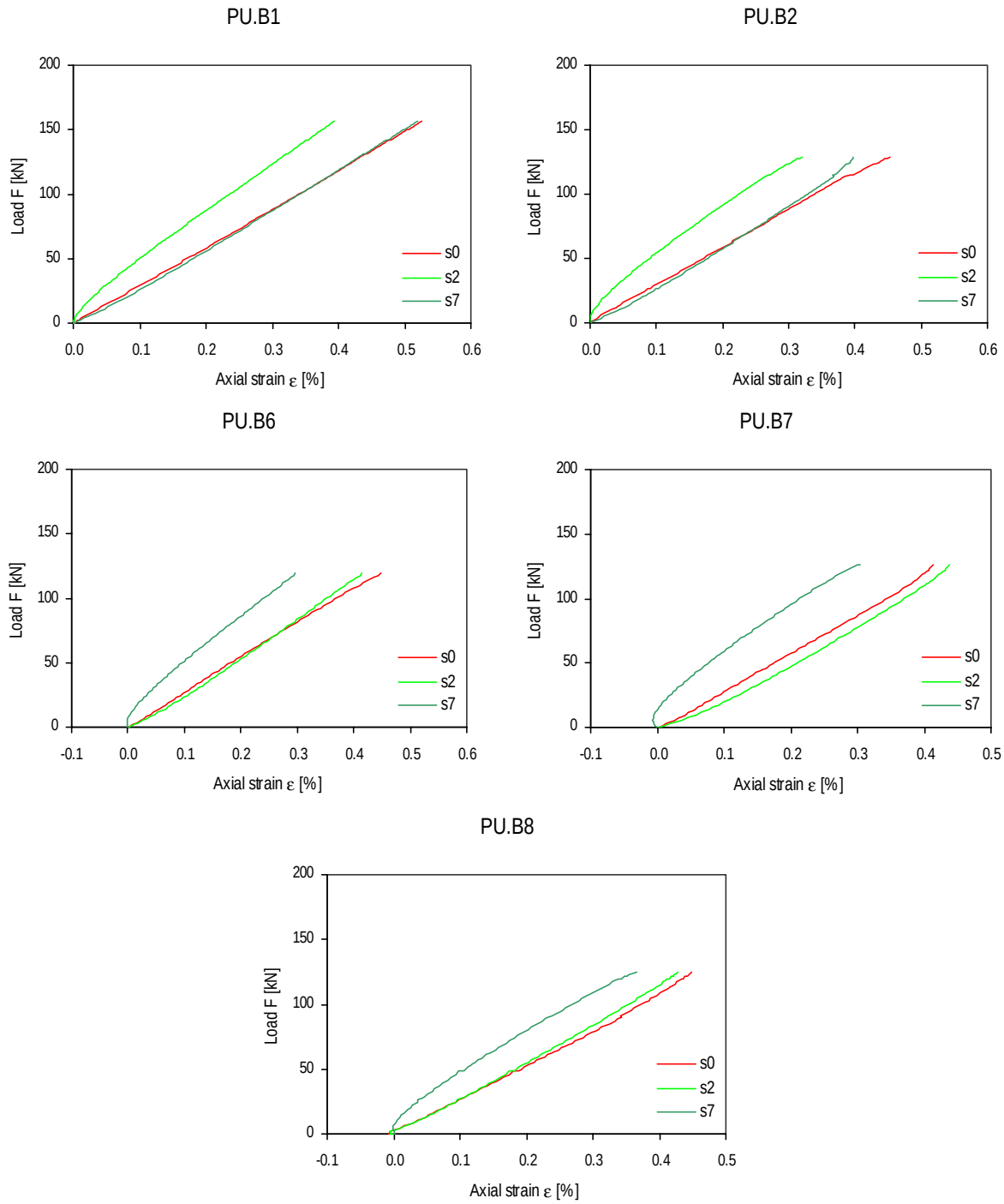

Figure 60 Load-strain curve of specimens PU.B1,2,6,7,8

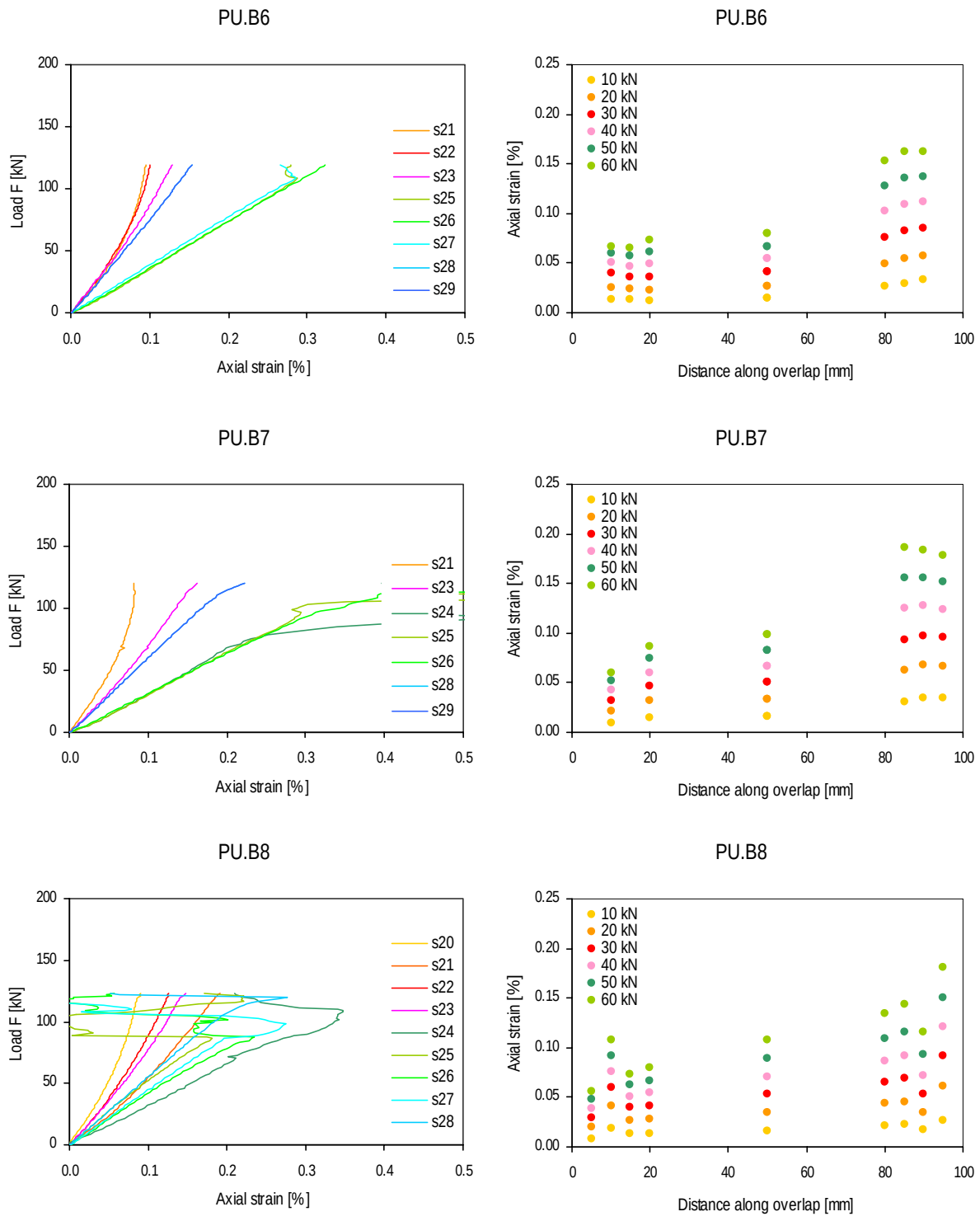

Figure 61 (a) Load-strain curves in joint; (b) Axial strain distribution along overlap length for different load levels of specimens PU.B6-8

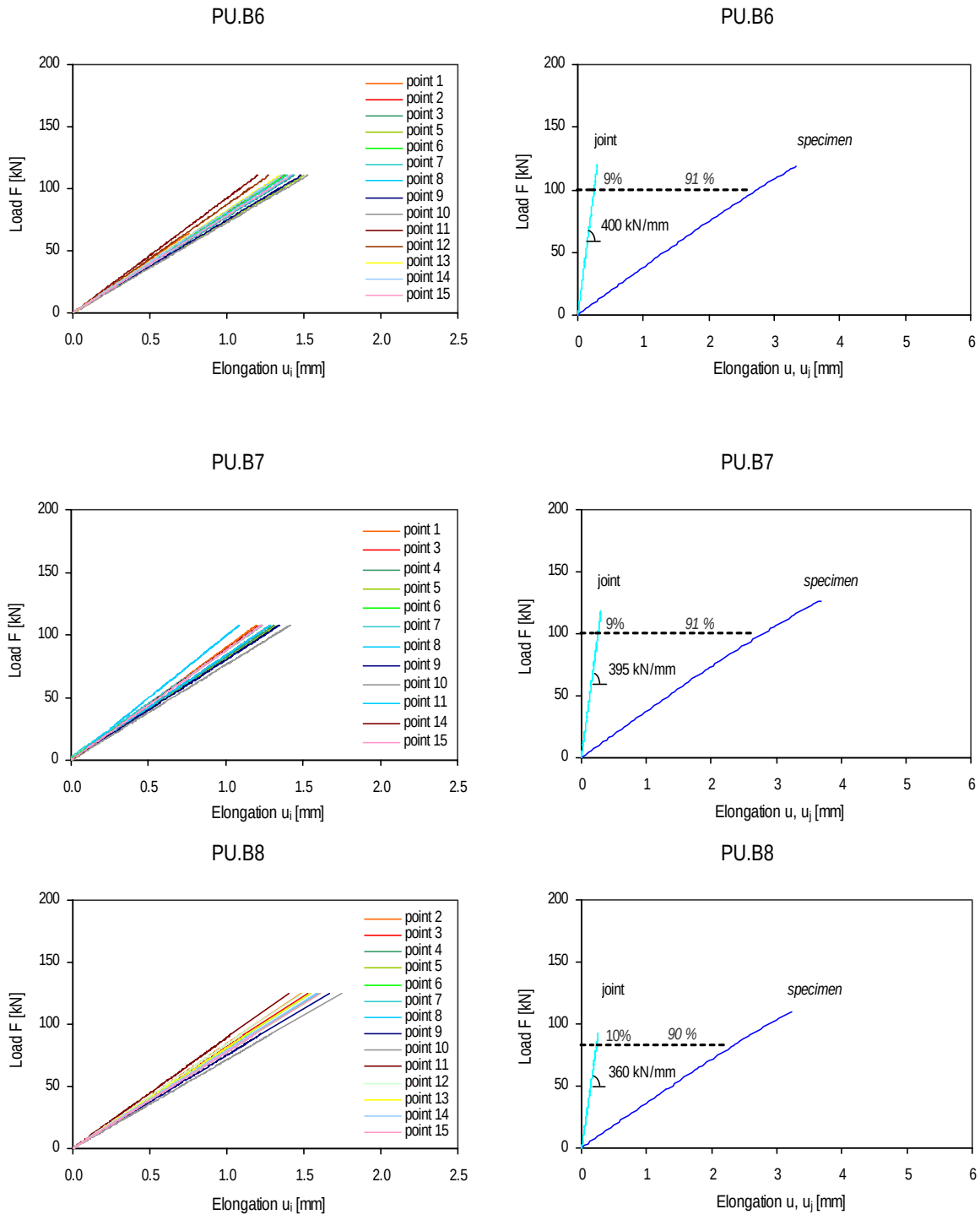

Figure 62 (a) Load-displacement curves measured with video-extensometer; (b) Load-displacement curves of joint and global specimen for specimens PU.B7,8,12

Table 30 Young's modulus of laminates for series PU.B [MPa]

Specimen	Laminates	
	5 mm	10 mm
PU.B1	33749	29412
PU.B2	32524	28878
PU.B6	32368	27424
PU.B7	32955	29333
PU.B8	29033	26244
m	32126	28258
s	1810	1381

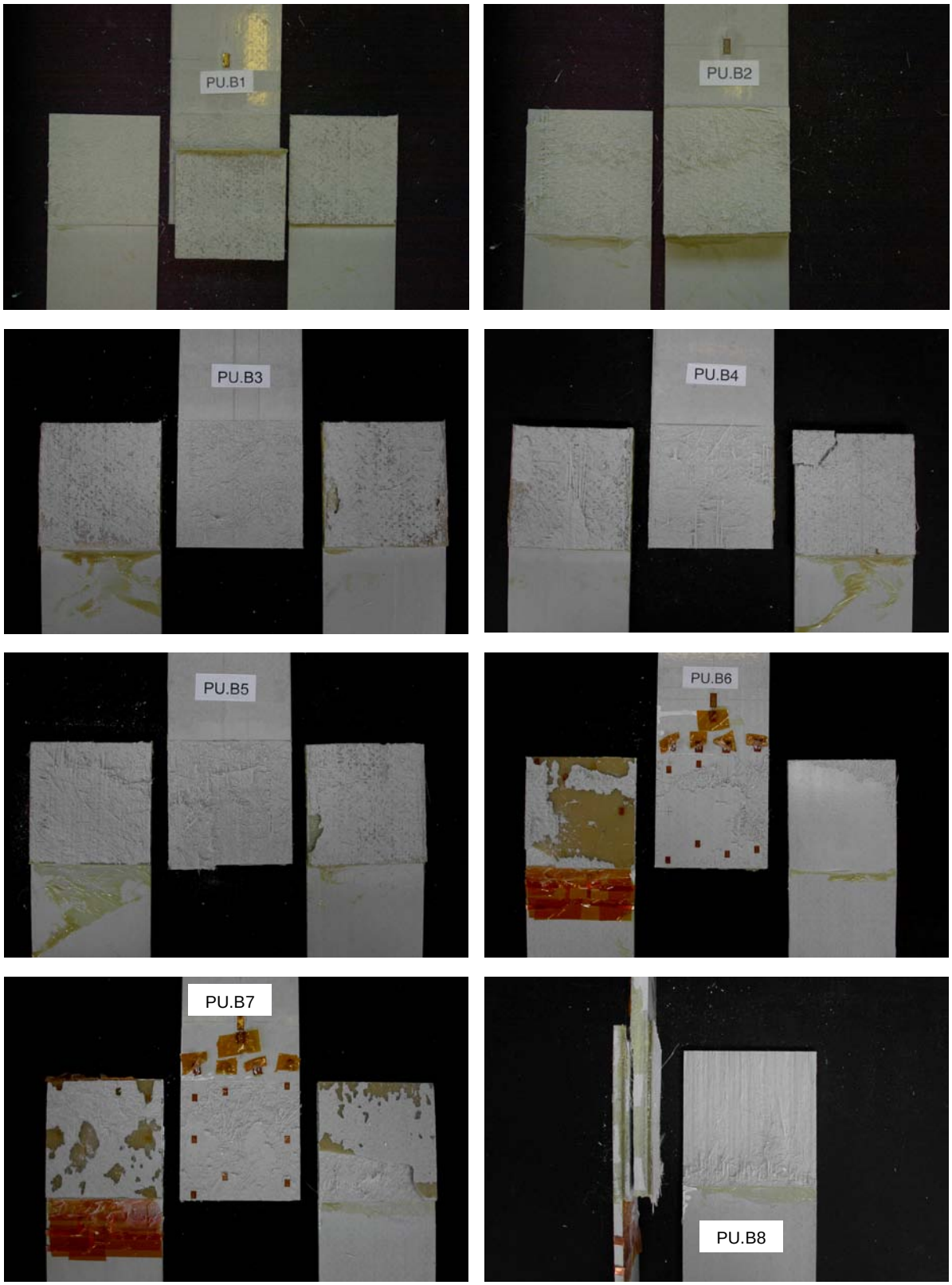

Figure 63 Failure of specimens PU.B1-8

7.5 Curves and Failure Pictures of Specimens PU.C

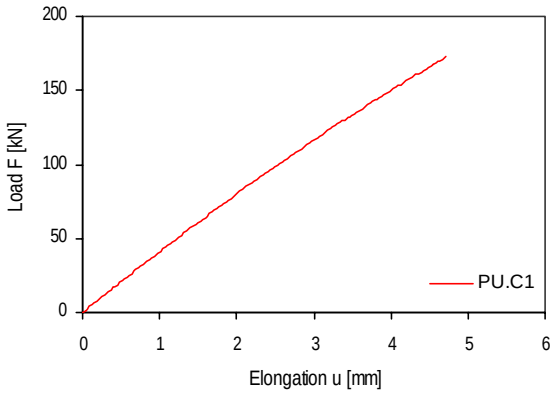

Figure 64 Load-elongation curve of specimen PU.C1

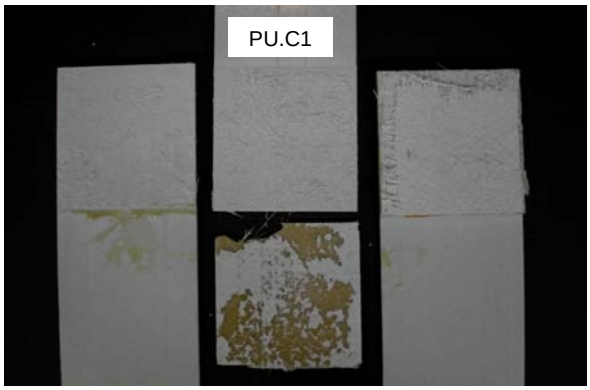

Figure 65 Failure of specimen PU.C1

7.6 Curves and Failure Pictures of Specimens ADP.A

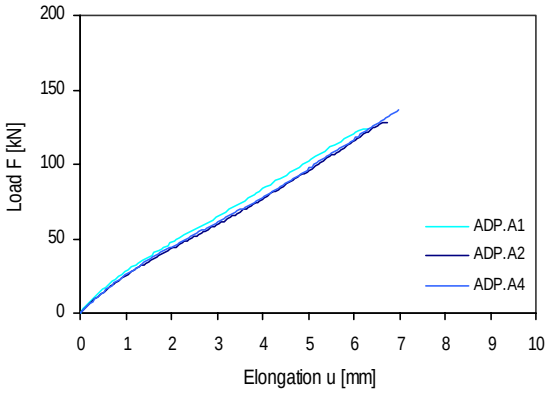

Figure 66 Load-elongation curve of specimens ADP.A

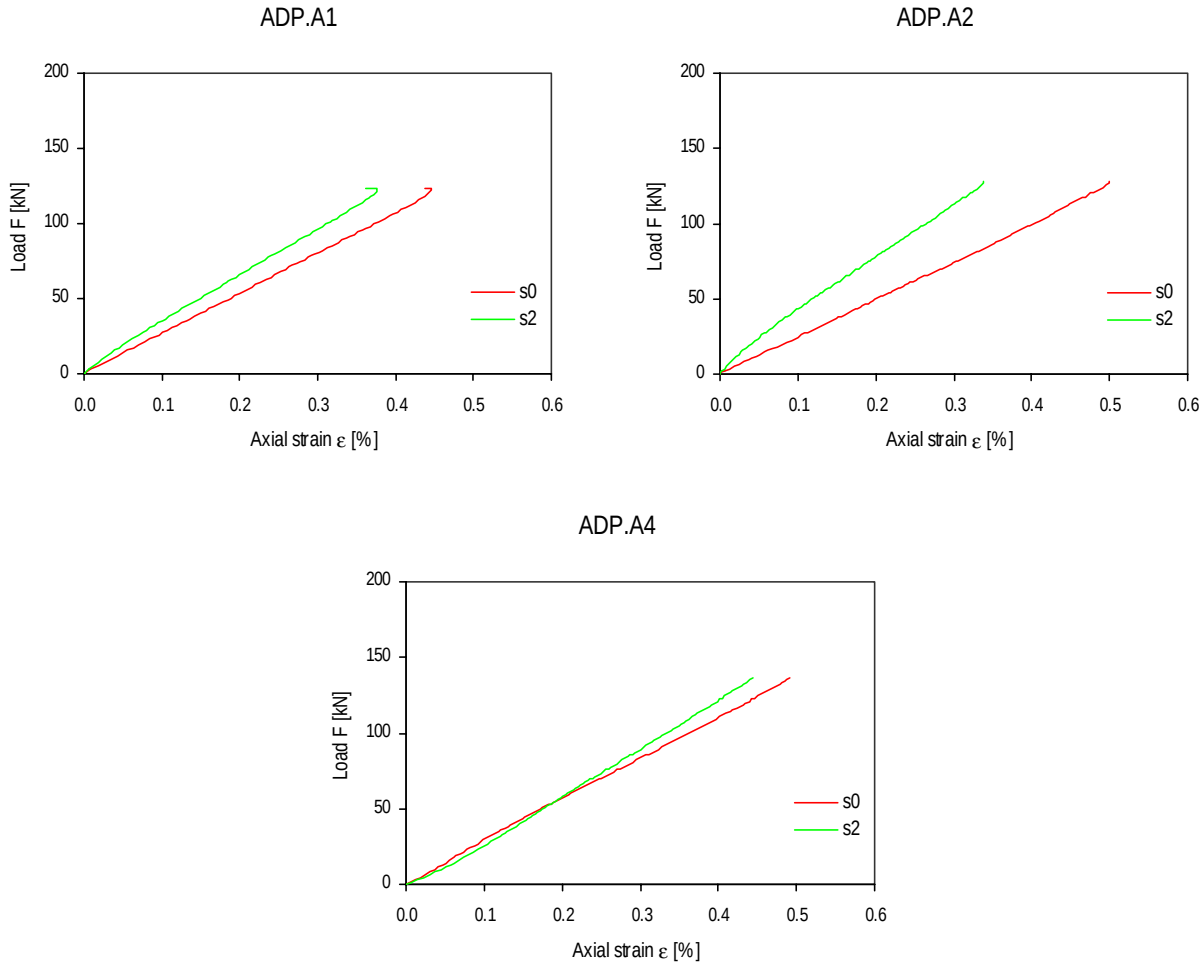

Figure 67 Load-strain curve of specimens ADP.A

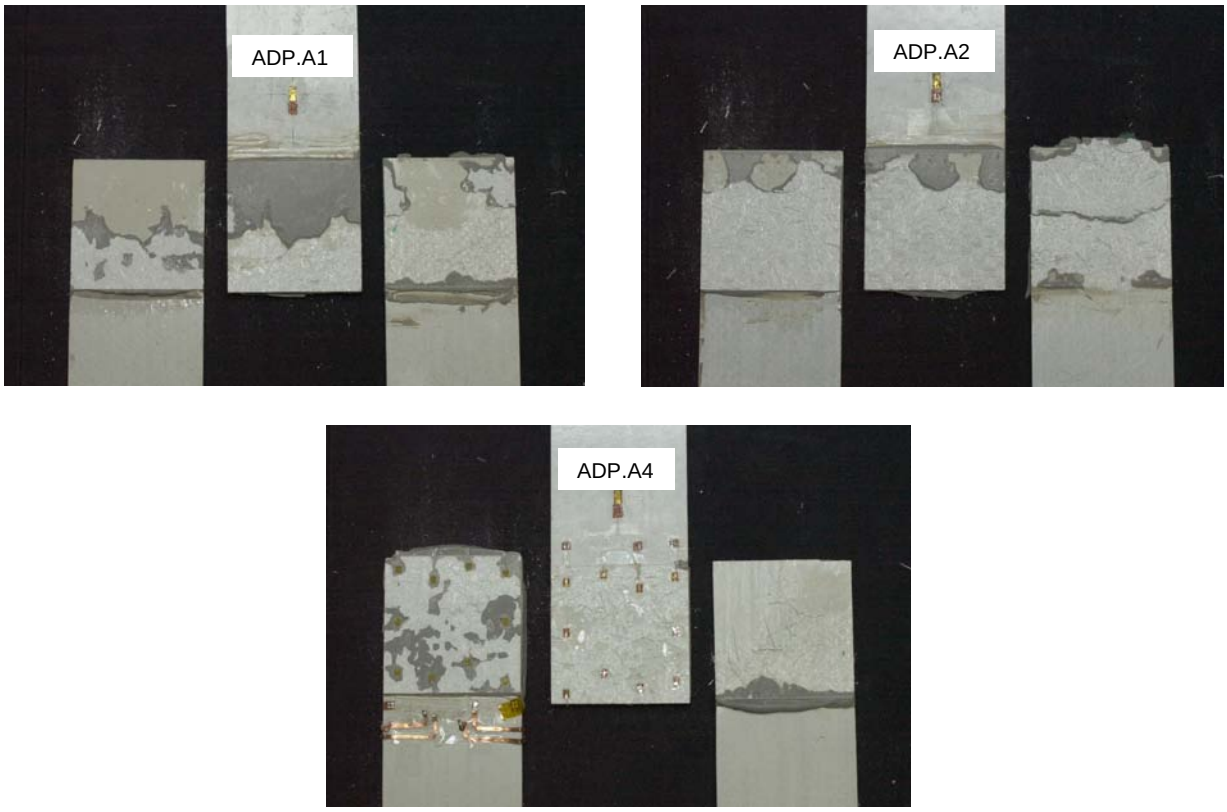

Figure 68 Failure of specimens ADP.A

7.7 Curves and Failure Pictures of Specimens ADP.B

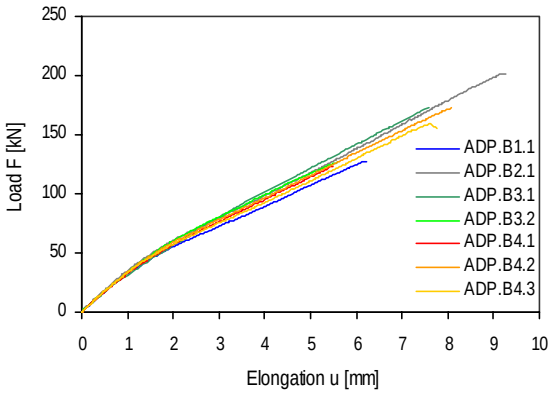

Figure 69 Load-elongation curve of specimens ADP.B

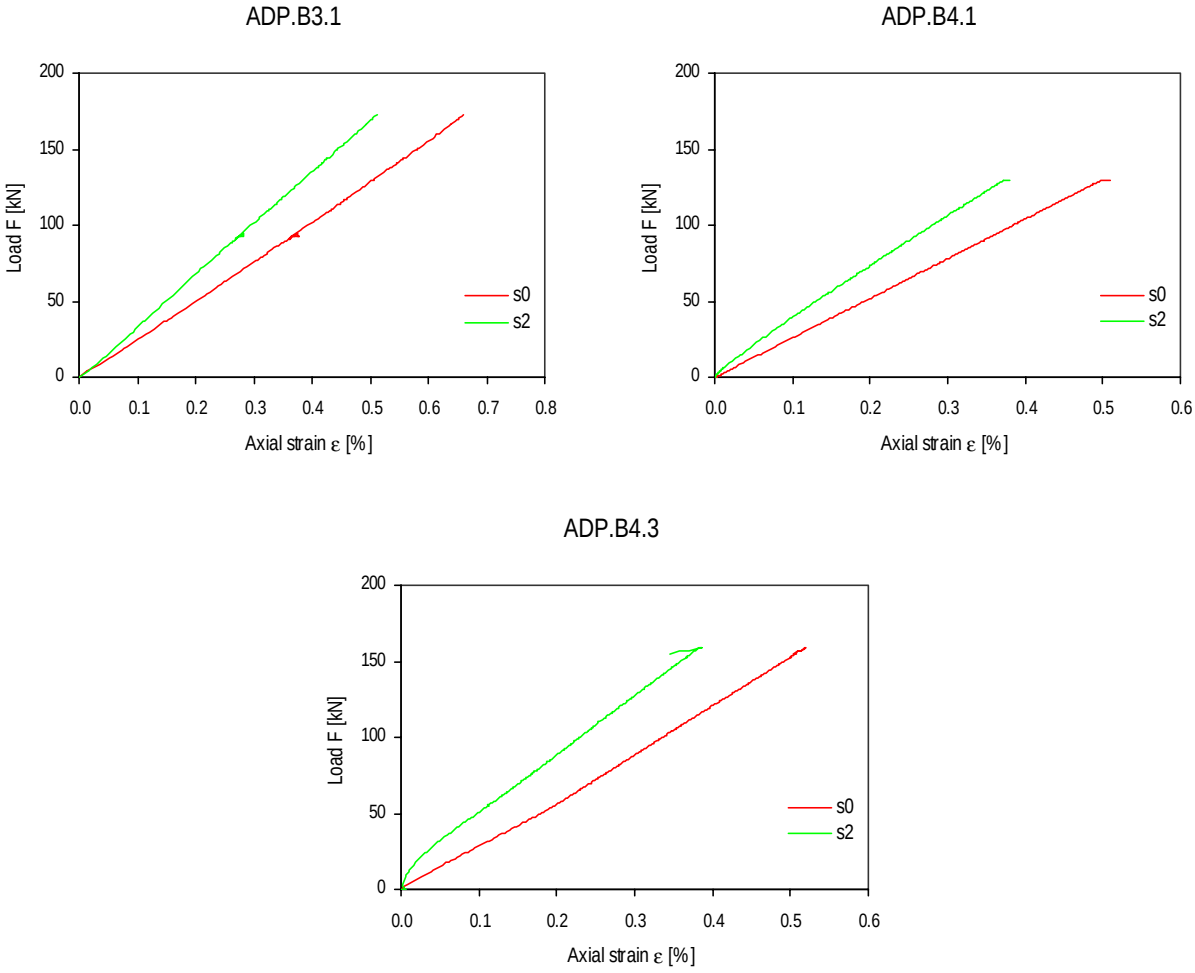

Figure 70 Load-strain curve of specimens ADP.B

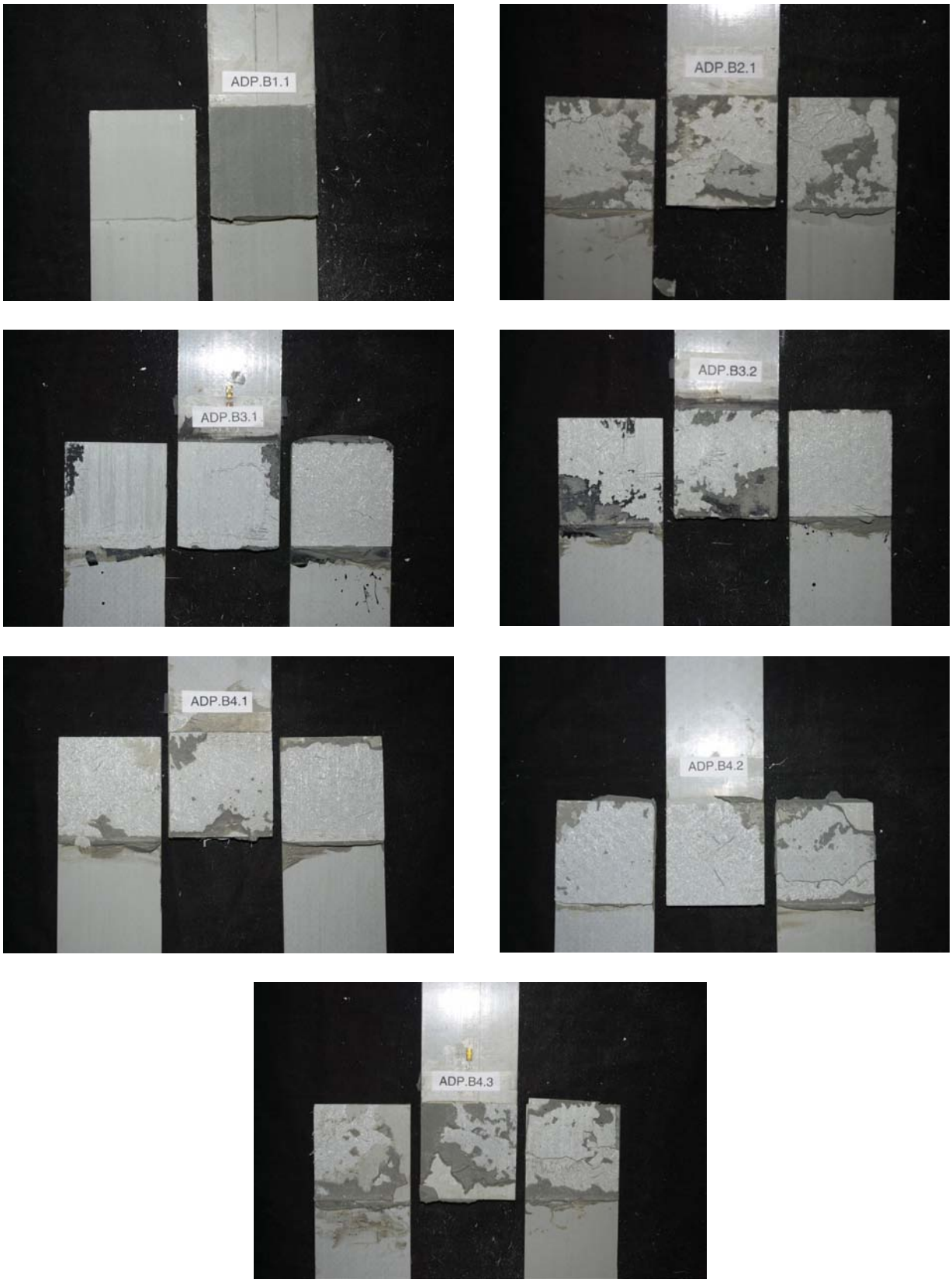

Figure 71 Failure of specimens ADP.B

7.8 Curves and Failure Pictures of Specimens ADP.C

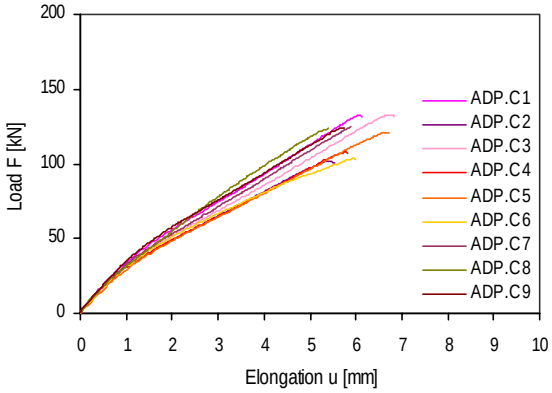

Figure 72 Load-elongation curve of specimens ADP.C

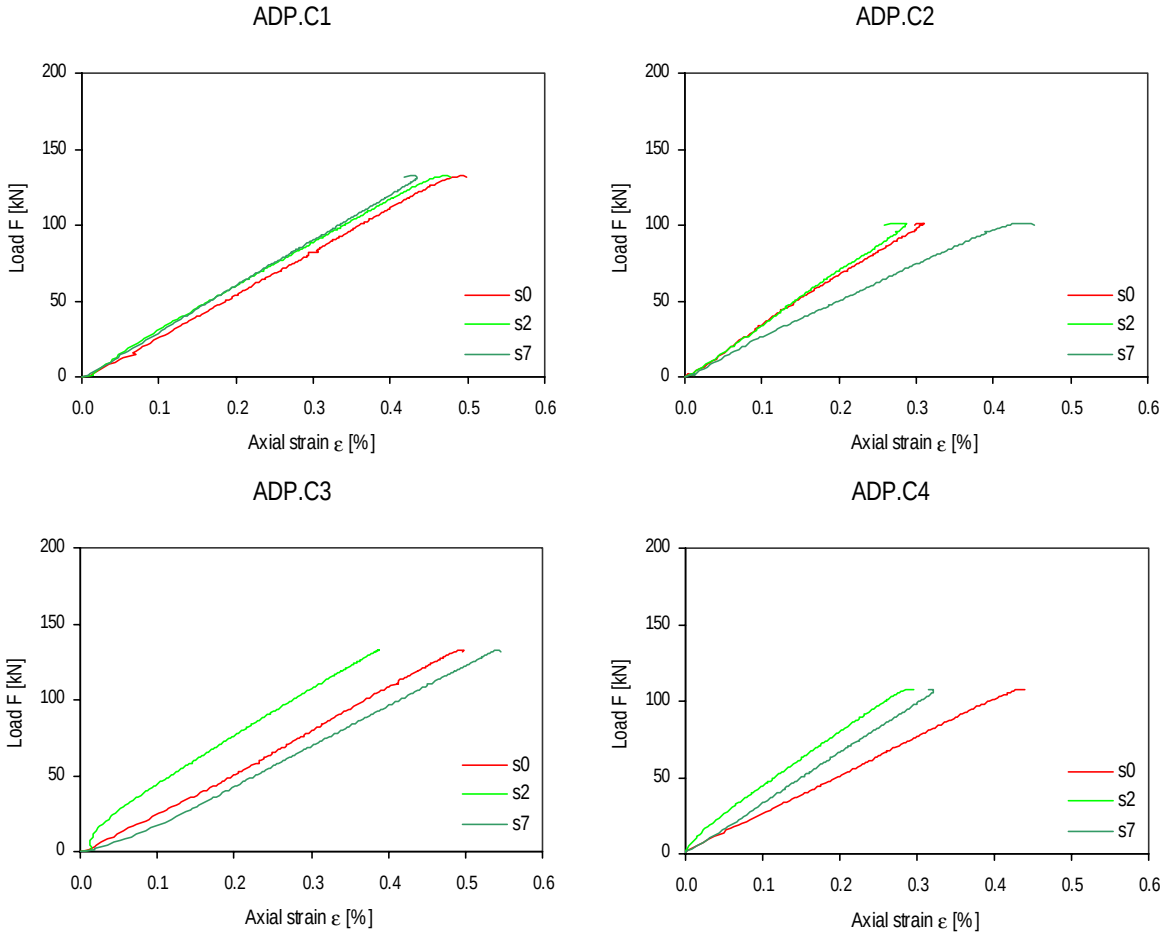

Figure 73 Load-strain curve of specimens ADP.C1-4

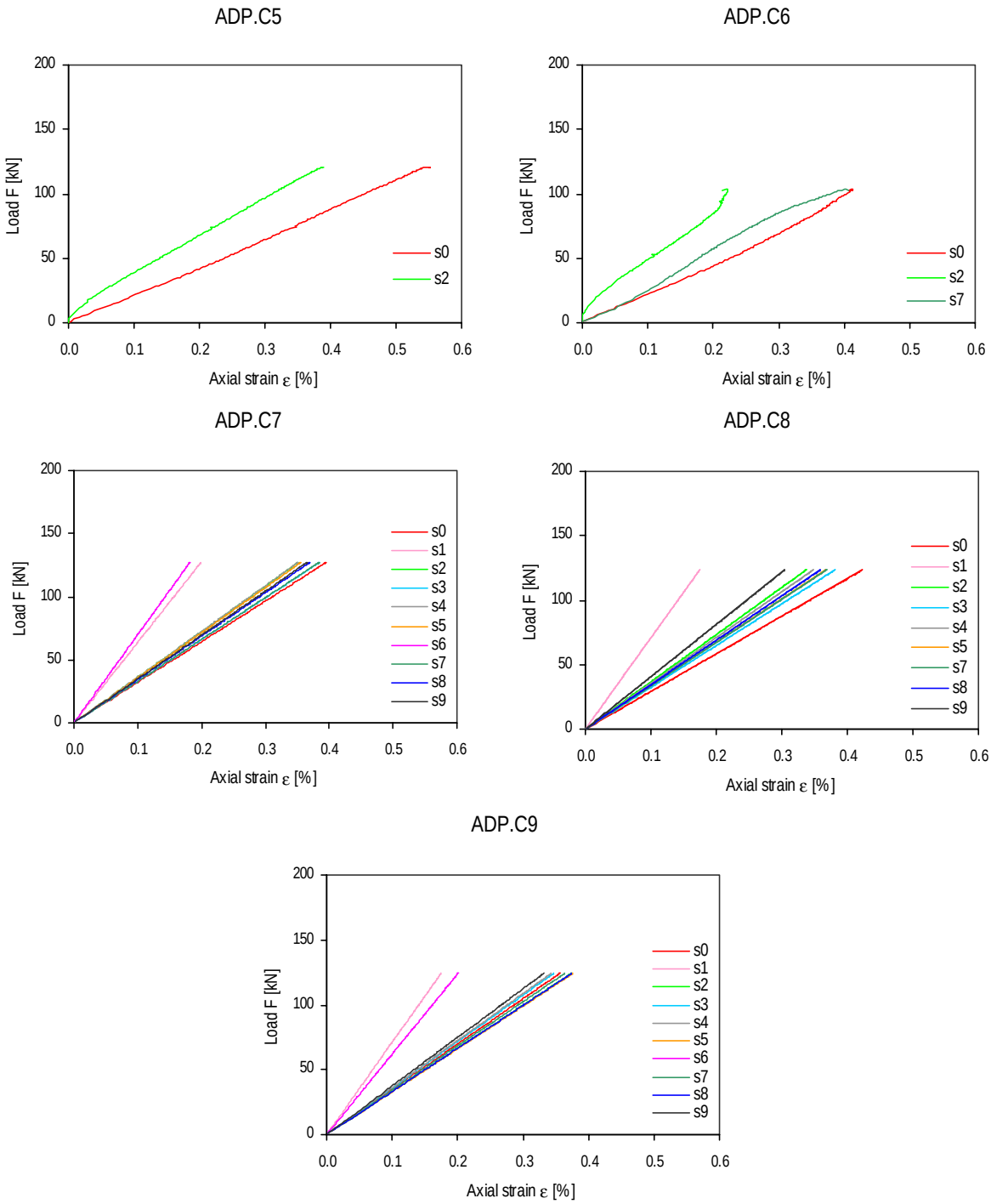

Figure 74 Load-strain curve of specimens ADP.C5-9

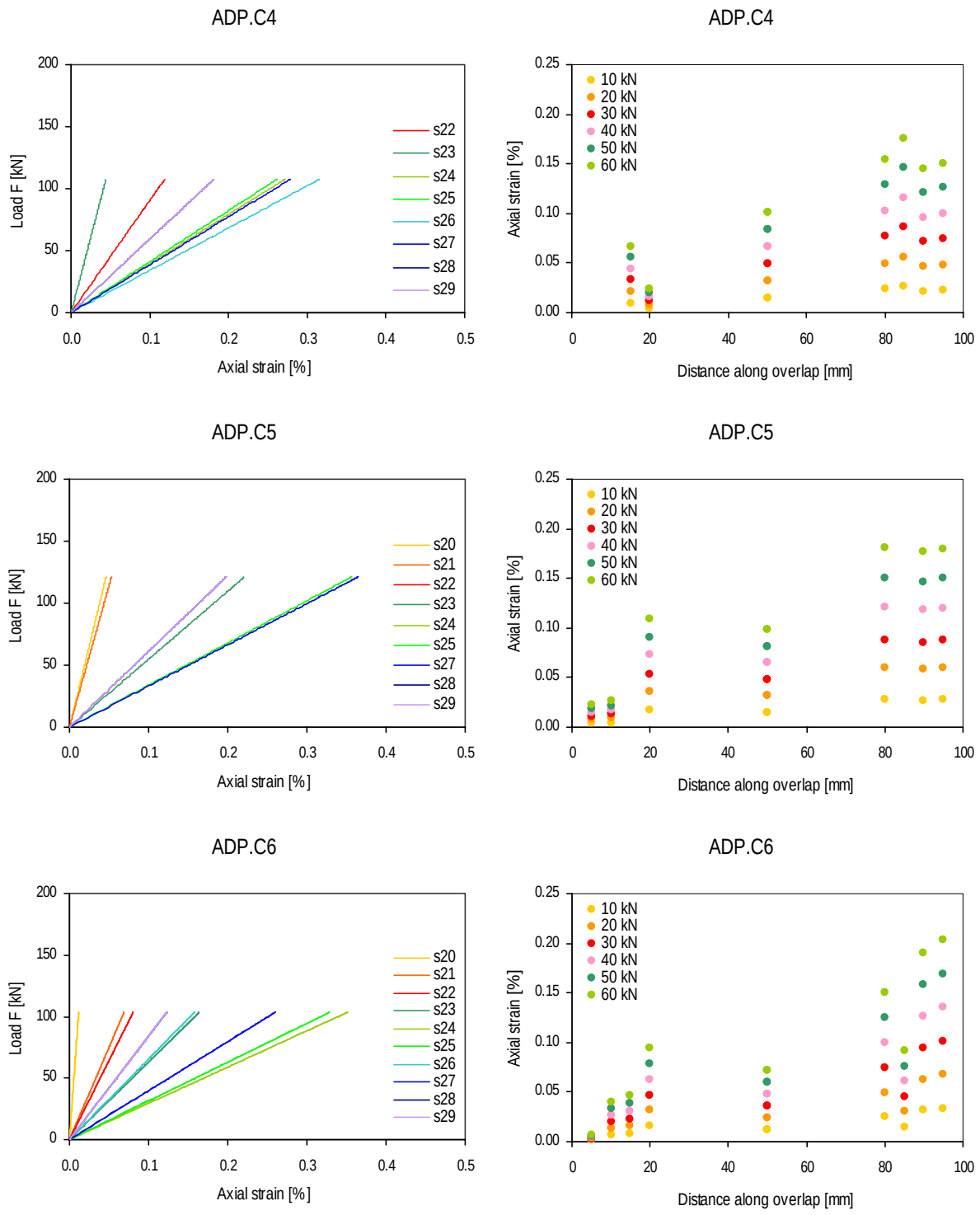

Figure 75 Load-strain curves in joint; (b) Axial strain distribution along overlap length for different load levels of specimens ADP.C4-6

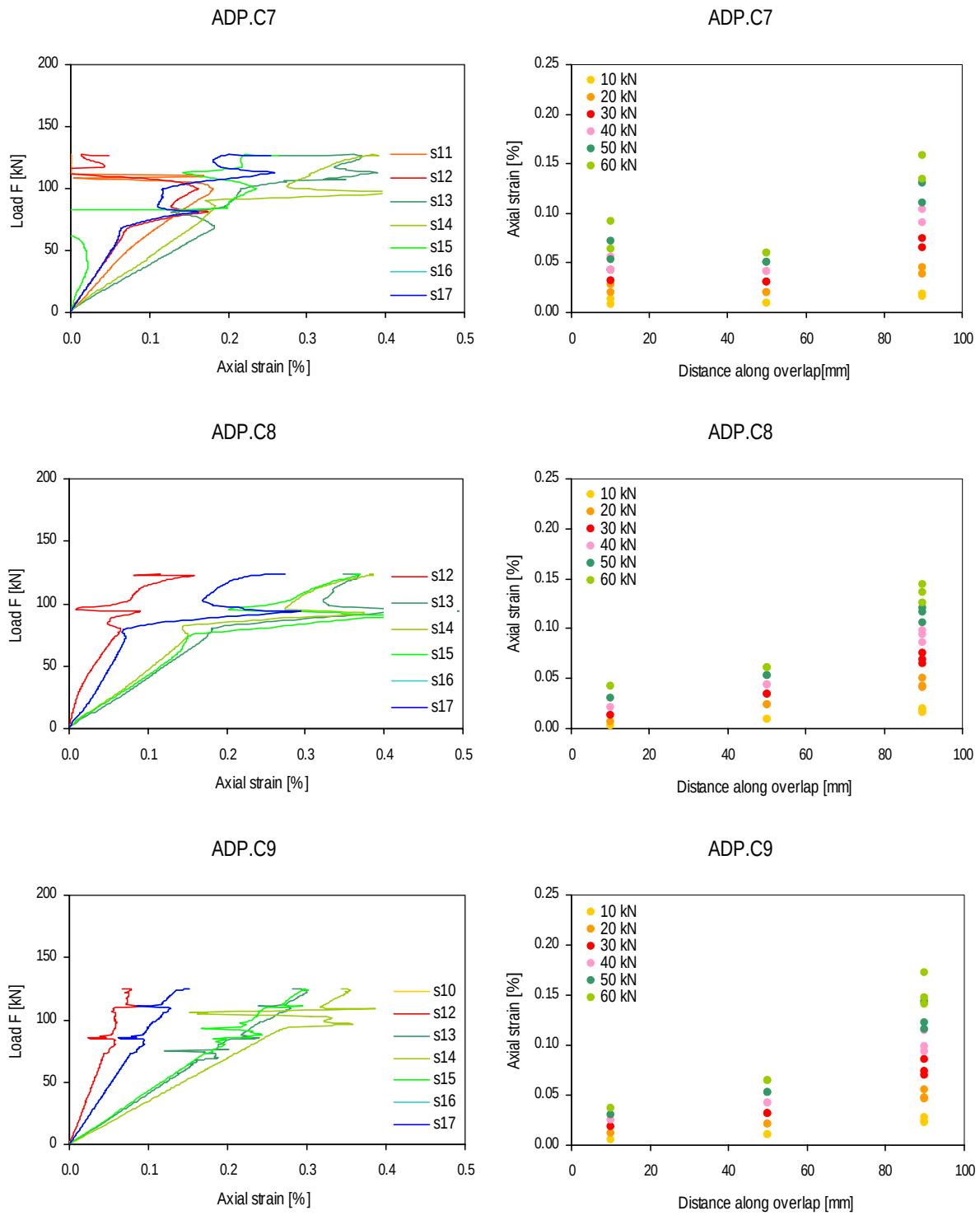

Figure 76 (a) Load-strain curves in joint; (b) Axial strain distribution along overlap length for different load levels of specimens ADP.C7-9

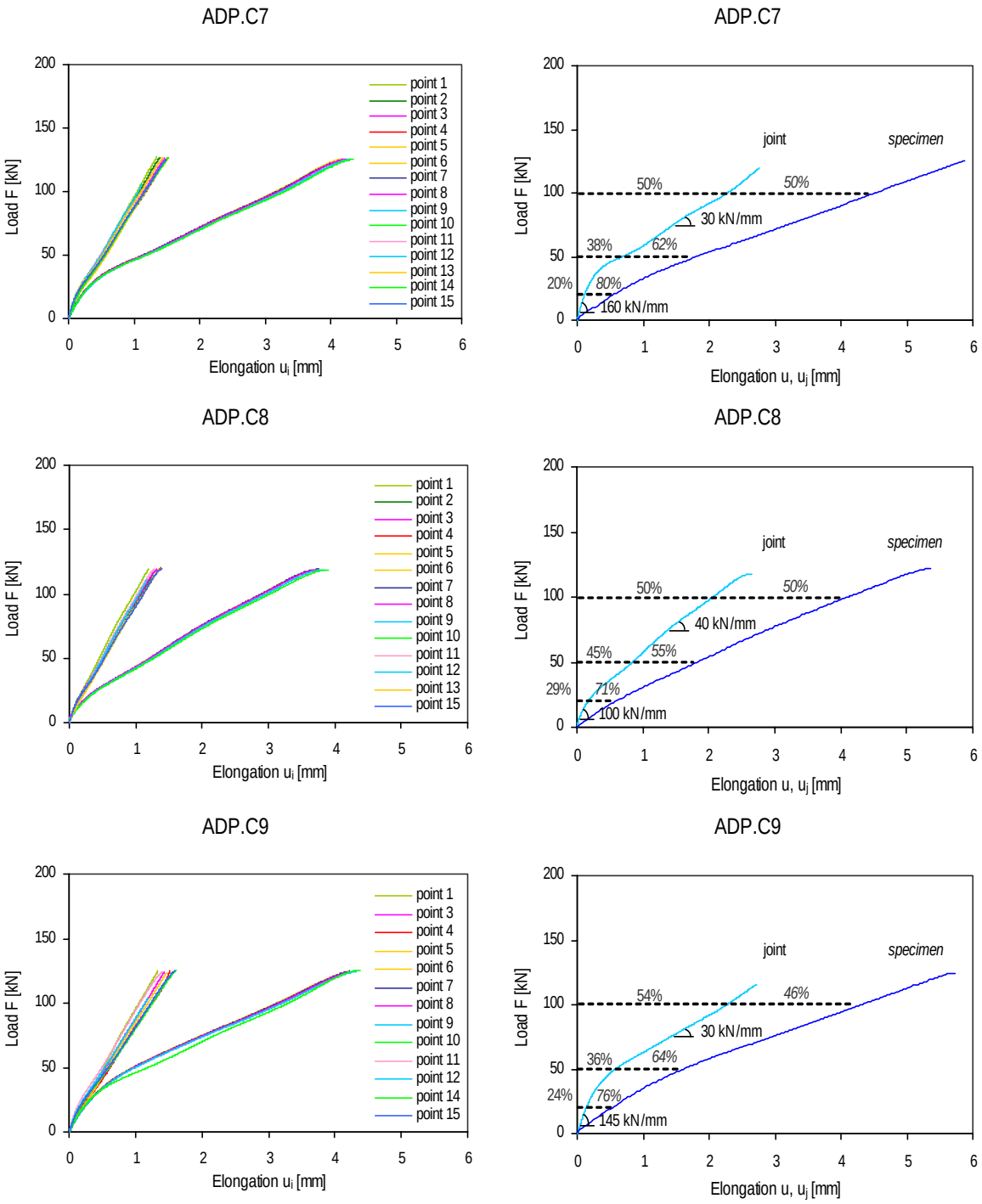

Figure 77 (a) Load-elongation curves measured with video-extensometer; (b) Load-elongation curves of joint and global specimen for specimens ADP.C7-9

Table 31 Young's modulus of laminates for series ADP.C [MPa]

Specimen	Laminates	
	5 mm	10 mm
ADP.C1	29715	27348
ADP.C2	29311	31984
ADP.C3	28756	28655
ADP.C4	33460	25449
ADP.C5	29183	22925[1]
ADP.C6	33746	29897
ADP.C7	33908	34341
ADP.C8	35124	31412
ADP.C9	33730	33977
m	31882	30380
s	2558	3139

[1] not considered in average and standard deviation values

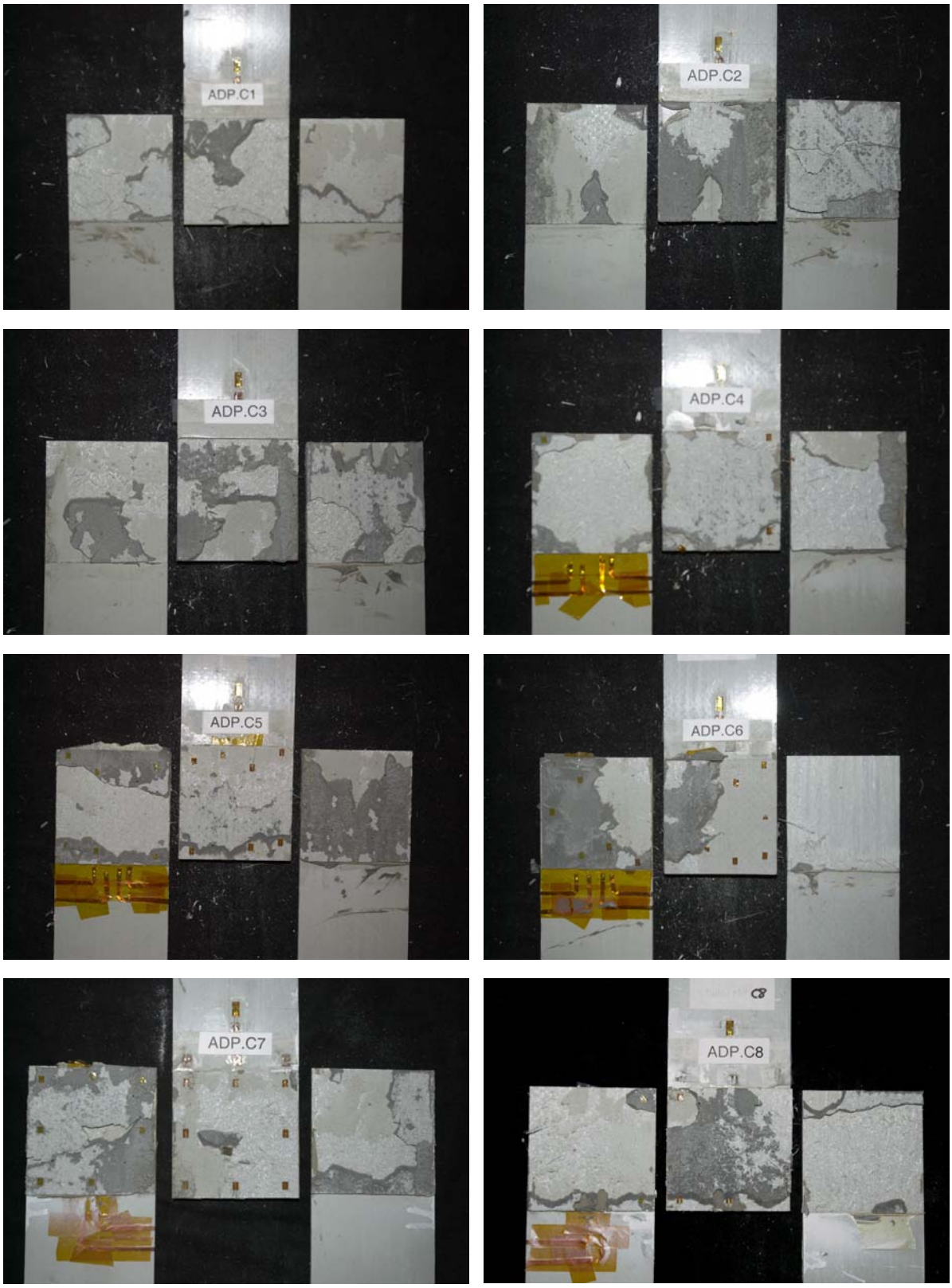

Figure 78 Failure of specimens ADP.C1-8

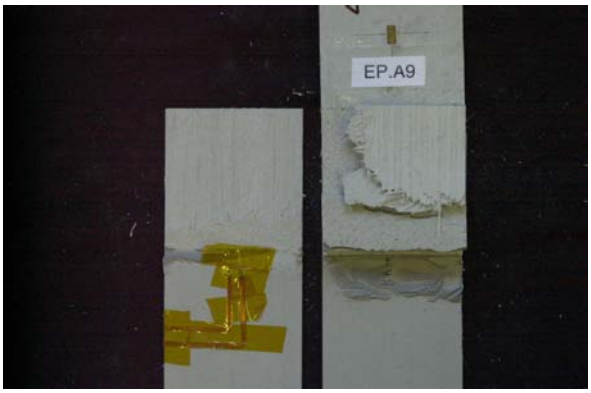

Figure 79 Failure of specimen ADP.C9

7.9 Curves and Failure Pictures of Specimens ADP.D

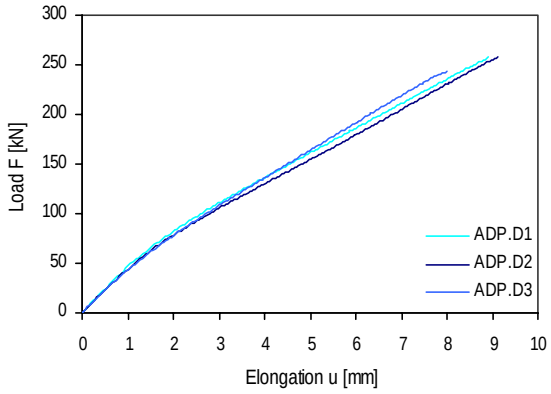

Figure 80 Load-elongation curve of specimens ADP.D

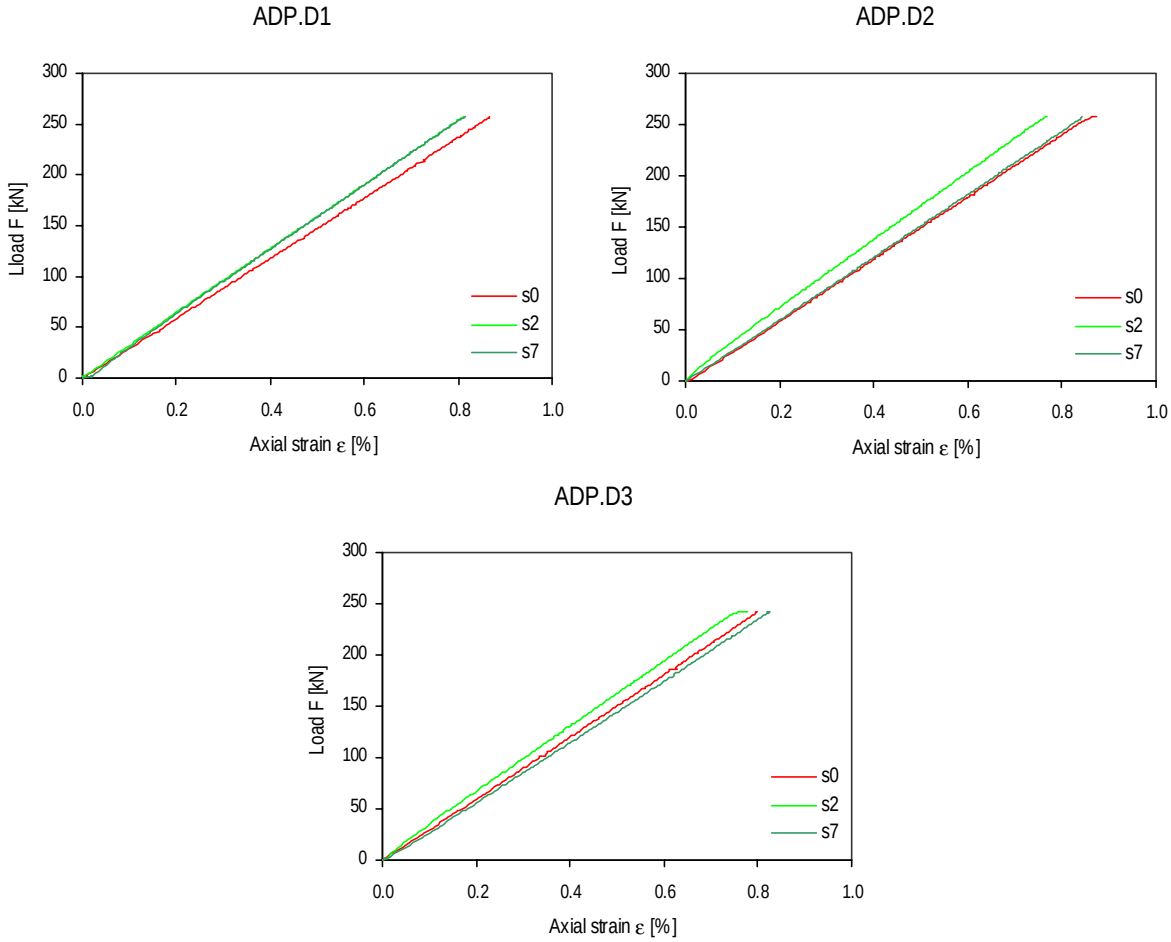

Figure 81 Load-strain curve of specimens ADP.D

Figure 82 Failure of specimens ADP.D

7.10 Curves and Failure Pictures of Specimens ADP-EP.A

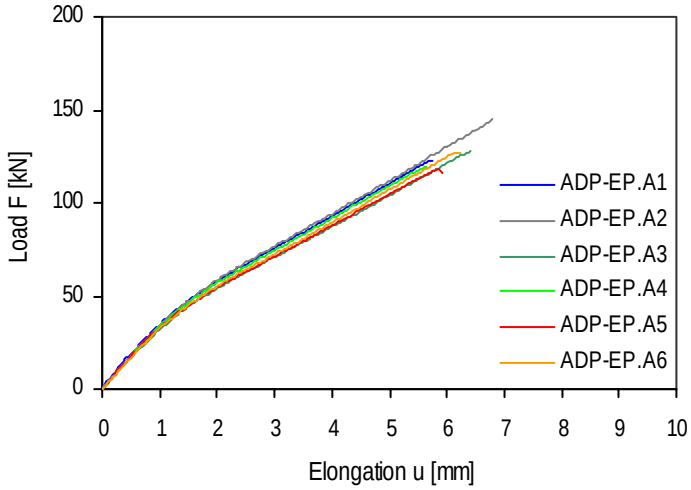

Figure 83 Load-elongation curve of specimens ADP-EP.A

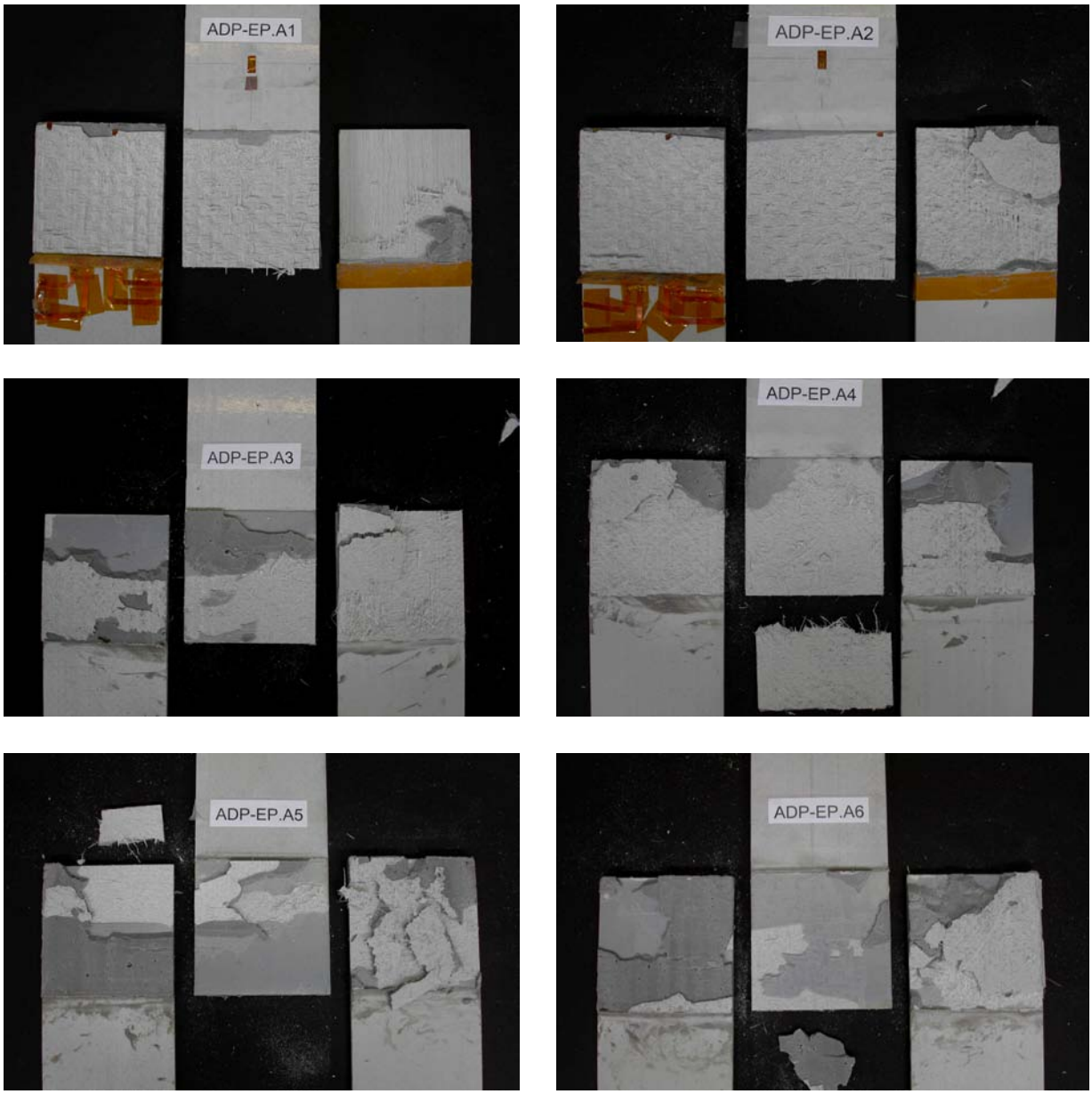

Figure 84 Failure of specimens ADP-EP.A

8 List of figures

9 List of tables

10 References

ABBOTT E.A., SCOTT M.L. (2002), The Case for Multidisciplinary Design Approaches for Smart Fibre Composite Structures, *Composite Structures*, Vol.58, No. 3, pp 349-362.

ADAMS R.D., CAWLEY P. (1989), Defect Types and Non-Destructive Testing Techniques for Composites and Bonded Joints, *Construction and Building Materials*, Vol.3, No. 4, pp 170-183.

ADAMS R.D. (1990), The Nondestructive Evaluation of Bonded Structures, *Construction and Building Materials*, Vol.4, No. 1, pp 3-8.

ADAMS R.D., COMYN J., WAKE W.C. (1997), *Structural Adhesive Joints in Engineering- Second Edition*, Chapman & Hall, London, United Kingdom.

ANON (2003), *Fiberline Design Manual*, Internet -http:/www.fiberline.com/gb/home/index.asp, July 6, 2004.

ASTM D 695M-96 (1996), Standard Test Method for Compressive Properties of Rigid Plastics [Metric][1], *Annual Book of ASTM Standards*, Vol. 08.01, pp 211-216.

ASUNDI A. (1987), Deformation in Adhesive Joints Using Moiré Interferomatry, *International Journal of Adhesion and Adhesives*, Vol. 7, No. 1, pp 39-42.

BASSETTI A. (2001), *Lamelles précontraintes en fibres carbone pour le renforcement de ponts rivetés endommagés par fatigue*, Dissertation ETH N° 2440, ETH Lausanne.

CRANE L.W., HAMERMESH C.L., MAUS L. (1976), Surface Treatment of Cured Epoxy Graphite Composites to Improve Adhesive Bonding, *SAMPE J.*, No. 2, pp 6-9.

DESSARTHE A. (1992), *Assemblages des matériaux composites, structures sandwichs et matières plastiques*, Publications CETIM, France.

DE CASTRO J. (2005 a), *Experiments on Epoxy, Polyurethane and Acrylic Adhesives*, Technical Report CCLab2000.1b/1, CCLab-EPFL, Lausanne, Switzerland.

DE CASTRO J. (2005 b), *System Ductility and Redundancy of FRP Structures with Ductile Adhesively-bonded Joints*, PhD Dissertation, ETH Lausanne, Switzerland.

EN ISO 527-2 (1996), *Determination of Tensile Properties - Part 2: Test Conditions for Moulding and Extrusion Plastics*, European Standard, Brussels, Belgium.

EN ISO 11003-1 (1996), *Determination of Shear Behaviour of Structural Adhesives - Part 1: Torsion test method using butt-bonded hollow cylinders*, European Standard, Brussels, Belgium.

EUREKA Project EU716 (1998), *Quality Assurance in Adhesive Technology*, Abington Publishing, Cambridge, United Kingdom.

GLEICH D.M. (2002), *Stress Analysis of Structural Bonded Joints*, Dissertation Technological University of Delft, The Netherlands.

HART-SMITH L.J., (1987), Joining, Mechanical Fastening, *Engineering Materials Handbook, Vol. 1, Composites*, ASM International, Ohio, United States of America, pp 479-495.

HART-SMITH L.J., OCHSNER R.W., RADECKY R.L. (1990), Surface Preparation of Composites for Adhesive-Bonded repair, *Engineering Materials, Handbook, Vol. 3, Adhesives and Sealants*, ASM International, Ohio, United States of America, pp 840-844.

HILL K.O., FUJII Y., JOHNSON D.C., KAWASAKI B. (1978), Photosensitivity in Optical Fibre Waveguides: Application to Reflection Filter Fabrication, *Applied Physics Letters*, Vol. 32, pp 647-649.

HOLLAWAY L.C., HEAD P.R. (2001), FRP Strengthening and Repair of Reinforced Concrete Systems, *Advanced Polymer Composites and Polymers in the Civil Infrastructure*, Chapter 5, Elsevier, Oxford, United Kingdom.

HUANG S., OHN M.M., LEBLANC M., MEASURES M.R. (1998), Continuous Arbitrary Strain Profile Measurements with Fibre Bragg Grating, *Journal Smart Material Structures*, Vol.7, pp 248-256.

HUTCHINSON A. (1999), Adhesive Bonded Joints Involving Fiber-Reinforced Polymer Composites, *Composite and Plastics in Construction*, Rapra Technology Limited, Shawbury, United Kingdom, paper 9.

JONES R., WYKES C. (1983), *Holographic and Speckle Interferometry*, Cambridge University Press, United Kingdom.

KELLER T. (2003), *Use of Fibre Reinforced Polymers in Bridge Construction*, Structural Engineering Documents 7, International Association for Bridge and Structural Engineering, Zürich, Switzerland.

LAMBERT A., RIVENEZ J., WACHE G., DESSARTHE A. (1994), *Les contrôles non destructifs Généralités*, Publications CETIM, France.

LAU K., CHAN CH., ZHOU L., JIN W (2001), Strain Monitoring in Composite-Strengthened Concrete Structures Using Optical Fibre Sensors, *Composites:Part II*, Vol.32, No. 1, pp 33-45.

MATTHEWS F.L., KILTY P.F., GODWIN E.W. (1982), A Review of the Strength of in Fiber-Reinforced Plastics, Part 2: Adhesively Bonded Joints, *Composites*, Vol. 13, No. 1, pp. 29-37.

MAASKANT R., ALAVIE T., MEASURES R.M., TADROS G., RIZKALLA S.H., GUHATHAKURTA A. (1997), Fibre-Optic Bragg Grating Sensor for Bridge Monitoring, *Journal Cement Concrete Composite*, Vol.19, No. 1, pp 21-33.

POCIUS A.V., WENZ R.P. (1985), Mechanical Surface Preparation of Graphite Epoxy Composite for Adhesive Bonding, *SAMPE J.*, Vol. 21, No. 5, pp 50-58.

RICHARDSON G., CROCOMBE A.D., SMITH P.A. (1993), A Comparison of Two- and Three-Dimensional Finite Element Analyses of Adhesive Joints, *International Journal of Adhesion and Adhesives*, Vol. 13, No. 3, pp 193-200.

SIEBRECHT J, VALLEE T. (2001), *Shear Test on Bonded Double Lap FRP-Joints*, Diploma dissertation, Chapter 7, CCLab-EPFL, Lausanne, Switzerland.

SOTIROPOULOS S.N., GANGARAO H.V.S., ALLISON R.W. (1994), Structural Efficiency of the Pultruded FRP Bolted and Adhesive Connections, *Composite Institute's 49th Annual* Conference, The Society of the Plastics Industry, New York, Session 8-A.

TIRELLI T. (2003), *Static and Fatigue Behavior of Pultruded GFRP Laminates*, Technical Report CCLab2000.1c/2, CCLab-EPFL, Lausanne, Switzerland.

TSUNO S. (2003), *Selection of Sika Primer for Adhesion to FRP (project of EPFL) by SikaFAst-5221*, Technical Report, Sika Technology AG, Tüffenwies, Switzerland

VALLEE T. (2004), *Adhesively Bonded Lap Joints of Pultruded GFRP Shape*, PhD Dissertation ETH No. 2964, ETH Lausanne, Switzerland.